N° d'ordre : 2017LYSEC19 Année 2017

THESE

présentée pour obtenir le titre de DOCTEUR de

L'ECOLE CENTRALE DE LYON

Spécialité: Acoustique

École Doctorale: Mécanique, Énergétique, Génie civile et Acoustique

Par Ahmed KESSENTINI

APPROCHE NUMERIQUE POUR LE CALCUL DE LA MATRICE DE DIFFUSION ACOUSTIQUE: APPLICATION POUR LES CAS CONVECTIFS ET NON CONVECTIFS.

A NUMERICAL APPROACH FOR THE CALCULATION OF THE ACOUSTICAL SCATTERING MATRIX: APPLICATION FOR THE CONVECTIVE AND THE NON CONVECTIVE CASES

Soutenue le 1 Juillet 2017 devant la commission d'Examen composée de :

M. C. KARRA	Professeur, U2MP- ENIS	Président
M. N. BOUHADDI	Professeur, FEMTO-ST-UBFC	Rapporteur
M. N. GMATI	Professeur, LAMSIN-ENIT	Rapporteur
M. J-L. DION	Professeur, LISMA-SUPMECA	Membre
M. F. CHAARI	Professeur, U2MP-ENIS	Membre
M. M. ICHCHOU	Professeur, LTDS-ECL	Directeur de thèse
M. M. TAKTAK	Maître de Conférences, U2MP-ENIS	Directeur de thèse
M. O. BAREILLE	Maître de Conférences, LTDS-ECL	Directeur de thèse

Laboratoire de Tribologie et Dynamique des Systèmes – UMR 5513

République Tunisienne
Ministère de l'Enseignement Supérieur
et de la Recherche Scientifique

Université de Sfax
École Nationale d'Ingénieurs de Sfax

Ecole Doctorale
Sciences et Technologies

Thèse de *DOCTORAT*

Génie Mécanique
N° d'ordre: 301/16

THESE

Présentée à

L'École Nationale d'Ingénieurs de Sfax

En co-tutelle avec

L'École Centrale de Lyon

En vue de l'obtention du

DOCTORAT

Dans la discipline Génie Mécanique

Par

Ahmed KESSENTINI

A numerical approach for the calculation of the acoustical scattering matrix: application for the convective and the non-convective cases

Approche numérique pour le calcul de la matrice de diffusion acoustique: application pour les cas convectifs et non convectifs

Soutenue le 1er Juillet 2017, devant le jury composé de :

M.	**Chafik KARRA**	Président
M.	**Noureddine BOUHADDI**	Rapporteur
M.	**Nabil GMATI**	Rapporteur
M.	**Jean-Luc DION**	Membre
M.	**Fakher CHAARI**	Membre
M.	**Mohamed ICHCHOU**	Directeur de Thèse
M.	**Mohamed TAKTAK**	Directeur de Thèse
M.	**Olivier BAREILLE**	Co-encadrant
M.	**Mohamed Amine BEN SOUF**	Co-encadrant

Remerciements

Alors que les parties qui suivent sont l'aboutissement d'un peu plus que trois ans de travail à Sfax ainsi qu'à Lyon, je profite de cet espace pour remercier les personnes qui ont marqué mes débuts dans la recherche scientifique.

Ce travail de recherche a été effectué dans le cadre d'une thèse en co-tutelle entre le **LAboratoitre de Mécanique, Modélisation et Productique** (LA2MP) du département de Génie Mécanique de L'Ecole Nationale d'Ingénieurs de Sfax et le **Laboratoire de Tribologie et Dynamique des Systèmes** (LTDS) de L'Ecole Centrale de Lyon. J'exprime ma profonde gratitude à Monsieur Mohamed Haddar pour la confiance qu'il m'a témoignée au cours de ces trois années de doctorat, et à Messieurs Mohamed Ichchou et Olivier Bareille pour m'avoir accueilli au sein de leur équipe à Lyon. Merci à mes encadrants, Messieurs Mohamed Taktak, Mohamed Ben Souf, Mohamed Ichchou et Olivier Bareille, pour leurs précieuses aides scientifiques. J'associe à ces remerciements Messieurs Nabil Gmati et Noureddine Bouhaddi qui m'ont fait l'honneur de bien vouloir examiner ce travail et Messieurs Chafik Karra et Fakher Chaari qui ont accepté de participer au jury.

Mes immenses remerciements s'adressent particulièrement à mes parents, avec qui j'ai surmonté les difficultés. Merci pour leur soutien et leurs conseils. Je tiens aussi à remercier mes amis. Ce fut un plaisir de partager avec eux des moments extraordinaires.
Je garde dans l'esprit tant de souvenirs spéciaux, des bons et des moins bons, et une expérience que j'espère me bien servir à l'avenir.

Résumé

Cette thèse s'intéresse à l'étude de la propagation acoustique en guides d'ondes. La méthode "Wave Finite Element" (WFEM) est d'abord appliquée à la propagation des ondes acoustiques dans des conduits périodiques rigides. Etant modélisés seulement en cellule typique de taille réduite, la théorie des milieux périodiques conduit ensuite à un problème dont les solutions sont extraites pour une section de guide d'ondes, pouvant être ensuite calculées dans tout le milieu en utilisant ces cellules répétitives. Puis, des conduits avec des discontinuités d'impédance acoustique sont étudiés. Une modélisation par Eléments Finis est utilisée pour ces parties traitées acoustiquement et la matrice de diffusion est calculée. Différentes configurations sont étudiées, et le comportement et la performance en terme d'atténuation acoustique de ces traitements sont discutés. Les réponses forcées des conduits à des conditions aux limites imposées sont également calculées et comparées aux solutions fournies par la méthode Eléments Finis conventionnelle. La propagation acoustique dans les applications industrielles, néanmoins, s'accompagne souvent par un écoulement de fluide. L'étude est alors étendue au cas de la propagation acoustique libre en présence d'écoulement moyen uniforme. Une reformulation est donc issue de l'équation de Helmholtz convectée et développée pour le calcul de la diffusion. L'effet de l'écoulement est enfin examiné.

Mots clés: Propagation acoustique guidée, Conduit, Matrice de diffusion, Wave Finite Element.

Abstract

This thesis deals with the study of the guided acoustical propagation. The Wave Finite Element method (WFEM) is first applied to the propagation of acoustic waves in rigid periodic ducts. Only a typical cell of reduced size being modelled, the theory of periodic media then leads to a problem whose solutions are extracted for a waveguide section, and can then be computed throughout the medium using these repetitive cells. Then, ducts with acoustic impedance discontinuities are studied. Finite element modelling is used for these acoustically lined parts and the scattering matrix is calculated. Different configurations are studied, and the behaviour and performance in terms of acoustic attenuation of these liners are discussed. The forced responses of ducts submitted to imposed boundary conditions are also calculated and compared to the solutions provided by the conventional Finite Element method. The acoustical propagation in industrial applications, however, is often accompanied by a flow. The study is therefore extended to the case of free acoustical propagation in the presence of uniform mean flow. A reformulation is derived from the convected Helmholtz equation and further developed for the calculation of the scattering. The effect of the flow is finally examined.

Keywords: Guided acoustical propagation, Duct, Scattering matrix, Wave Finite Element.

Contents

List of Figures

List of Tables

Introduction

Duct acoustics has been a widely investigated research topic, as it has various engineering applications such as aircraft engines, compressors, and ventilation systems. Acoustic liners are the most used techniques to attenuate sound levels in duct systems. Aero-structures, such as an aircraft nacelle, are made of honeycombs and designed to be environmentally friendly through a reduced engine noise. In other engineering applications, porous liners are preferred since their performance is less frequency dependent. Whether honeycombs or porous materials are used, these systems involve heterogeneous and multi-scaled media, and therefore different behaviours of the acoustic waves propagation within these media. A lined waveguide can be completely characterised by its scattering matrix. Therefore, it will be worth finding ways to express this matrix taking into consideration the multi-modal aspect of the guided acoustical propagation and almost realistic conditions.

The scattering matrix is considered as a characterisation of a waveguide element regardless of the upstream and downstream conditions [9]. For instance, the scattering matrix was calculated to study the scattering at elbow junctions of structural features through a semi-analytical finite element (SAFE) method [10]. Kharrat *et al.* [11] studied the waves diffusion due to defects in pipes. In other works, the scattering matrix of acoustical propagation inside waveguides with impedance discontinuities was calculated [12, 13]. Some previous works dealt with its measuring not only for the acoustical scattering due to passive elements [14], but also hybrid cells [15]. The acoustical scattering matrix can be also computed for a discontinuity of diameter using a mode matching approach (MMA) [16].

Several theoretical works focused on the study of the acoustical propagation and scattering within ducts. For the axisymmetric cases, analytical approaches used a series expansion of solutions that result from Helmholtz equation, and a projection over a basis of orthogonal

functions for the rigid duct. Coupling of modes with same circumferential order is added for the lined part. Vector of pressure projections obeys then a second-order differential equation. A subsequent method for the computation of scattering matrix is detailed in [17, 12]. An improvement of this method was later published [18]. These works studied sound propagation in cylindrical ducts without mean flow. Auregan *et al.* [5] presented a "multi-modal method" to compute the scattering matrix of propagation in a 2D lined duct with flow , which aimed to measure the liner impedance. Nevertheless, for 3D ducts of arbitrary cross section, it is laborious to express solutions within a duct analytically. Numerical approaches were alternatively proposed in literature [19, 13, 20]. These methods used the Finite Element formulation, and results of the adopted numerical methods were compared to the analytical results. However, Finite Element models get impractical for high frequencies causing an insufficiency of accuracy, or CPU capacity and time related computing issues. Although the Finite Element method was preferred, the scattering matrix was computed for a frequency range such as only uncoupled modes are cut-on. Experimental procedures for the multi-modal measuring of the acoustical scattering matrix using a pressure source composed of the cut-on modes were detailed in [21, 22, 4]. Five cut-on modes allowed the determination of a (10×10) scattering matrix. A comparison with theoretical results was also included.

When a waveguide is periodic, assuming that it is uniform following the waves propagation direction, a FE based approach can be used for an elementary modelling. This is the Wave Finite Element method, commonly referred to as the WFE method, and it will be mainly used in this thesis. The WFE method has many potential advantages compared to the above mentioned approaches. A significantly lower computing cost makes it a powerful alternative to the conventional FE method. The method remains efficient up to high frequencies, that is, study of high order modes is possible. Indeed, a FE model with a small size is involved. Mass and stiffness matrices, typically extracted using commercial FE tools, are then post-processed using the periodicity conditions to obtain an eigenvalue problem. The eigenvalues are divided into two sets corresponding to forward and backward going waves and the wavenumbers and wave modes are provided. Moreover, this method can be extended to the multi-layers [23] and the two dimensional propagation [24]. The WFE method for two dimensional structures was studied in [25]. Manconi and Mace [26] used the WFE method to analyse wave propagation

in axisymmetric structures. Renno and Mace [27] calculated the forced response of two dimensional homogeneous media through the WFE approach. The method does not have limitations for the type of element used for modelling. However, it may be prone to ill-conditioning issues. In fact, the cross-sectional mesh density can be increased to add high order modes to the wave basis, but time consuming matrix inversions and ill-conditioned matrices must be handled while raising the degrees of freedom number. For example, some authors kept only a reduced wave basis while computing the forced response [28]. Numerical issues were discussed and some solutions were provided in [29, 23]. The scattering matrix computation procedure is actually a hybrid WFE/FE method. The conventional FE method is used for the lined part of the duct while the WFE method is used for the rigid duct parts. The continuity conditions at the right and the left edges of the coupling element corresponding to the lined duct part are then exploited.

This thesis proposes a numerical approach to calculate the acoustical scattering within periodic lined ducts, with and without mean flow, with very few restricting hypotheses. The thesis includes four chapters:

In chapter 1, the literature is reviewed. Theory of acoustic duct modes is summarised. The conventional methods principles are briefly presented. Methods are compared and limitations are discussed.

In chapter 2, The WFE method formulation is presented. The scattering matrix computation method is detailed. Then, the computation procedure of the forced response of both single and coupled periodic waveguides is given. The chapter is ended by numerical validation of some typical examples. The scattering matrix calculated by the WFE method is compared to results of the analytical method, and the forced response is validated by the FE method [30].

Chapter 3 is devoted to advanced modelling of the lined duct parts. Two liner configurations are dealt with. The scattering due to locally reacting lining is first studied. Calculation of the equivalent surface impedance of the interface is used in this case. Then, scattering due to bulk reacting liners is considered. Three dimensional modelling of the lining is rather preferred. The response of rigid and lined waveguides submitted to prescribed boundary conditions (e.g. pressures or velocity excitations, anechoic or partially reflective ends, PML

layers ...) can be calculated. Results are always compared to conventional methods.

In chapter 4, the convective propagation case is considered. For the standard case of a uniform medium without flow, modes are related to the eigensolutions of Laplace operator . For a medium with mean flow, the details become more complicated, but the concept of duct modes remains the same. Results are then discussed and concluding remarks are finally given.

Chapter 1

Bibliographic survey

1.1 Introduction

Several methods, including analytical and numerical ones, have been used in literature for the study of the acoustical propagation inside waveguides. Acoustical waveguides were characterised in different ways such as calculating the transfer matrix [31, 32], the mobility matrix [33], the reflection matrix [34, 21], the transmission matrix [21] and the determination of the scattering matrix either theoretically [12, 13] or experimentally [20, 22]. Particularly, the scattering matrix provides a full multi-modal description of transmission, reflection and conversion between the modes. Moreover, it is an intrinsic characterisation of waveguides which does not depend on the upstream and downstream conditions.

This chapter is organised as following: Theoretical bases of duct acoustics are reviewed in the first part. An application of noise reduction by absorbing materials is illustrated. Then, the main methods dealt with in literature for the study of the guided acoustical propagation and the calculation of the scattering matrix are summarised. The chapter is ended by presenting the Wave Finite Element Method through a comparison with the other approaches.

1.2 Theoretical bases

1.2.1 Conservation equations

Let us suppose that perturbations are small and equations are linear in the acoustic quantities. The fluid is assumed to be homogeneous, non-viscous and thermally non-conductive. The propagation equation of the acoustic pressure is the result of a system of three fundamental equations governing the fluctuation of the fluid density ρ, the acoustic velocity $\mathbf{v}$ and the acoustic pressure p.

Equation of mass conservation and equation of momentum conservation are given respectively by:

$$\frac{\partial \rho}{\partial t} + \rho_0 div(\mathbf{v}) = 0 \tag{1.1}$$

$$\rho_0 \frac{\partial \mathbf{v}}{\partial t} + \boldsymbol{\nabla} p = 0 \tag{1.2}$$

The state equation is:

$$p = \rho c^2 \tag{1.3}$$

where c is the celerity of the sound in the fluid and ρ_0 is the density of the fluid.

1.2.2 Acoustic impedance

The complexity of the aeroacoustic phenomena in the surface of a liner makes the definition of a macroscopic quantity describing the effects of absorption necessary. The presence of an absorbent material can be taken into account as boundary conditions in guided propagation equations. We define:

– Acoustic impedance: the ratio of the pressure to the velocity normal to the material.

– Characteristic acoustic impedance: the acoustic impedance in the free field given by $\rho_0 c$.

– Normalised acoustic impedance: a dimensionless quantity that normalises the acoustic impedance to the characteristic acoustic impedance of the air.

– Acoustic admittance: the inverse of the acoustic impedance.

It should be noted that the acoustic impedance is frequency dependent. Although the

impedance depends also on spatial coordinates, a homogenised acoustic impedance which represents the whole material is usually considered. Furthermore, it was shown that an acoustic impedance depends on fluid flow characteristics too [35].
The real part of the impedance is called resistance. The resistance of a passive material is necessarily positive. The imaginary part is called reactance. Three particular values of the acoustic impedance have special meanings: if the impedance is infinite, then the normal velocity is zero which corresponds to a rigid wall. If the impedance is equal to zero, then it corresponds to the soft wall condition. If the impedance is equal to $\rho_0 c$, it corresponds to the transparent boundary condition (no reflection condition) under normal incidence.
Several methods, including theoretical and experimental ones, were used in literature for the eduction of the acoustic impedance of absorbers under different propagation conditions [36, 37, 38, 39, 6, 40] .

1.2.3 Acoustic field inside ducts

Let us consider a hard-walled duct of arbitrary cross section with a uniform medium without mean flow. Consider the two-dimensional cross-sectional area $\mathcal{A}$ of the duct and the outward unit normal to the wall $\mathbf{n}_R$. The duct $\mathcal{D}$ is defined:

$$\mathcal{D} = \{(x, y, z) | (y, z) \in \mathcal{A}\} \tag{1.4}$$

The acoustic field satisfies in the duct the Helmholtz equation for harmonic time dependence:

$$\boldsymbol{\nabla}^2 p + \frac{\omega^2}{c^2} p = 0 \tag{1.5}$$

where c is the celerity of the sound in the fluid and ω is the angular frequency.
The hard wall boundary condition can be written as:

$$\mathbf{v}\mathbf{n}_R = 0 \tag{1.6}$$

where $\mathbf{v}$ is the velocity and $\mathbf{n}_R$ is the normal to the rigid wall.
Solutions of Eq. (1.5) are of the form $p(x, y, z) = X(x)\psi(y, z)$ with $X(x) = \mathrm{e}^{-\mathrm{i}k_x x}$. Functions

ψ associated to particular values of k_x are determined up to a multiplicative factor. When the exponential term is dropped, we get:

$$\boldsymbol{\nabla}_{yz}^2\psi + (\frac{\omega^2}{c^2} - k_x^2)\psi = 0 \tag{1.7}$$

where $\boldsymbol{\nabla}_{yz}^2$ denotes the Laplacian $\boldsymbol{\nabla}^2$ in y and z. As ψ is a function of y and z, it is same to replace by $\boldsymbol{\nabla}^2$ instead. The general solutions are therefore:

$$p(x, y, z) = \sum_{j=0}^{\infty} A_j \psi_j(y, z) \mathrm{e}^{-\mathrm{i}k_{xj}x} \tag{1.8}$$

where ψ_j are the eigenfunctions of Laplace operator reduced to $\mathcal{A}$, which, for $(y, z) \in \mathcal{A}$, are solutions of

$$-\boldsymbol{\nabla}^2\psi = \alpha^2\psi \tag{1.9}$$

and α is the transversal wavenumber.

The axial wavenumbers k_{xj} are given by one of the square roots (+ for right running waves and − for left running waves)

$$k_{xj}^{+-} = \pm\sqrt{\frac{\omega^2}{c^2} - \alpha_j^2} \tag{1.10}$$

Each term in the series expansion is called a duct mode. If $\omega/c > \alpha_j$, the j^{th} mode is cut-on. If $\omega/c = \alpha_j$, the j^{th} mode is at resonance and the axial wave length is infinite (Fig. 1.1). If $\omega/c < \alpha_j$, the j^{th} mode is cut-off (exponentially decaying). In a rectangular duct, $\psi(y, z) = f(y)g(z)$: The eigensolutions consist of combinations of trigonometric functions. In a circular duct in polar coordinates (r,θ), $\psi(y, z) = f(\theta)g(r)$. These eigensolutions consist of exponentials in θ and Bessel functions [41] in r. For ellipses, explicit solutions can be also expressed, but only in special cases such as with hard walls. The eigensolutions consist of Mathieu functions [41]. For other geometries, numerical methods have to be used for the eigenvalue problem.

For (y, z) belonging to the duct wall, we have:

$$\boldsymbol{\nabla}\psi\mathbf{n}_R = 0 \tag{1.11}$$

where $\mathbf{n}_R$ represents the normal to the rigid wall.

The use of Green's theorem, Eq.(1.9) and Eq.(1.11) leads to:

for $i \neq j$:

$$\int\int_{\mathcal{A}} \left[\psi_i(\boldsymbol{\nabla}^2\psi_j + \alpha_j^2\psi_j) - \psi_j(\boldsymbol{\nabla}^2\psi_i + \alpha_i^2\psi_i)\right] \mathrm{d}S = (\alpha_j^2 - \alpha_i^2) \int\int_{\mathcal{A}} \psi_j\psi_i \mathrm{d}S = 0 \tag{1.12}$$

for $i = j$,

$$\int\int_{\mathcal{A}} \left[\psi_j\boldsymbol{\nabla}^2\psi_j + \alpha_j^2\psi_j^2\right] \mathrm{d}S = \alpha_j^2 \int\int_{\mathcal{A}} \psi_j^2 \mathrm{d}S - \int\int_{\mathcal{A}} |\boldsymbol{\nabla}\psi_j|^2 \mathrm{d}S = 0 \tag{1.13}$$

Any $\alpha_j \neq 0$ is an eigenvalue only if $\int\int_{\mathcal{A}} \psi_j^2 \mathrm{d}S \neq 0$. If $\alpha_j = 0$, then $\psi_0 = 1$ and $\int\int_{\mathcal{A}} \psi_0^2 \mathrm{d}S = |\mathcal{A}| \neq 0$.

The orthogonality of $\{\psi_j\}$ has been shown from Eq. (1.12) and Eq. (1.13). That is to say:

$$\int\int_{\mathcal{A}} \psi_i\psi_j \mathrm{d}S = \begin{cases} = 0 & \text{if } i \neq j \\ \neq 0 & \text{if } i = j \end{cases} \tag{1.14}$$

It is noted that the above solutions only need a minor adaptation to include a uniform mean flow inside the duct.

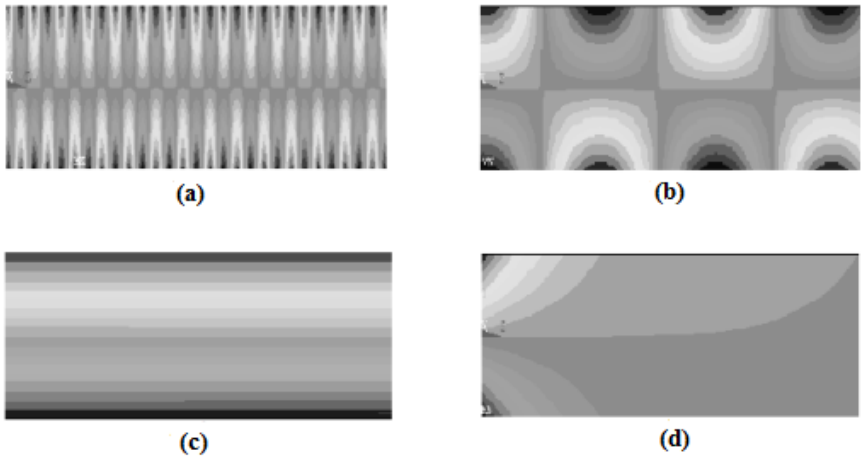

Figure 1.1. *Pressure's real part contours: Axial patterns for (a)large axial wavenumber (b)small axial wavenumber (c)zero axial wavenumber (d)imaginary axial wavenumber.*

- ***Rectangular cross-section***

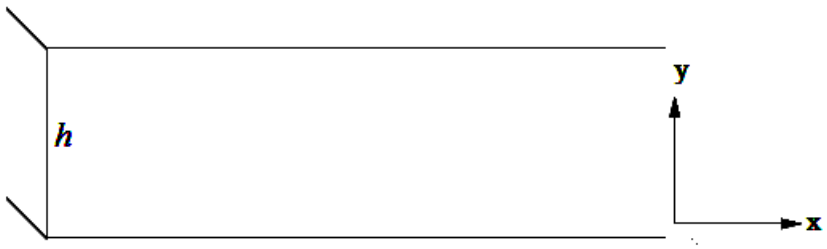

Figure 1.2. *Waveguide with a rectangular cross-section (problem set in the xy-plane).*

The resolution of the Helmholtz equation here is only detailed in 2D since resolution for the third dimension can be done by analogy to the transversal dimension. Thus, a two-dimensional problem, set in the xy-plane, where the x- (resp., y-) axis is parallel (resp., normal) to the walls of the duct is considered (Fig. 1.2). The separation of variables $p = X(x)Y(y)$ is used for the resolution of Eq. (1.5). We obtain:

$$Y(y)\frac{\mathrm{d}^2X(x)}{\mathrm{d}x^2} + X(x)\frac{\mathrm{d}^2Y(y)}{\mathrm{d}y^2} + \frac{\omega^2}{c^2}X(x)Y(y) = 0 \tag{1.15}$$

Dividing by $X(x)Y(y)$ yields to:

$$\frac{1}{X(x)}\frac{\mathrm{d}^2X(x)}{\mathrm{d}x^2} + \frac{1}{Y(y)}\frac{\mathrm{d}^2Y(y)}{\mathrm{d}y^2} + \frac{\omega^2}{c^2} = 0 \tag{1.16}$$

The first term is only dependent on x and the second term depends only on y. Hence, we can write:

$$\frac{\mathrm{d}^2X(x)}{\mathrm{d}x^2} + k_x^2X(x) = 0 \tag{1.17}$$

Solutions of $X(x)$ are:

$$X_j(x) = \mathrm{e}^{\mp \mathrm{i}k_jx} \tag{1.18}$$

k_j is the j^{th} axial wavenumber.

Solutions $Y_j(y)$ verify:

$$\frac{1}{Y_j(y)}\frac{\mathrm{d}^2Y_j(y)}{\mathrm{d}y^2} + k^2 - k_j^2 = 0 \tag{1.19}$$

where $k = \omega/c$.

From the boundary condition,

$$\frac{\partial p}{\partial y}|_{y=0} = 0 \tag{1.20}$$

we get:

$$Y_j(y) = C_1 \cos(\alpha_j y) \tag{1.21}$$

where $\alpha_j = \sqrt{k^2 - k_j^2}$ (dispersion relation). The other boundary condition at $y = h$, where h is the dimension of the duct $\mathcal{D}$ following y,:

$$\frac{\partial p}{\partial y}|_{y=h} = 0 \tag{1.22}$$

gives:

$$\begin{aligned} C_1 \sin\left(\sqrt{k^2 - k_j^2} h\right) &= 0, \\ \sqrt{k^2 - k_j^2} h &= j\pi, \\ \sqrt{k^2 - k_j^2} &= \frac{j\pi}{h} \end{aligned} \tag{1.23}$$

The coefficient C_1 can be determined by normalisation of modes $\psi_j = Y_j$.

$$\begin{aligned} &\int_0^h \psi_j \psi_j \mathrm{d}y = \int_0^h C_1^2 \cos^2\left(\frac{j\pi}{h} y\right) \mathrm{d}y = \int_0^h \frac{1}{2} C_1^2 + \frac{1}{2} C_1^2 \cos\left(\frac{2j\pi}{h} y\right) \mathrm{d}y = \\ &C_1^2 \left[\frac{1}{2} y + \frac{h}{4j\pi} \sin\left(\frac{2j\pi}{h} y\right)\right]_0^h = \frac{1}{2} h C_1^2 = 1 \end{aligned} \tag{1.24}$$

Hence, $C_1 = \sqrt{2/h}$ for $j \neq 0$ and $C_1 = \sqrt{1/h}$ for $j = 0$. Finally, expression of the pressure inside the duct is given by:

$$p_j(x, y, t) = \begin{cases} \sqrt{\dfrac{1}{h}}\, \mathrm{e}^{\mathrm{i}(\mp k x - \omega t)} & \text{if } j = 0 \\ \sqrt{\dfrac{2}{h}} \cos\left(\dfrac{j\pi}{h} y\right) \mathrm{e}^{\mathrm{i}(\mp k_j x - \omega t)} & \text{if } j \neq 0 \end{cases} \tag{1.25}$$

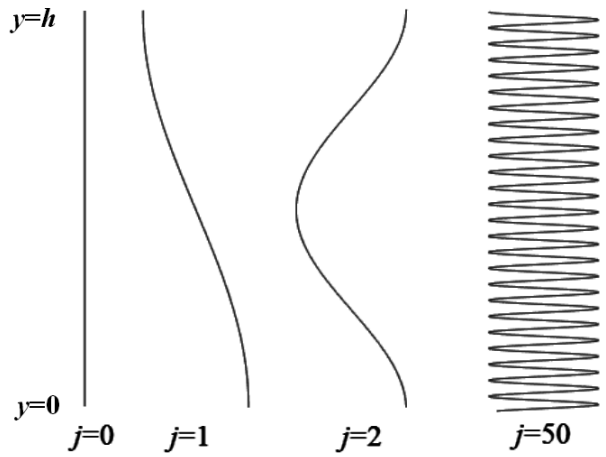

Figure 1.3. *Mode shapes in a rigid channel.*

The phase velocity is defined such as:

$$c_{ph} = \frac{w}{k_j} = \frac{c}{\sqrt{1 - \pi^2 j^2 \dfrac{c^2}{h^2\omega^2}}} \tag{1.26}$$

and the group velocity is given by:

$$c_g = \frac{\mathrm{d}\omega}{\mathrm{d}k_j} = c\sqrt{1 - \pi^2 j^2 \frac{c^2}{h^2\omega^2}} \tag{1.27}$$

The duct is now assumed to be lined at $y = h$. This leads to write:

$$\boldsymbol{\nabla}^2 p + k^2 p = 0 \quad \text{if } y \in]0, h[\tag{1.28}$$

$$\frac{\partial p}{\partial y} = 0 \quad \text{if } y = 0 \tag{1.29}$$

$$\frac{\partial p}{\partial y} = \frac{\mathrm{i}\omega\rho_0}{Z} p \quad \text{if } y = h \tag{1.30}$$

where Z is the impedance of the lined wall.

The transversal wavenumbers in this case, say β_j, must satisfy the boundary condition at $y = h$ given by (1.30). Eqs. (1.28) and (1.29) allow expressing solutions $Y_j(y)$ as $C_1 \cos(\beta_j y)$. Thus, β_j are given by:

$$-\beta_j \tan(\beta_j h) = \frac{\mathrm{i}\omega\rho_0}{Z} \tag{1.31}$$

Solutions of (1.31) can be found by the Newton–Raphson method. It is an iterative method which requires an initial guess. It is easy to see that an initial guess can not be equal to $(2j + 1)\pi/(2h)$ since the function must be differentiable at each point of the iteration. Propagation constants are then calculated by the dispersion relation [42].

- ***Circular cross-section***

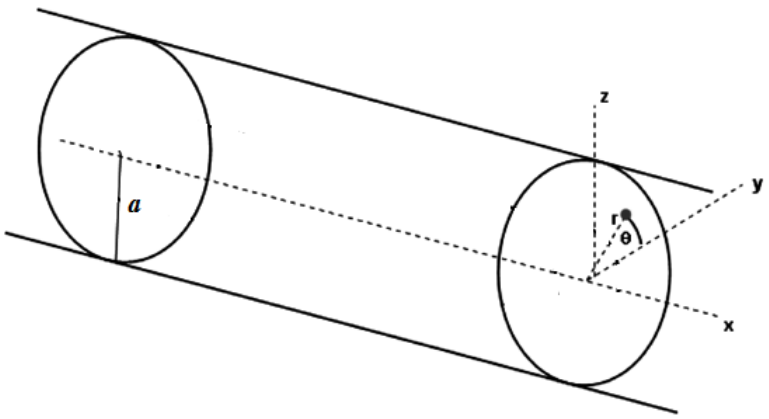

Figure 1.4. *Cylindrical duct.*

In cylindrical coordinates, the Laplacien is given by:

$$\boldsymbol{\nabla}^2 = \frac{\mathrm{d}^2}{\mathrm{d}r^2} + \frac{1}{r}\frac{\mathrm{d}}{\mathrm{d}r} + \frac{1}{r^2}\frac{\mathrm{d}^2}{\mathrm{d}\theta^2} + \frac{\mathrm{d}^2}{\mathrm{d}x^2} \tag{1.32}$$

The pressure distribution inside the duct $\mathcal{D}$ is x-, r- and θ- dependent (Fig. 1.4). Assuming a time harmonic dependence and using the separation of variables $p = X(x)R(r)\Theta(\theta)$,

Helmholtz equation (1.5) in cylindrical coordinates is:

$$X\Theta\left(\frac{\mathrm{d}^2R}{\mathrm{d}r^2}+\frac{1}{r}\frac{\mathrm{d}R}{\mathrm{d}r}\right)+XR\frac{1}{r^2}\frac{\mathrm{d}^2\Theta}{\mathrm{d}\theta^2}+R\Theta\frac{\mathrm{d}^2X}{\mathrm{d}x^2}+k^2XR\Theta=0 \tag{1.33}$$

Multiplying Eq. (1.33) by $r^2/(XR\Theta)$ gives:

$$-\frac{1}{\Theta}\frac{\mathrm{d}^2\Theta}{\mathrm{d}\theta^2}=\frac{r^2}{R}\left(\frac{\mathrm{d}^2R}{\mathrm{d}r^2}+\frac{1}{r}\frac{\mathrm{d}R}{\mathrm{d}r}\right)+r^2\left(\frac{1}{X}\frac{\mathrm{d}^2X}{\mathrm{d}x^2}+k^2\right)=m^2 \tag{1.34}$$

m is an integer and stands for the circumferential mode order.
Multiplying Eq. (1.33) by $r^2/(X\Theta)$ yields to:

$$r^2\frac{\mathrm{d}^2R}{\mathrm{d}r^2}+r\frac{\mathrm{d}R}{\mathrm{d}r}+\left(\left(\frac{1}{X}\frac{\mathrm{d}^2X}{\mathrm{d}x^2}+k^2\right)r^2-m^2\right)R=0 \tag{1.35}$$

Physical solutions of R are the Bessel functions of first kind. For each circumferential order m, the transversal wavenumbers α_{mi} must satisfy the boundary condition:

$$J_m^{'}(\alpha_{mi}a)=0 \tag{1.36}$$

where a is the radius of the duct $\mathcal{D}$, and $J_m^{'}$ denotes the derivative of the m^{th} order Bessel function of first kind.

$$\alpha_{mi}=\frac{\chi_{mi}}{a} \tag{1.37}$$

where χ_{mi} is the i^{th} root of $J_m^{'}$.
The associated solutions of Helmholtz equation $J_m(\alpha_{mi}r)\mathrm{e}^{\mathrm{i}(\mp k_{mi}x-m\theta-\omega t)}$ are the duct modes. The solution of Helmholtz equation (1.5) can be written as following:

$$p(x,r,\theta,t)=\sum_{m=-\infty}^{+\infty}\sum_{i=0}^{+\infty}A_{mi}\mathrm{e}^{\mathrm{i}(\pm k_{mi}x)}J_m(\chi_{mi}r/a)\mathrm{e}^{\mathrm{i}(-m\theta-\omega t)} \tag{1.38}$$

Only the plane wave mode propagates for frequencies below the cut-off frequency of the first higher order mode:

$$f < 1.84\frac{c}{2\pi a} \tag{1.39}$$

Pressure is constant in every cross-sectional area of the duct for these frequencies. Above the cut-off frequency given by (1.39) , the pressure distribution in a given section of the duct will not be uniform [43]. Generally, a mode is propagative or evanescent (exponentially decaying) depending on the frequency being higher or lower than the cut-off frequency. Cut-off frequencies of higher order modes are calculated in a similar way as Eq. (1.39) replacing coefficient 1.84 by the corresponding Bessel function derivative's zero.

i \ m	0	1	2	3	4	5
0	0	1.8412	3.0542	4.2012	5.3176	6.4156
1	3.8317	5.3314	6.7061	8.0152	9.2824	10.5199
2	7.0156	8.5363	9.9695	11.3459	12.6819	13.9872
3	10.1735	11.7060	13.1704	14.5858	15.9641	17.3128
4	13.3237	14.8636	16.3475	17.7888	19.1960	20.5755

Table 1.1. *Zeros of* J'_m.

Modes with a circumferential order $m = 0$ are called symmetric (No dependency on θ). For these modes, the acoustic field is symmetric over the axis of revolution.

When the wall of the duct is lined, for each circumferential order m, the transversal wavenumbers β_{mi} are determined such as the boundary condition at $r = a$ is satisfied [44]

$$\frac{J_m(\beta_{mi}a)}{\beta_{mi}J'_m(\beta_{mi}a)} = \frac{\mathrm{i}Z}{\rho_0\omega} \tag{1.40}$$

where ρ_0 is the density of the fluid and Z is the wall impedance.

For a hard boundary condition ($Z = \infty$), $\beta_{mi} = \alpha_{mi}$ (Eq. (1.36)). For a soft boundary condition ($Z = 0$), β_{mi} are simply given by the zeros of the Bessel function.

- ***Annular duct***

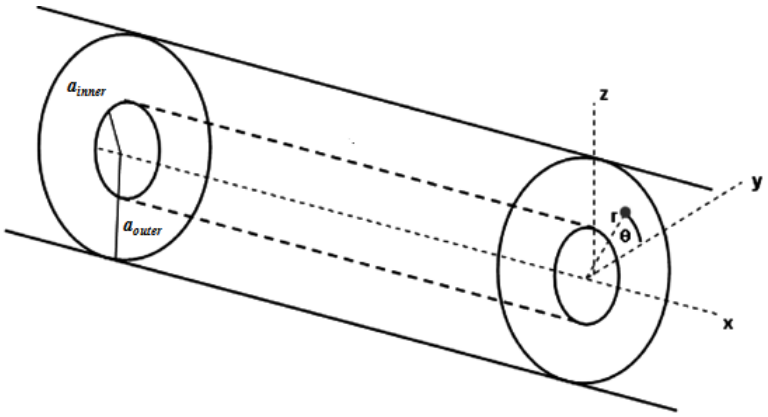

Figure 1.5. *Annular duct.*

For an annular duct, angular and axial dependencies are determined similarly as for a circular duct section. However, while R is only dependent on Bessel function of first kind for a cylindrical duct, R is given for an annular duct as:

$$R(r) = A_{mi} J_m(\alpha_{mi} r) + B_{mi} \mathcal{Y}_m(\alpha_{mi} r) \tag{1.41}$$

where J_m and $\mathcal{Y}_m$ are the m^{th} order Bessel functions of first kind and second kind respectively [45]. For a cylindrical duct, B_{mi} are necessarily zeros as $\mathcal{Y}_m$diverge at $r = 0$. A_{mi} and B_{mi} are given by the boundary conditions, and for a rigid duct are of the form:

$$A_{mi} = \cos(\tau_{mi}) \tag{1.42}$$

$$B_{mi} = \sin(\tau_{mi}) \tag{1.43}$$

with

$$\tau_{mi} = \arctan\left(-\frac{J'_m(\alpha_{mi} a_{outer})}{\mathcal{Y}'_m(\alpha_{mi} a_{outer})}\right) \tag{1.44}$$

where a_{outer} is the outer radius of the duct (Fig. 1.5).

1.3 Passive noise reduction

Reduction of sound levels of aircraft engines has been one of the important engineering challenges. Sources of noise are multiple: fan, turbine, compressor and jet noise (Fig. 1.6).

Sound propagation in a duct of large transversal dimensions induces the presence of many propagating high modes, and their superposition is the origin of the complexity of noise in the aircraft engines. Lining at the wall of the nacelle is used to attenuate the noise. It consists of SDOF and DDOF thin resistive sheets and honeycombs [2] (Fig. 1.7). In a turbojet nacelle, acoustic treatments are submitted to high acoustic pressure levels (up to 160 dB) and important flows (Mach numbers up to 0.6) [46]. The lined waveguide can be characterised by its scattering matrix.

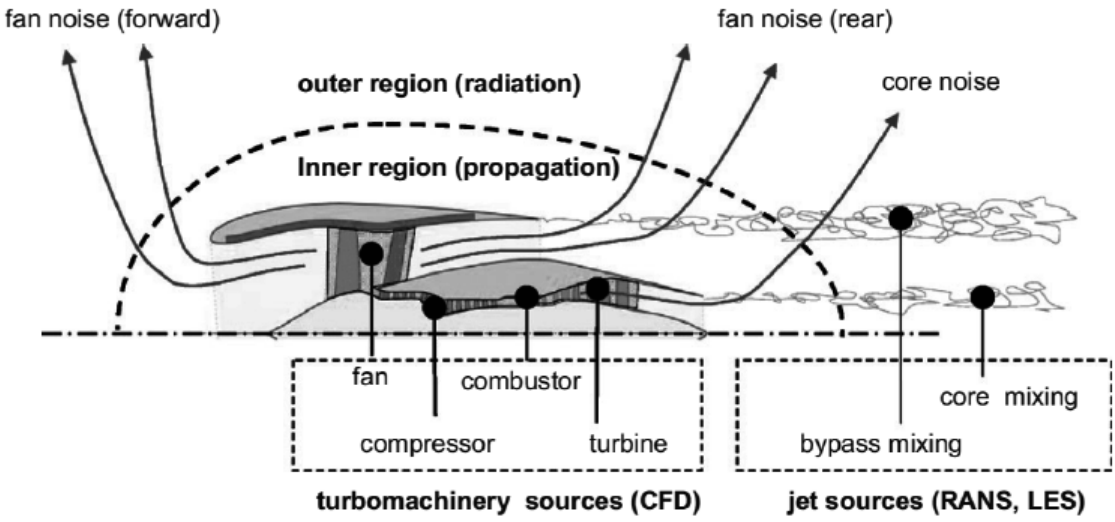

Figure 1.6. *Illustration of aircraft engine's principal sources of noises [1].*

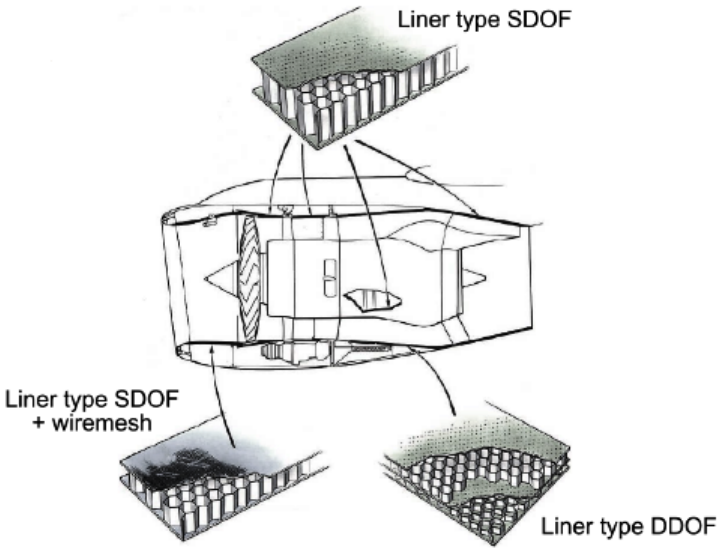

Figure 1.7. *Types of liners used in an aircraft engine [2].*

1.4 Scattering matrix definition

Absorbing materials are represented by their acoustic impedance. A homogenised impedance which represents the whole material is used. Scattering due to impedance discontinuities of lined parts will be studied (See Fig. 1.8).

The scattering matrix is a $(2n \times 2n)$ matrix such as it relates the $2n$ reflected (output) modal pressure amplitudes at the left and right sides of a duct element $\mathbf{Q}_{wg_1}^{ref}$ and $\mathbf{Q}_{wg_2}^{ref}$ to the $2n$ incident (input) modal pressure amplitudes at the left and right sides $\mathbf{Q}_{wg_1}^{inc}$ and $\mathbf{Q}_{wg_2}^{inc}$.

$$\begin{pmatrix} \mathbf{Q}_{wg_1}^{ref} \\ \mathbf{Q}_{wg_2}^{ref} \end{pmatrix} = \mathbf{C} \begin{pmatrix} \mathbf{Q}_{wg_1}^{inc} \\ \mathbf{Q}_{wg_2}^{inc} \end{pmatrix} \tag{1.45}$$

where square blocks of $\mathbf{C}$ are such as $\mathbf{C} = \begin{pmatrix} \mathbf{C}_{11} & \mathbf{C}_{12} \\ \mathbf{C}_{21} & \mathbf{C}_{22} \end{pmatrix}$

- $\mathbf{C}_{11}$ corresponds to reflection of the waves entering the element from the left side
- $\mathbf{C}_{21}$ corresponds to transmission of the waves entering the element from the left side
- $\mathbf{C}_{12}$ corresponds to transmission of the waves entering the element from the right side
- $\mathbf{C}_{22}$ corresponds to reflection of the waves entering the element from the right side

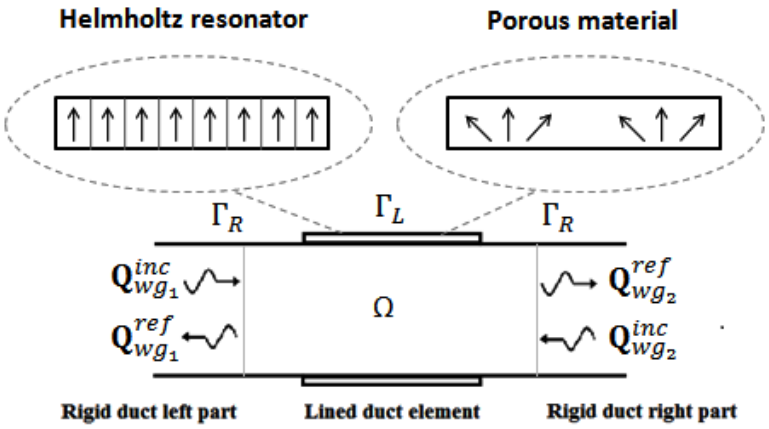

Figure 1.8. *Illustration of an acoustical scattering problem and description of wave propagation behaviours due to lining on the duct's walls (to be studied later on in the manuscript).*

It is worth noting that a same square block may stand for a transmission or reflection matrix depending on how the vectors of modal pressure amplitudes were arranged. Several works aimed to compute the multi-modal scattering matrix. Others dealt with some experimental facilities to measure it. These methods are summarised hereafter.

1.5 Review of the theoretical methods of the scattering matrix calculation

1.5.1 Analytical Method (MMPM)

Bi *et al.* [12, 17] presented an analytical technique to calculate the scattering matrix. The proposed method was called "**M**ulti-**M**odal **P**ropagation **M**ethod" (MMPM), and applied to

cylindrical ducts. Here is the principle of the method. The Euler and continuity equations are projected over the eigenfunctions of rigid duct. As a result of the local impedance boundary condition, a second order differential equation of the form $\mathbf{P}'' + \mathbf{AP} = \mathbf{0}$ relating the vector $\mathbf{P}$ composed by the pressure projections over these eigenfunctions and its second derivative (with respect to the spatial coordinate) is then written. The matrix $\mathbf{A}$ is the sum of two terms: the first diagonal term comes from using the rigid duct basis functions. Rigid duct modes do not obey the wall boundary conditions, and so a second coupling term $\mathbf{\Gamma}$, which can be considered as the expression of scattering effects due to the liner, is added.

$$\mathbf{A} = (K^2\mathbf{I} - \mathbf{L}^2) + \mathbf{\Gamma} \tag{1.46}$$

with K is the dimensionless wavenumber, $\mathbf{I}$ is the identity matrix, $\mathbf{L}$ is a diagonal matrix with the transversal wavenumbers α_j on the diagonal, and coefficients of the matrix $\mathbf{\Gamma}$, which represent the coupling between modes (m, i) and (m', i'), are given by:

$$\Gamma_{mi,m'i'} = \frac{-1}{\pi\sqrt{\left(1 - \dfrac{m^2}{\alpha_{mi}^2}\right)\left(1 - \dfrac{m'^2}{\alpha_{m'i'}^2}\right)}} \int_0^{2\pi} \frac{\mathrm{i}K}{\bar{Z}}\, \mathrm{e}^{-\mathrm{i}\left(m'-m\right)\theta}\, \mathrm{d}\theta \tag{1.47}$$

where m and i are the circumferential and radial mode orders respectively, and $\bar{Z}$ is the complex conjugate of the normalised impedance of the liner. It is easy to see from Eq. (1.47) that only modes with same circumferential orders are coupled. Eigenvalues square roots of matrix $\mathbf{A}$ are the axial wavenumbers inside the lined duct part. The continuity conditions at interfaces rigid-lined parts are then applied. A subsequent procedure for the calculation of the scattering matrix is detailed in [12]. The scattering matrix blocs are then given in terms of the eigenvalues and eigenvectors of matrix $\mathbf{A}$ with truncation at a sufficient number of modes. For further details, the reader may refer to [17, 12]. The scattering of a segmented liner can be calculated using a cascade of scatterers as in [47]. The convergence of the method was discussed in [12, 18]. This method is used later on in this thesis to validate results of the WFE method. However, for arbitrary cross-sections, analytical solutions are not obvious.

Therefore, Finite Element based methods are alternatively used.

1.5.2 Finite Element Method (FEM)

Taktak *et al.* [13] used a Finite Element method to compute the scattering matrix. The studied duct element does not represent a change in the cross section, but in the wall impedance. Moreover, the duct is assumed to be cylindrical and the impedance of the liner is locally reacting. The weak variational formulation is written:

$$\Pi = -\int_{\Omega} \boldsymbol{\nabla} q \boldsymbol{\nabla} p \mathrm{d}v + k^2 \int_{\Omega} qp \mathrm{d}v + \int_{\cup \Gamma_i} q \frac{\partial p}{\partial n_i} \mathrm{d}S = 0 \tag{1.48}$$

Ω denotes the acoustic domain inside the duct element. Γ_i are the boundaries of the duct element, $\mathbf{n}_i$ are the outward normal to Γ_i, p is the acoustic pressure, q is a test function and k is the wavenumber. Later on , in chapter 4, the convected formulation of the problem will be used to calculate the mass, stiffness and damping matrices.

The acoustic pressure in the duct is the solution of the system composed of Helmholtz equation and boundary conditions of the rigid and the lined parts:

$$\begin{cases} \boldsymbol{\nabla}^2 p + k^2 p = 0 \text{ in } \Omega & (1.49) \\ \dfrac{\partial p}{\partial n_R} = 0 \text{ on } \Gamma_R & (1.50) \\ Z \dfrac{\partial p}{\partial n_L} = \mathrm{i}\omega\rho_0 p \text{ on } \Gamma_L & (1.51) \end{cases}$$

where k is the free field wavenumber, $\mathbf{n}_R$ and $\mathbf{n}_L$ are the outward normals to the rigid and lined parts respectively, Z is the impedance of the liner, ρ_0 is the density of the fluid, ω is the angular frequency and i is the complex number such as $\mathrm{i}^2 = -1$.

The third integral term of the weak variational formulation is calculated per circumferential order and for each boundary. Solution of Eq. (1.49) is used for the left and right edges of the duct element. Eq. (1.50) and Eq. (1.51) are used for the rigid and lined boundaries respectively. The domain Ω is meshed with finite elements, and the Eq. (1.48) leads finally

to a system of the following form:

$$\begin{cases} \mathbf{H}_1\mathbf{p} + \mathbf{H}_2 \begin{pmatrix} \mathbf{Q}_{wg_1}^{inc} \\ \mathbf{Q}_{wg_2}^{inc} \end{pmatrix} + \mathbf{H}_3 \begin{pmatrix} \mathbf{Q}_{wg_1}^{ref} \\ \mathbf{Q}_{wg_2}^{ref} \end{pmatrix} = \mathbf{0} \\ \mathbf{H}_4\mathbf{p} + \mathbf{H}_5 \begin{pmatrix} \mathbf{Q}_{wg_1}^{inc} \\ \mathbf{Q}_{wg_2}^{inc} \end{pmatrix} + \mathbf{H}_6 \begin{pmatrix} \mathbf{Q}_{wg_1}^{ref} \\ \mathbf{Q}_{wg_2}^{ref} \end{pmatrix} = \mathbf{0} \end{cases} \tag{1.52}$$

where $\mathbf{p}$ is the vector of nodal pressures.

The system is then rearranged in order to express the relation between left running and right running modal pressures on the left and right boundaries of the duct element. A loop along with the circumferential orders must be then performed to have the total scattering matrix.

1.5.3 Boundary Element Method (BEM)

An integral equation can be derived from the Helmholtz equation by applying the Green's theorem. The integral equation is of the form [48, 49]:

$$\int_S \frac{\partial G}{\partial n}(\mathcal{P}, \mathcal{Q}) p(\mathcal{Q}) \mathrm{d}S + \frac{1}{2} p(\mathcal{Q}) = \int_S G(\mathcal{P}, \mathcal{Q}) \frac{\partial p}{\partial n} \mathrm{d}S \tag{1.53}$$

The function G is a Green's function. Physically, $G(\mathcal{P}, \mathcal{Q})$ represents the effect observed at a point $\mathcal{P}$ of a unit source at the point $\mathcal{Q}$. $\dfrac{\partial}{\partial n}$ represents the partial derivative with respect to the unit outward normal at the point $\mathcal{Q}$ on the boundary. G is defined as follows:

$$\begin{aligned} G(\mathcal{P}, \mathcal{Q}) &= \frac{\mathrm{i}}{4} H_0^{(1)}(kr) \quad \text{in two dimensions} \\ G(\mathcal{P}, \mathcal{Q}) &= \frac{1}{4\pi} \frac{\mathrm{e}^{\mathrm{i}kr}}{r} \qquad \text{in three dimensions} \end{aligned} \tag{1.54}$$

where $r = |\mathrm{r}|$, $\mathrm{r} = \mathcal{Q} - \mathcal{P}$. The function $H_0^{(1)}$ is the spherical Hankel function of the first kind of order zero.

Figure 1.9. *Illustration of modelling by the FEM and BEM approaches [3].*

The main advantage of the BEM is that only the boundary has to be modelled in order to obtain a solution. Unlike the FEM, no discretisation of the interior region is required (Fig. 1.9). However, the method is still limited to low frequencies applications.

1.5.4 Spectral Finite Element Method (SFEM)

The Spectral Finite Element Method is based on a variational formulation for non-conservative motion in the frequency domain [50]. The studied duct region is decomposed into rectangular elements. Acoustic propagation through the inhomogeneous waveguide $\Omega = \bigcup \Omega_i$ with various geometries, linings, and fluid properties can be investigated (Fig. 1.10).

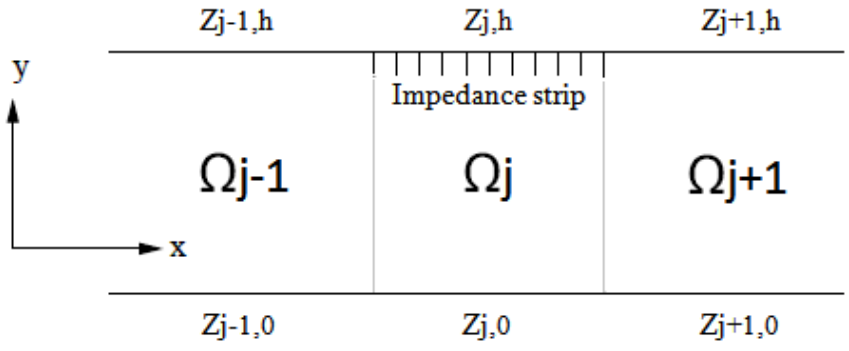

Figure 1.10. *Schematic of the computation regions inside the duct.*

The weak variational formulation is given by:

$$\mathcal{L}_\Omega(p,\bar{p}) = \int_\Omega \left(\frac{1}{\rho\omega^2} k^2 p\bar{p} - \frac{1}{\rho\omega^2} \nabla p \nabla \bar{p} \right) \mathrm{d}v + \int_\Gamma \frac{1}{\rho\omega^2} \frac{\mathrm{i}k}{Z} p\bar{p} \mathrm{d}S \tag{1.55}$$

$\bar{p}$ denotes the conjugate of the sound pressure p in the adjoint system. Z is the normalised impedance defined at Γ.

The approximate solution p may be represented by the expression:

$$p = \mathbf{N}^t(y)\mathbf{W}(x) \tag{1.56}$$

where N_i are polynomial shape functions ($\mathbf{N}$ is the vector of shape functions) and W_i are the spectral wave functions.

Integration of the variational form is performed by region.

$$\mathcal{L}_{\Omega_j} = \int (\bar{\mathbf{W}}_j)^t \mathbf{K}_1 \mathbf{W}_j \mathrm{d}x - \int (\bar{\mathbf{W}}_j)^t \mathbf{K}_2 \mathbf{W}_j \mathrm{d}x + \int (\bar{\mathbf{W}}_j)^t \mathbf{K}_3 \mathbf{W}_j \mathrm{d}x - \int \left(\frac{\mathrm{d}\bar{\mathbf{W}}_j}{\mathrm{d}x} \right)^t \mathbf{K}_4 \frac{\mathrm{d}\mathbf{W}_j}{\mathrm{d}x} \mathrm{d}x \tag{1.57}$$

with submatrices

$$\mathbf{K}_1 = \frac{k^2}{\rho\omega^2} \int \mathbf{N}\mathbf{N}^t \mathrm{d}y \tag{1.58}$$

$$\mathbf{K}_2 = \frac{1}{\rho\omega^2} \int \frac{\mathrm{d}\mathbf{N}}{\mathrm{d}y} \left(\frac{\mathrm{d}\mathbf{N}}{\mathrm{d}y} \right)^t \mathrm{d}y \tag{1.59}$$

$$\mathbf{K}_4 = \frac{1}{\rho\omega^2} \int \mathbf{N}\mathbf{N}^t \mathrm{d}y \tag{1.60}$$

and for a $(q,r)^{\text{th}}$ element,

$$K_3^{q,r} = \frac{\mathrm{i}k}{Z_{j,h}} \frac{1}{\rho\omega^2} \delta_{qn_e} \delta_{rn_e} + \frac{\mathrm{i}k}{Z_{j,0}} \frac{1}{\rho\omega^2} \delta_{q1} \delta_{r1} \tag{1.61}$$

$Z_{j,0}$ and $Z_{j,h}$ are the normalised impedances defined at lower ($y = 0$) and upper ($y = h$) boundaries of the j^{th} region respectively. δ is the Kronecker index. n_e is the polynomial interpolation order. The final forms of the matrices $\mathbf{K}_1$,..,$\mathbf{K}_4$ are constructed by a combination

of their submatrices.

Letting

$$\mathbf{K}_0 = \mathbf{K}_1 - \mathbf{K}_2 + \mathbf{K}_3 \tag{1.62}$$

a system of $(n_e \times n_e)$ second order ordinary differential equations for $W_i(x)$ follows:

$$\mathbf{K}_4 \frac{\mathrm{d}^2\mathbf{W}}{\mathrm{d}x^2} + \mathbf{K}_0\mathbf{W} = 0 \tag{1.63}$$

Solutions are expressed as follows:

$$\mathbf{W} = C\mathbf{\Phi}\mathrm{e}^{-\mathrm{i}\mu x} \tag{1.64}$$

where $\mathbf{\Phi}$ is a vector representing the nodal and interior amplitudes, C is a constant and eigenvalues μ come in pairs of eigenmodes with the same phase speed propagating in the positive and negative axial directions. The dimension of the eigenvalue problem is $(n_e \times n_e)$ and a finite $2n_e$ number of eigenvalues are obtained. Within each region the pressure is given by the combination of polynomials and wave functions as in Eq. (1.56).

1.6 Review of the experimental methods of the scattering matrix calculation

Several experiments have been carried out to predict the scattering matrix [22, 4, 51, 52, 53]. Fig. 1.11 shows the experimental set up at the University of Technology of Compiegne.
The equipment is composed by a source, two measurement duct elements, a test duct element and an anechoic termination. The experimental process, as presented by Sitel *et al.*, is as follows [22]: Considering n cut-on modes, the $2n$ scattering matrix coefficients are obtained after repeating the experiment for n linearly independent pressure distributions for at least two load configurations. The frequency spectra of the total modal coefficients in two closed cross sections located in both measurement duct elements are collected, and the incident and reflected modal pressure vectors are separated for each load and source configuration. Then, the incident and reflected modal pressure vectors on both sides of the test duct element for the n source configurations and two or several loads are post processed. The scattering

matrix is finally computed.

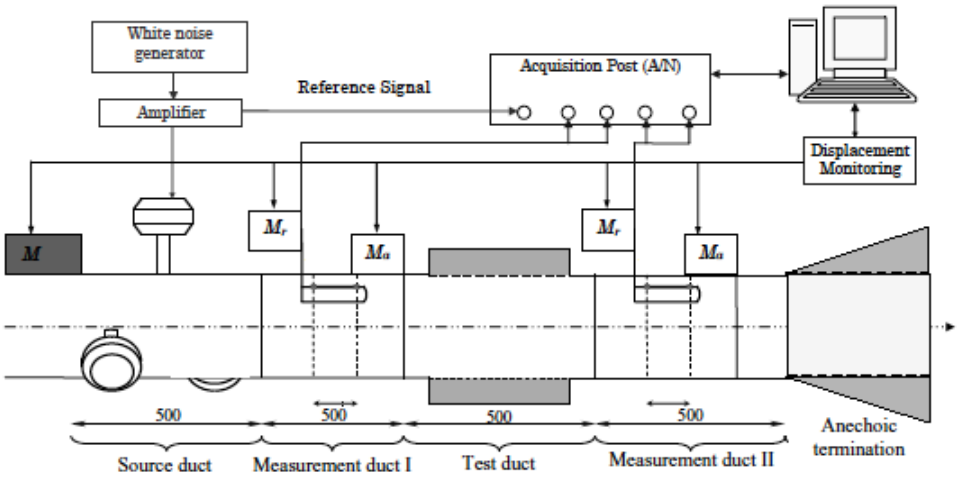

Figure 1.11. *Experimental set up of the scattering matrix measurement [4].*

Similar experiments were performed at University of Maine for a rectangular cross section configuration in presence of flow [5]. The experiment aimed to measure the wall impedance by an inverse method through the calculation of the scattering matrix.

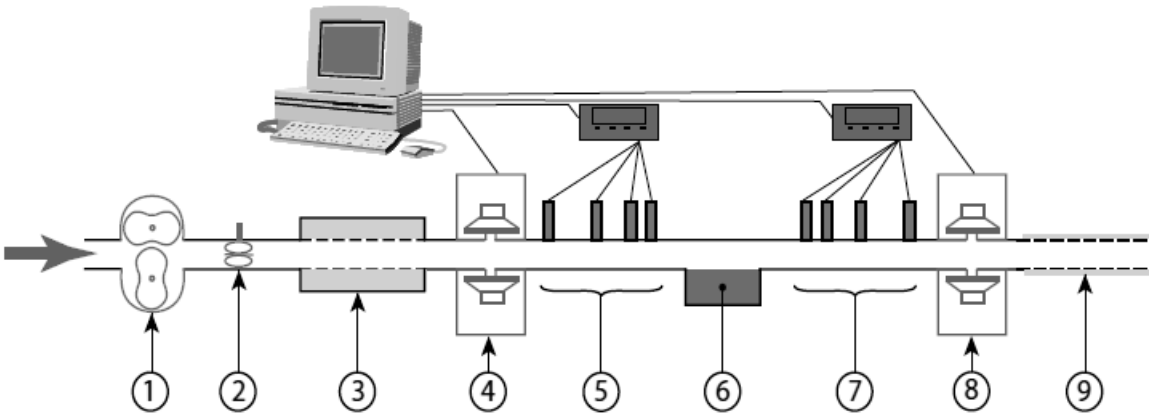

Figure 1.12. *Schematic description of the experimental set-up. 1: Compressor, 2: Flowmeter, 3: Upstream anechoic termination, 4: Upstream source , 5: upstream microphones, 6: Lined wall, 7: downstream microphones, 8: Downstream source, 9: Downstream anechoic termination [5].*

The set-up includes a compressor generating the air flow, downstream and upstream acoustic sources made of loudspeakers, and two anechoic terminations (See Fig. 1.12). Two measurements are made in two different states of the system: switching on the upstream source, the downstream source being switched off (first measurement), and then by switching on the downstream source, the upstream source being switched off (second measurement).

Some other experiments dealt with the eduction of liners impedance. Eduction technique matches between numerical simulations and acoustic measurements. Fig. 1.13 shows the Aero-Thermo-Acoustic test bench of the French Aerospace Laboratory ONERA.

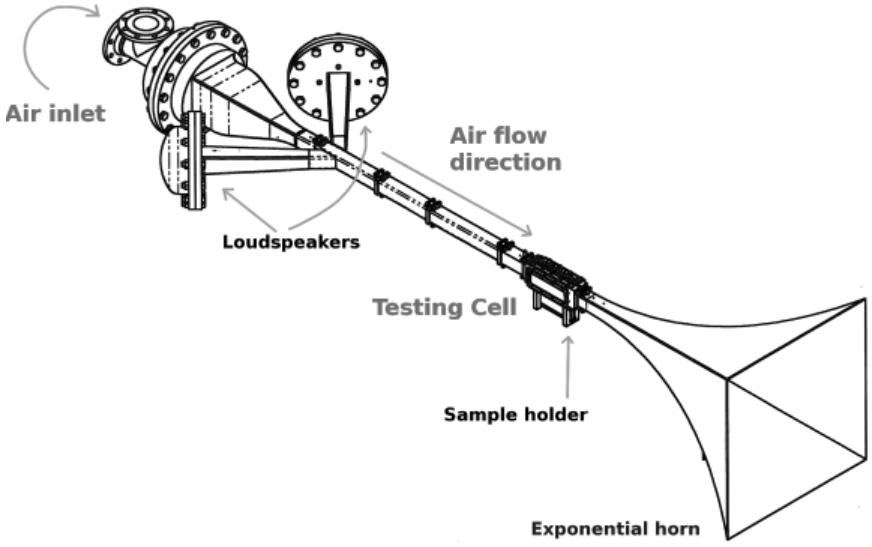

Figure 1.13. *ONERA's Aero-Thermo-Acoustic test bench in grazing configuration [6].*

ONERA's impedance eduction method is based on acoustic Laser Doppler Anemometry (LDA) measurements and Discontinuous Galerkin (DG) simulations. Excitation is provided by two loudspeakers installed in pressurised cabinets. Upstream of the test section, two microphone probes are flush-mounted, which allow the measurement of the incident acoustic plane waves amplitude. A Laser Doppler Velocimeter allows the measurement of the velocity components. The equipment is ended by an anechoic outlet.

1.7 An introduction to the Wave Finite Element Method (WFEM)

The Wave Finite Element approach has recently attracted many researchers for the study of wave propagation either in one dimensional (Fig. 1.14) or two dimensional (Fig. 1.15) periodic structures. The method combines a Finite Element elementary modelling and relations provided by the periodicity condition.

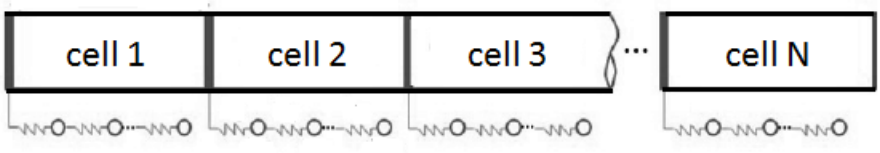

Figure 1.14. *Illustration of cells decomposition for the 1D WFE method.*

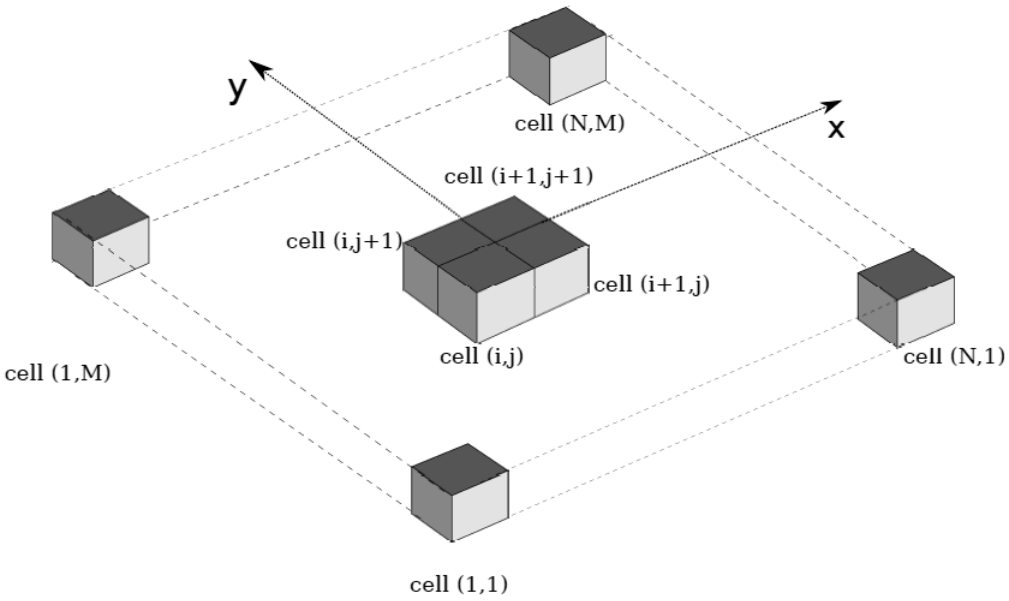

Figure 1.15. *Illustration of cells decomposition for the 2D WFE method [7].*

The principle of the method is as following: The periodic waveguide is divided into similar cells following the direction of propagation. Once the eigensolutions are extracted for the waveguide section, the state vectors can be determined for the whole waveguide using these repeating cells and avoiding the costly approach of meshing the entire waveguide. A unit cell is meshed using commercial FE packages and internal nodes are condensed onto the cell's edges. The Bloch theorem is applied to the cells composing the periodic waveguides. A propagation constant μ, representing the change in the amplitude and the phase in the propagation directions, relates the displacements on the cell edges, (eventually the cell corners for 2D periodic structures [7, 54]).

$$\mathbf{q}_r = \mu\ \mathbf{q}_l \tag{1.65}$$

where $\mathbf{q}$ is the vector of displacements, and subscripts l and r stand for the left and right edges of a cell.
The equilibrium of forces at the cell's scale is also expressed as follows [55]:

$$\mu\mathbf{f}_l + \mathbf{f}_r = \mathbf{0} \tag{1.66}$$

where $\mathbf{f}$ is the vector of forces.

Finally, the method leads to an eigenvalue problem. Wavenumbers can be then calculated through eigenvalues. If the waveguide is undamped, then the wavenumber is purely real or purely imaginary, associated with a propagating or an evanescent wave respectively. If there is damping, then the wavenumber is complex and the wave is an oscillating decaying wave. Wave mode shapes are given by the eigenvectors. The method can be further applied to identify the forced response regarding the boundary conditions.

The WFE method has been widely used in previous works for studying the wave propagation in structures. It has been used for beam-like structures [56], laminates [57], fluid-filled pipes [58, 59], tyres [60], rails [61], poroelastic media [62, 63] and damaged structures for damage detection and sizing purposes [64, 65]. The method was not only applied to straight waveguides but to curved ones also [64].

Numerical instabilities may arise when it comes to solve the so-called eigenproblem. Deal-

ing with matrices singularities and choices of mesh density and cells length are important to ensure a satisfying convergence of the method. Some authors proposed better conditioned forms to the eigenvalue problem [66] so that numerical problems are avoided particularly when the cross-section's mesh involves a large number of degrees of freedom. Some authors have later proposed significant improvements to the method allowing a reduction of the computational cost [67, 68, 69]. Thus, the use of the method seems to be particularly interesting as it represents an efficient alternative to the conventional FE method, regarding its applicability to the mid and high frequencies ranges.

1.8 Bibliographic synthesis

Several methods dealing with duct acoustics have been presented in this chapter. Comparison between methods is summarised in the following table:

Method	**Application to duct acoustics**	**Advantages**	**Limits**
MMPM	[12] Scattering matrix	Exact solutions	Restricted to simple geometries
FEM	[13] Scattering matrix	Possible extension to the complex geometries modelling	Time consuming for high frequencies ranges
BEM	[32] Transfer matrix	Only boundary of the domain needs to be discretised	Time consuming for high frequencies ranges
SFEM	[50] Acoustic fields inside ducts with impedance and geometry non-uniformities	Possible extension to modelling of ducts with irregular regions[50]	-Requiring higher order polynomial interpolation -Numerical issues
WFEM		Lower computational time	Numerical issues (Solutions to be provided later on in the manuscript)

Table 1.2. *A summary on duct acoustics methods.*

1.9 Conclusion

The scattering matrix is an intrinsic characterisation of a waveguide element which does not depend on the upstream and downstream conditions. It is only dependent on the acoustic and geometric properties of the characterised element and provides a complete description of the modal reflection, transmission and modes conversion.

This chapter has also led to a comparison of various methods dealing with the study of the guided acoustical propagation and scattering of acoustic waves. It has been shown that the use of the Wave Finite Element Method is mostly advantageous compared to methods used in literature as it uses an elementary FE modelling and allows an efficient study for the mid and high frequencies ranges. Nonetheless, it is noted that the method could be prone to numerical issues and therefore some scaling strategies are yet to be proposed to avoid erroneous results. The WFE formulation will be presented in details within the next chapter and will be later applied to the acoustical guided propagation.

Chapter 2

Wave Finite Element Method: Theoretical background and numerical validations

2.1 Introduction

Studying the free and forced wave propagation using purely analytical methods might be arduous for complex geometries. For such geometries, a Finite Element modelling is recommended. However, full modelling by the conventional Finite Element method could be costly particularly when the model size is important. Analysis for the high frequencies ranges requires a refined mesh and makes the use of the full model even more inappropriate. The Wave Finite Element method represents an efficient alternative for periodic waveguides as commercial packages can be exploited for a reduced FE modelling, and an analytical extension of periodicity relations follows.

In this chapter, the formulation of the Wave Finite Element method is introduced. Theoretical notes are given: the scattering matrix and forced response computation techniques are presented. Then, some examples of simple cases are considered for validation at the end of the chapter. The proposed approach results are verified by comparison with either analytical or Finite Element methods, and the main advantages of the approach are reviewed.

2.2 The Wave Finite Element approach

2.2.1 Assumptions

The different properties of waves propagating in periodic waveguides can be given by the WFE approach. A waveguide is supposed to be made of similar segments which are modelled using same FE models and are connected along a main axis, called direction of propagation (See Fig. 2.1). Δ is the length of each one. It is assumed that the wall impedance is infinite inside the waveguide, which corresponds to a rigid wall, and that either there are no internal degrees of freedom or internal degrees of freedom have been already condensed onto the left and right edges of each segment. The meshing compatibility of coupling interfaces provides identical nodal distribution in the left and right faces. i.e. Each face is supposed to have the same degree of freedom, noted n.

2.2.2 Eigenvalue problem formulation

First, the relation between velocities and pressures of one waveguide segment has to be expressed:

$$\begin{pmatrix} \mathbf{v}_l \\ \mathbf{v}_r \end{pmatrix} = \begin{pmatrix} \mathbf{D}_{ll} & \mathbf{D}_{lr} \\ \mathbf{D}_{rl} & \mathbf{D}_{rr} \end{pmatrix} \begin{pmatrix} \mathbf{p}_l \\ \mathbf{p}_r \end{pmatrix} \tag{2.1}$$

where $\mathbf{p}$ and $\mathbf{v}$ are respectively the pressures and particles velocities vectors.
The subscripts l and r respectively refer to as the left and right edges of the segment.
$\mathbf{D}$ is given by $\mathbf{D} = -\omega^2\mathbf{M} + \mathbf{K}$ where $\mathbf{M}$ and $\mathbf{K}$ are respectively the mass and stiffness matrices of the waveguide segment, and ω is the angular frequency.

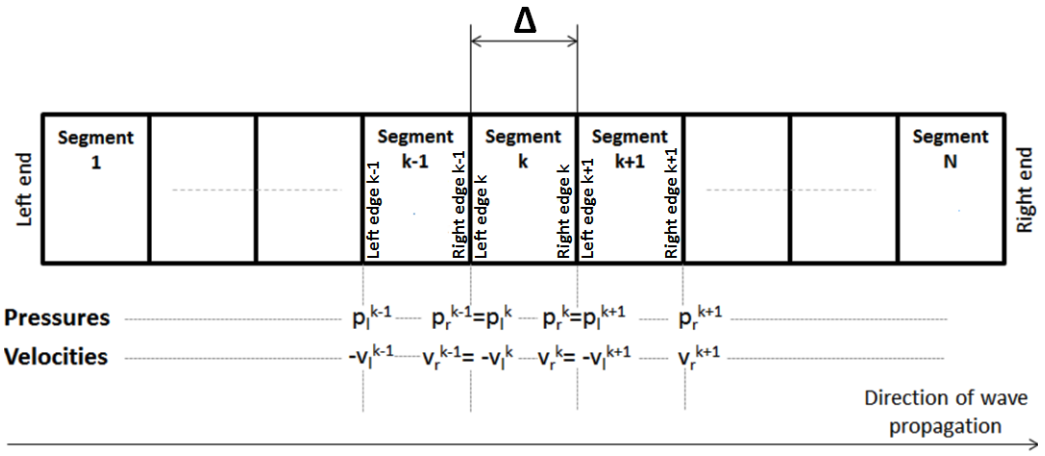

Figure 2.1. *Illustration of a periodic waveguide.*

Using the Zhong and Williams theory [70], Eq. (2.1) may be reformulated in terms of state vectors as (See Appendix A):

$$\mathbf{u}_r = \mathbf{S}\mathbf{u}_l \tag{2.2}$$

where $\mathbf{S}$ is a $(2n \times 2n)$ symplectic matrix verifying:

$$\mathbf{J}_n = \mathbf{S}^t \mathbf{J}_n \mathbf{S} \tag{2.3}$$

and $\mathbf{J}_n = \begin{pmatrix} \mathbf{0} & \mathbf{I}_n \\ -\mathbf{I}_n & \mathbf{0} \end{pmatrix}$; $\mathbf{u}_l^t = [(\mathbf{p}_l)^t(-\mathbf{v}_l)^t]$ and $\mathbf{u}_r^t = [(\mathbf{p}_r)^t(\mathbf{v}_r)^t]$. t denotes the matrix transpose.

The matrix $\mathbf{S}$ is expressed as [71]:

$$\mathbf{S} = \begin{pmatrix} -\mathbf{D}_{lr}^{-1}\mathbf{D}_{ll} & -\mathbf{D}_{lr}^{-1} \\ \mathbf{D}_{rl} - \mathbf{D}_{rr}\mathbf{D}_{lr}^{-1}\mathbf{D}_{ll} & -\mathbf{D}_{rr}\mathbf{D}_{lr}^{-1} \end{pmatrix} \tag{2.4}$$

Considering the coupling conditions between two successive waveguide segments k and $k+1$, $\mathbf{u}_l^{(k+1)} = \mathbf{u}_r^{(k)}$ in Eq. (2.2) leads to:

$$\mathbf{u}_l^{(k+1)} = \mathbf{S}\mathbf{u}_l^{(k)} \tag{2.5}$$

Using Bloch's theorem [72], the solutions of Eq. (2.5) can be expressed as:

$$\mathbf{u}_l^{(k+1)} = \mu \mathbf{u}_l^{(k)} \tag{2.6}$$

These solutions are $(\mu_j, \mathbf{\Phi}_j)$ and represent the wave modes propagating along the whole waveguide. They are numerically calculated by means of the following eigenvalue problem:

$$\mathbf{S}\mathbf{\Phi}_j = \mu_j \mathbf{\Phi}_j \tag{2.7}$$

$$det(\mathbf{S} - \mu \mathbf{I}_{2n}) = 0 \tag{2.8}$$

For a particular mode j, $\mu_j = \exp(-\mathrm{i}k_j\Delta)$ where k_j is the axial wavenumber, while the vector $\mathbf{\Phi}_j$ represents the wave mode shape. It is worth noting that every single eigenvector may be partitioned into components of pressure and velocity, given $\mathbf{\Phi}_j^t = [(\mathbf{\Phi_p})_j^t (\mathbf{\Phi_v})_j^t]$. Considering a specific eigenvalue μ_j, left multiplying of Eq. (2.7) by $\mathbf{S}^t\mathbf{J}_n$ gives:

$$\mathbf{S}^t\mathbf{J}_n\mathbf{S}\mathbf{\Phi}_j = \mu_j \mathbf{S}^t\mathbf{J}_n\mathbf{\Phi}_j \tag{2.9}$$

As the matrix $\mathbf{S}$ is symplectic, Eq. (2.9) can be written as follows:

$$\mathbf{J}_n\mathbf{\Phi}_j = \mu_j \mathbf{S}^t\mathbf{J}_n\mathbf{\Phi}_j \tag{2.10}$$

Then if we consider the transpose of Eq. (2.10), we can write:

$$(\mathbf{\Phi}_j^t\mathbf{J}_n)\mathbf{S} = \frac{1}{\mu_j}\ \mathbf{\Phi}_j^t\ \mathbf{J}_n \tag{2.11}$$

It is clear that $(\mathbf{\Phi}_j^t\mathbf{J}_n)$ is a left eigenvector of matrix $\mathbf{S}$. Hence, eigenvalues are defined for $j \in \{1, .., n\}$ such as:

$$\mu_{n+j} = \frac{1}{\mu_j} \tag{2.12}$$

Hence, if eigenvalues $\{\mu_i\}_{i=1,..,n}$ associated with eigenvectors $\{\mathbf{\Phi}_i\}_{i=1,..,n}$ correspond to the forward going waves ($|\mu| < 1$), eigenvalues $\{\mu_i\}_{i=n+1,..,2n}$ associated with eigenvectors $\{\mathbf{\Phi}_i\}_{i=n+1,..,2n}$ correspond to the backward going waves ($|\mu| > 1$). Matrix $\mathbf{\Phi}$ of the eigenvectors

can be detailed in this way:

$$\mathbf{\Phi} = \begin{pmatrix} \mathbf{\Phi_p}^{inc} & \mathbf{\Phi_p}^{ref} \\ \mathbf{\Phi_v}^{inc} & \mathbf{\Phi_v}^{ref} \end{pmatrix} \tag{2.13}$$

As shown in [73] , the eigenvalue problem defined by Eq. (2.7) must be solved at particular frequencies. This means that the wave modes established by Eq. (2.13) have to be arranged for each frequency. Correspondence between two sets of modes defined at two frequencies, close to each other, can be achieved in the WFE framework using the following criterion: Given two wave modes $b \in \{1, .., n\}$ and $j \in \{n+1, .., 2n\}$ defined at pulsation ω , such that $\mu_b(\omega) = 1/\mu_j(\omega)$, and for sufficiently little Δ_ω, wave mode j defined at pulsation $\omega + \Delta_\omega$ is such that [58]:

$$\left| \frac{\mathbf{\Phi}_b(\omega)^t}{\left\|\mathbf{\Phi}_b(\omega)^t\right\|} \mathbf{J}_n \frac{\mathbf{\Phi}_j(\omega+\Delta_\omega)}{\|\mathbf{\Phi}_j(\omega+\Delta_\omega)\|} \right| = max_{k\in\{n+1,..,2n\}} \left\{ \left| \frac{\mathbf{\Phi}_b(\omega)^t}{\left\|\mathbf{\Phi}_b(\omega)^t\right\|} \mathbf{J}_n \frac{\mathbf{\Phi}_k(\omega+\Delta_\omega)}{\|\mathbf{\Phi}_k(\omega+\Delta_\omega)\|} \right| \right\} \tag{2.14}$$

where $\|\mathbf{y}\|$ stands for the hermitian norm of a vector $\mathbf{y}$, defined as $\|\mathbf{y}\| = \sqrt{\mathbf{y}^h\mathbf{y}}$ where h is the conjugate transpose.

This criterion is the result of the orthogonality relations between the left and right eigenvectors:

For $\mu_s(\omega) \neq 1/\mu_j(\omega)$:

$$\mathbf{\Phi}_s^t(\omega)\,\mathbf{J}_n\mathbf{\Phi}_j(\omega) = 0 \tag{2.15}$$

Finally, state vectors $\mathbf{u}_l^{(k)}$ and $\mathbf{u}_r^{(k)}$ of a substructure k are given by means of eigenvectors $\{\mathbf{\Phi}_i\}_{i=1,..,2n}$ as:

$$\mathbf{u}_l^{(k)} = \sum_{i=1}^{2n} \mathbf{\Phi}_i Q_i^{(k)} \tag{2.16}$$

and

$$\mathbf{u}_r^{(k)} = \sum_{i=1}^{2n} \mathbf{\Phi}_i Q_i^{(k+1)} \tag{2.17}$$

where $\{Q_i\}_{i=1,..,2n}$ stand for the amplitudes of the wave modes.

2.2.3 Numerical conditioning

The computation of wave characteristics by the WFE method may suffer from various numerical issues. First, issues related to the FE discretisation must be reduced. The segments length is chosen such as it is at least six times smaller than the minimal wavelength. As the frequency increases, the length of segment is meant to be smaller. However when re-meshing the waveguide with shorter segments, round-off errors due to truncation of inertia terms appear for the low frequencies. This is because K_{ij} is much larger than $\omega^2 M_{ij}$. Some digits associated with the inertia terms in $D_{ij} = K_{ij} - \omega^2 M_{ij}$ are truncated after the subtraction. The number of the digits truncated is approximately [29]:

$$n_{ij} = \log_{10} \frac{|K_{ij}|}{|\omega^2 M_{ij}|} \tag{2.18}$$

It is clear from Eq. (2.18) that there is a frequency below which errors become unacceptable. In this case, a higher precision arithmetic must be used.

Furthermore, the resolution of the eigenvalue problem in the form (2.7) may be prone to numerical issues especially when the FE model has a large number of degrees of freedom. The eigenvalue problem includes both very small eigenvalues μ and very large eigenvalues $1/\mu$, standing for waves that decay rapidly over a segment in the positive and negative directions, respectively. Moreover, $\mathbf{D}_{lr}$ can be ill-conditioned. The condition number, given by the ratio of the largest singular value to the smallest, of the matrix $\mathbf{D}_{lr}$ is large and numerical errors are likely to occur when computing its inverse. It may be useful to convert problem (2.7) to the quadratic eigenvalue problem which is better-conditioned [74, 29]:

$$\begin{pmatrix} \mathbf{0} & \mathbf{I}_n \\ -\mathbf{D}_{lr}^{-1}\mathbf{D}_{rl} & -\mathbf{D}_{lr}^{-1}(\mathbf{D}_{ll} + \mathbf{D}_{rr}) \end{pmatrix} \begin{pmatrix} \mathbf{p}_l \\ \mu \mathbf{p}_l \end{pmatrix} = \mu \begin{pmatrix} \mathbf{p}_l \\ \mu \mathbf{p}_l \end{pmatrix} \tag{2.19}$$

The velocities component can be then obtained by:

$$\mathbf{v}_l = (\mathbf{D}_{ll} + \mu \mathbf{D}_{lr})\ \mathbf{p}_l \tag{2.20}$$

Another reformulation of the eigenvalue problem can be also considered. The following

generalised eigenvalue problem is used to mitigate the ill-conditioning [28, 75, 76]:

$$\mathbf{F}\begin{pmatrix}\mathbf{p}_l\\ \mathbf{p}_r\end{pmatrix} = \mu_j \mathbf{G}\begin{pmatrix}\mathbf{p}_l\\ \mathbf{p}_r\end{pmatrix} \tag{2.21}$$

where $\mathbf{F} = \begin{pmatrix}\mathbf{0} & \mathbf{I}_n\\ \mathbf{D}_{rl} & \mathbf{D}_{rr}\end{pmatrix}$; $\mathbf{G} = \begin{pmatrix}\mathbf{I}_n & \mathbf{0}\\ -\mathbf{D}_{ll} & -\mathbf{D}_{lr}\end{pmatrix}$; and $\mathbf{\Phi}_j = \mathbf{G}\begin{pmatrix}\mathbf{p}_l\\ \mathbf{p}_r\end{pmatrix}$.
Matrices $\mathbf{F}$ and $\mathbf{G}$ could still have large condition numbers because terms of matrix $\mathbf{I}_n$ have a different order compared to matrices $\mathbf{D}_{rr}$ and $\mathbf{D}_{ll}$. The first row is multiplied by the factor $||\mathbf{D}_{rr}||_2$ so that the condition number is significantly reduced.

$$\left(\begin{bmatrix}\mathbf{0} & ||\mathbf{D}_{rr}||_2\mathbf{I}_n\\ \mathbf{D}_{rl} & \mathbf{D}_{rr}\end{bmatrix} - \mu_j \begin{bmatrix}||\mathbf{D}_{rr}||_2\mathbf{I}_n & \mathbf{0}\\ -\mathbf{D}_{ll} & -\mathbf{D}_{lr}\end{bmatrix}\right)\begin{pmatrix}\mathbf{p}_l\\ \mathbf{p}_r\end{pmatrix} = \mathbf{0} \tag{2.22}$$

The present form is better-conditioned than form (2.7) and there are not numerical problems any more.

2.2.4 Scattering matrix computation

Let us suppose that an acoustic treatment covers partially the external surface of the duct. Transmission and reflection, for the different modes, may be predicted by computing the scattering matrix.

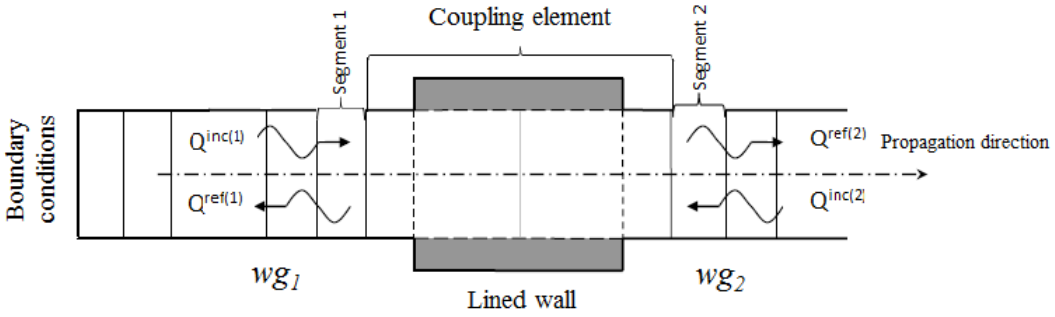

Figure 2.2. *Description of the lined duct model.*

As presented in Fig. 2.2, the studied problem can be modelled as two waveguides wg_1 and wg_2 linked through a coupling element which could be discretised using p-only fluid elements under FE software. Unless the determination of the phase of the scattering coefficients is of interest, the length of the coupling element can be larger than the lined part length.
The pressure and velocity vectors are related such as:

$$\mathbf{v}_{(N_c\times 1)} = \mathbf{D}_{\mathbf{c}(N_c\times N_c)}\mathbf{p}_{(N_c\times 1)} \tag{2.23}$$

where N_c is the total number of degrees of freedom of the coupling element.

From the equation of mass conservation combined with the equation of state, and the equation of momentum conservation [12], the radial boundary conditions for a sound-hard boundary Γ_R and an absorbing boundary Γ_L, are expressed respectively by:

$$\frac{\partial p}{\partial n_R} = 0 \tag{2.24}$$

$$\frac{\partial p}{\partial n_L} = \mathrm{i}\frac{\omega}{cZ}p \tag{2.25}$$

where $\mathbf{n}_i$ is the outward normal to the boundary, c is the celerity of the sound in the air,ω is the angular frequency and Z is the normalised impedance of the liner.

Following the pressure finite elements formulation, terms of the elementary damping matrix are further given by:

$$C^e_{cij} = \int_{\Gamma^e_L} \frac{1}{cZ} N_i N_j \mathrm{d}S \tag{2.26}$$

where N_i and N_j are the two dimensional element shape functions [77].
The dynamic stiffness matrix $\mathbf{D_c}$ is then given in terms of mass, damping and stiffness matrices of the coupling element as follows:

$$\mathbf{D_c} = -\omega^2\mathbf{M_c} + \mathrm{i}\omega\mathbf{C_c} + \mathbf{K_c} \tag{2.27}$$

A block matrix formulation of the matrix $\mathbf{D_c}$ can be written as follows:

$$\mathbf{D_c} = \begin{pmatrix} \tilde{\mathbf{D}}_{ll(n\times n)} & \tilde{\mathbf{D}}_{li(n\times(N_c-2n))} & \tilde{\mathbf{D}}_{lr(n\times n)} \\ \tilde{\mathbf{D}}_{il((N_c-2n)\times n)} & \tilde{\mathbf{D}}_{ii((N_c-2n)\times(N_c-2n))} & \tilde{\mathbf{D}}_{ir((N_c-2n)\times n)} \\ \tilde{\mathbf{D}}_{rl(n\times n)} & \tilde{\mathbf{D}}_{ri(n\times(N_c-2n))} & \tilde{\mathbf{D}}_{rr(n\times n)} \end{pmatrix} \tag{2.28}$$

where n is the number of degrees of freedom per cross-section.

$$\begin{pmatrix} \tilde{\mathbf{D}}_{ll} & \tilde{\mathbf{D}}_{li} & \tilde{\mathbf{D}}_{lr} \\ \tilde{\mathbf{D}}_{il} & \tilde{\mathbf{D}}_{ii} & \tilde{\mathbf{D}}_{ir} \\ \tilde{\mathbf{D}}_{rl} & \tilde{\mathbf{D}}_{ri} & \tilde{\mathbf{D}}_{rr} \end{pmatrix} \begin{pmatrix} \mathbf{p}_l^{(c)} \\ \mathbf{p}_i^{(c)} \\ \mathbf{p}_r^{(c)} \end{pmatrix} = \begin{pmatrix} \mathbf{v}_l^{(c)} \\ \mathbf{0} \\ \mathbf{v}_r^{(c)} \end{pmatrix} \tag{2.29}$$

where superscript (c) refers to the coupling element.

Replacing $\mathbf{p}_i^{(c)}$ by its expression from the second row in the first and third rows allows suppression of the internal nodes. Finally, after eliminating the internal degrees of freedom the condensed dynamic stiffness matrix $\mathbf{D_c^*}$ can be written as:

$$\mathbf{D_c^*} = \begin{pmatrix} \tilde{\mathbf{D}}_{ll} - \tilde{\mathbf{D}}_{li}\tilde{\mathbf{D}}_{ii}^{-1}\tilde{\mathbf{D}}_{il} & \tilde{\mathbf{D}}_{lr} - \tilde{\mathbf{D}}_{li}\tilde{\mathbf{D}}_{ii}^{-1}\tilde{\mathbf{D}}_{ir} \\ \tilde{\mathbf{D}}_{rl} - \tilde{\mathbf{D}}_{ri}\tilde{\mathbf{D}}_{ii}^{-1}\tilde{\mathbf{D}}_{il} & \tilde{\mathbf{D}}_{rr} - \tilde{\mathbf{D}}_{ri}\tilde{\mathbf{D}}_{ii}^{-1}\tilde{\mathbf{D}}_{ir} \end{pmatrix} \tag{2.30}$$

It should be noted that the calculation of the dynamic stiffness matrix of the coupling element condensed onto the interfaces must be done at each frequency. Thus, direct inversion of $\tilde{\mathbf{D}}_{ii}$ has a high computational cost especially if the coupling element includes many degrees of freedom. The inverse of $\tilde{\mathbf{D}}_{ii}$ can be given by:

$$\tilde{\mathbf{D}}_{ii}^{-1} = (\tilde{\mathbf{K}}_{ii} + \mathrm{i}\omega\tilde{\mathbf{C}}_{ii} - \omega^2\tilde{\mathbf{M}}_{ii})^{-1} = (\mathbf{I} - \omega^2\tilde{\mathbf{K}}_{ii}^{-1}(\tilde{\mathbf{M}}_{ii} - \frac{\mathrm{i}}{\omega}\tilde{\mathbf{C}}_{ii}))^{-1}\tilde{\mathbf{K}}_{ii}^{-1} \tag{2.31}$$

When $||\omega^2\tilde{\mathbf{K}}_{ii}^{-1}(\tilde{\mathbf{M}}_{ii} - \frac{\mathrm{i}}{\omega}\tilde{\mathbf{C}}_{ii})||$ remains less than 1, a less costly approach is to use a second order expansion in Neumann series of $\tilde{\mathbf{D}}_{ii}^{-1}$:

$$\tilde{\mathbf{D}}_{ii}^{-1} = [\mathbf{I} + \omega^2\tilde{\mathbf{K}}_{ii}^{-1}(\tilde{\mathbf{M}}_{ii} - \frac{\mathrm{i}}{\omega}\tilde{\mathbf{C}}_{ii}) + \omega^4\tilde{\mathbf{K}}_{ii}^{-1}(\tilde{\mathbf{M}}_{ii} - \frac{\mathrm{i}}{\omega}\tilde{\mathbf{C}}_{ii})\tilde{\mathbf{K}}_{ii}^{-1}(\tilde{\mathbf{M}}_{ii} - \frac{\mathrm{i}}{\omega}\tilde{\mathbf{C}}_{ii})]\tilde{\mathbf{K}}_{ii}^{-1} \tag{2.32}$$

To calculate the condensed dynamic stiffness matrix, $\tilde{\mathbf{K}}_{ii}^{-1}$ is calculated only once in the frequency range for which the condition for the expansion in Neumann series is verified, so the computational cost is reduced.

Two coupled waveguide segments (1) and (2) belonging respectively to the waveguides wg_1 and wg_2 are modelled (Fig. 2.2). It can be shown that amplitudes $(\mathbf{Q}^{ref(1)};\mathbf{Q}^{ref(2)})$ of the modes reflected by the coupling element at the interface are related to the amplitudes $(\mathbf{Q}^{inc(1)};\mathbf{Q}^{inc(2)})$ of the modes incident to the coupling element at the interface by means of the scattering matrix [56, 78].

Indeed, expressions of state vectors $\mathbf{u}_r^{(1)}$ and $\mathbf{u}_l^{(2)}$ of segments (1) and (2) give:

$$\begin{pmatrix} \mathbf{p}_r^{(1)} \\ \mathbf{p}_l^{(2)} \end{pmatrix} = \begin{pmatrix} {\boldsymbol{\Phi}_\mathbf{p}}^{inc(1)} & \mathbf{0} & {\boldsymbol{\Phi}_\mathbf{p}}^{ref(1)} & \mathbf{0} \\ \mathbf{0} & {\boldsymbol{\Phi}_\mathbf{p}}^{inc(2)} & \mathbf{0} & {\boldsymbol{\Phi}_\mathbf{p}}^{ref(2)} \end{pmatrix} \begin{pmatrix} \mathbf{Q}^{inc(1)} \\ \mathbf{Q}^{inc(2)} \\ \mathbf{Q}^{ref(1)} \\ \mathbf{Q}^{ref(2)} \end{pmatrix} \tag{2.33}$$

$$\begin{pmatrix} \mathbf{v}_r^{(1)} \\ \mathbf{v}_l^{(2)} \end{pmatrix} = \begin{pmatrix} {\boldsymbol{\Phi}_\mathbf{v}}^{inc(1)} & \mathbf{0} & {\boldsymbol{\Phi}_\mathbf{v}}^{ref(1)} & \mathbf{0} \\ \mathbf{0} & {\boldsymbol{\Phi}_\mathbf{v}}^{inc(2)} & \mathbf{0} & {\boldsymbol{\Phi}_\mathbf{v}}^{ref(2)} \end{pmatrix} \begin{pmatrix} \mathbf{Q}^{inc(1)} \\ \mathbf{Q}^{inc(2)} \\ \mathbf{Q}^{ref(1)} \\ \mathbf{Q}^{ref(2)} \end{pmatrix} \tag{2.34}$$

Considering the coupling's conditions of interfaces guides-coupling element which state that:

$$\begin{pmatrix} \mathbf{p}_l^{(c)} \\ \mathbf{p}_r^{(c)} \end{pmatrix} = \begin{pmatrix} \mathbf{p}_r^{(1)} \\ \mathbf{p}_l^{(2)} \end{pmatrix} \; ; \; \begin{pmatrix} \mathbf{v}_l^{(c)} \\ \mathbf{v}_r^{(c)} \end{pmatrix} = - \begin{pmatrix} \mathbf{v}_r^{(1)} \\ \mathbf{v}_l^{(2)} \end{pmatrix} ,$$

Eqs. (2.33) and (2.34) lead to:

$$-\mathbf{D}_\mathbf{c}^* \left[{\boldsymbol{\Psi}_\mathbf{p}}^{inc} {\boldsymbol{\Psi}_\mathbf{p}}^{ref} \right] \begin{pmatrix} \mathbf{Q}^{inc(1)} \\ \mathbf{Q}^{inc(2)} \\ \mathbf{Q}^{ref(1)} \\ \mathbf{Q}^{ref(2)} \end{pmatrix} = \left[{\boldsymbol{\Psi}_\mathbf{v}}^{inc} {\boldsymbol{\Psi}_\mathbf{v}}^{ref} \right] \begin{pmatrix} \mathbf{Q}^{inc(1)} \\ \mathbf{Q}^{inc(2)} \\ \mathbf{Q}^{ref(1)} \\ \mathbf{Q}^{ref(2)} \end{pmatrix} \tag{2.35}$$

$$\boldsymbol{\Psi_p}^{inc} = \begin{pmatrix} \boldsymbol{\Phi_p}^{inc(1)} & \mathbf{0} \\ \mathbf{0} & \boldsymbol{\Phi_p}^{inc(2)} \end{pmatrix} \quad \boldsymbol{\Psi_p}^{ref} = \begin{pmatrix} \boldsymbol{\Phi_p}^{ref(1)} & \mathbf{0} \\ \mathbf{0} & \boldsymbol{\Phi_p}^{ref(2)} \end{pmatrix}$$

where

$$\boldsymbol{\Psi_v}^{inc} = \begin{pmatrix} \boldsymbol{\Phi_v}^{inc(1)} & \mathbf{0} \\ \mathbf{0} & \boldsymbol{\Phi_v}^{inc(2)} \end{pmatrix} \quad \boldsymbol{\Psi_v}^{ref} = \begin{pmatrix} \boldsymbol{\Phi_v}^{ref(1)} & \mathbf{0} \\ \mathbf{0} & \boldsymbol{\Phi_v}^{ref(2)} \end{pmatrix}$$

The scattering matrix $\mathbf{C}$ is defined such as :

$$\begin{pmatrix} \mathbf{Q}^{ref(1)} \\ \mathbf{Q}^{ref(2)} \end{pmatrix} = \mathbf{C} \begin{pmatrix} \mathbf{Q}^{inc(1)} \\ \mathbf{Q}^{inc(2)} \end{pmatrix} \tag{2.36}$$

where

$$\mathbf{C} = -\left(\mathbf{D_c^*}\boldsymbol{\Psi_p}^{ref} + \boldsymbol{\Psi_v}^{ref}\right)^{+}\left(\mathbf{D_c^*}\boldsymbol{\Psi_p}^{inc} + \boldsymbol{\Psi_v}^{inc}\right) \tag{2.37}$$

and $^{+}$ refers to the pseudo-inverse [79].

2.2.5 Computation of the forced response of rigid waveguides

A rigid cylindrical duct submitted to acoustical pressure $p(\omega)$ and a normalised impedance Z at its left and right ends respectively is considered. The duct is divided into N segments whose lengths are satisfying the following condition:

$$\Delta \leq \frac{c}{12 f_{max}} \tag{2.38}$$

where c stands for the celerity of sound in the air, (c/f_{max}) is the minimal wave length.
Boundary condition in the left side can be expressed as following:

$$\boldsymbol{\Phi_p}^{inc}\mathbf{Q}^{inc(1)} + \boldsymbol{\Phi_p}^{ref}\mathbf{Q}^{ref(1)} = \mathbf{p}_0 \tag{2.39}$$

Superscript (i) refers to the i^{th} cross-sectional surface of the waveguide and $\mathbf{p}_0$ is the magnitude of the imposed pressure.
The right side boundary condition can be written as follows [80]:

$$\boldsymbol{\mu}^{-N}\mathbf{Q}^{ref(1)} = \mathbf{R}\boldsymbol{\mu}^{N}\mathbf{Q}^{inc(1)} \tag{2.40}$$

where N is the number of segments composing the duct. $\boldsymbol{\mu}$ is the $(n \times n)$ diagonal matrix of eigenvalues corresponding to the incident modes, and $\mathbf{R}$ stands for a reflection matrix and can be given as:

$$\mathbf{R} = \begin{pmatrix} R_1 & \cdots & 0 \\ \vdots & \ddots & \vdots \\ 0 & \cdots & R_n \end{pmatrix} \tag{2.41}$$

where [40]:

$$R_n = \frac{Z\cos\theta_n - 1}{Z\cos\theta_n + 1} \tag{2.42}$$

$$\theta_n = \cos^{-1}\left(\sqrt{1 - \left(\frac{f_n^c}{f}\right)^2}\right) \tag{2.43}$$

and f_n^c is the cut-off frequency of the n^{th} mode . Note also that, if the modes eigenvalues are sorted in ascending order for the first frequency in criterion (2.14), the n^{th} mode corresponds to the plane wave mode, the $(n-1)^{\text{th}}$ mode to the first cross-sectional mode, and so on. Given Eqs. (2.39) and (2.40), we can write:

$$\begin{pmatrix} (\boldsymbol{\Phi_{\mathbf{p}}}^{inc})^{-1}\mathbf{p_0} \\ \mathbf{0} \end{pmatrix} = \begin{pmatrix} \mathbf{I}_n & (\boldsymbol{\Phi_{\mathbf{p}}}^{inc})^{-1}(\boldsymbol{\Phi_{\mathbf{p}}}^{ref}) \\ \mathbf{R}\boldsymbol{\mu}^N & -\boldsymbol{\mu}^{-N} \end{pmatrix} \begin{pmatrix} \mathbf{Q}^{inc(1)} \\ \mathbf{Q}^{ref(1)} \end{pmatrix} \tag{2.44}$$

Solving Eq. (2.44) needs appropriate manipulations to avoid numerical errors due to close-to-singular or badly scaled matrices. Hence, it will be worth solving Eq. (2.44) this way:

$$\begin{pmatrix} \mathbf{Q}^{inc(1)} \\ \mathbf{Q}^{ref(1)} \end{pmatrix} = \begin{pmatrix} \mathbf{I}_n & \mathbf{0} \\ \mathbf{0} & \boldsymbol{\mu}^N \end{pmatrix} \begin{pmatrix} \mathbf{I}_n & (\boldsymbol{\Phi_{\mathbf{p}}}^{inc})^{-1}(\boldsymbol{\Phi_{\mathbf{p}}}^{ref})\boldsymbol{\mu}^N \\ \mathbf{R}\boldsymbol{\mu}^N & -\mathbf{I}_n \end{pmatrix}^{-1} \begin{pmatrix} (\boldsymbol{\Phi_{\mathbf{p}}}^{inc})^{-1}\mathbf{p}_0 \\ \mathbf{0} \end{pmatrix} \tag{2.45}$$

The pressure vector for the k^{th} cross-section is given by:

$$\mathbf{p}^{(k)} = \begin{pmatrix} \boldsymbol{\Phi_{\mathbf{p}}}^{inc} & \boldsymbol{\Phi_{\mathbf{p}}}^{ref} \end{pmatrix} \begin{pmatrix} \boldsymbol{\mu}^{k-1} & \mathbf{0} \\ \mathbf{0} & \boldsymbol{\mu}^{-(k-1)} \end{pmatrix} \begin{pmatrix} \mathbf{Q}^{inc(1)} \\ \mathbf{Q}^{ref(1)} \end{pmatrix} \tag{2.46}$$

It should be noted that, when the k^{th} cross-section is far from the 1^{st} cross-section, calculation of the forced response may be prone to numerical difficulties. This is because terms in $\boldsymbol{\mu}^{-(k-1)}$ in Eq. (2.46) tend to infinity in this case. A solution for this issue is to retain only the propagating and the less decaying waves and eliminate the strongly evanescent waves for which $|\mu| < \kappa$, where κ is a user-defined value [27, 28]. The waves for which $|\mu|$ is too small are rapidly decaying and almost with no contribution to the overall response while they do cause numerical issues.

2.2.6 Computation of the forced response of coupled waveguides

Two coupled waveguides are assumed to be submitted to prescribed pressure and impedance on their uncoupled limits. $N1$ and $N2$ segments constitute respectively the waveguides wg_1 and wg_2.

The boundary conditions will be expressed as:

For waveguide wg_1:

$$(\boldsymbol{\Phi}_{\mathbf{p}}{}^{inc})_{wg_1}\mathbf{Q}_{wg_1}^{inc(1)} + (\boldsymbol{\Phi}_{\mathbf{p}}{}^{ref})_{wg_1}\mathbf{Q}_{wg_1}^{ref(1)} = \mathbf{p}_0 \tag{2.47}$$

$$\boldsymbol{\mu}_{wg_1}^{-N1}\mathbf{Q}_{wg_1}^{ref(1)} = \mathbf{C}_{11}\boldsymbol{\mu}_{wg_1}^{N1}\mathbf{Q}_{wg_1}^{inc(1)} + \mathbf{C}_{12}\boldsymbol{\mu}_{wg_2}^{N2}\mathbf{Q}_{wg_2}^{inc(1)} \tag{2.48}$$

For waveguide wg_2:

$$\boldsymbol{\mu}_{wg_2}^{-N2}\mathbf{Q}_{wg_2}^{ref(1)} = \mathbf{C}_{21}\boldsymbol{\mu}_{wg_1}^{N1}\mathbf{Q}_{wg_1}^{inc(1)} + \mathbf{C}_{22}\boldsymbol{\mu}_{wg_2}^{N2}\mathbf{Q}_{wg_2}^{inc(1)} \tag{2.49}$$

$$\mathbf{Q}_{wg_2}^{ref(1)} = \mathbf{R}\mathbf{Q}_{wg_2}^{inc(1)} \tag{2.50}$$

where $\{\mathbf{C}_{ij}\}_{i=1,2,j=1,2}$ represent the square block components of the scattering matrix $\mathbf{C}$. Diagonal blocks $\{\mathbf{C}_{ii}\}_{i=1,2}$stand for reflection matrices, while off-diagonal blocks stand for transmission matrices. $\mathbf{R}$ is given by Eq. (2.41). Superscript (i) refers to the i^{th} cross-sectional surface of the waveguide. $\boldsymbol{\mu}_{wg_1}$ and $\boldsymbol{\mu}_{wg_2}$ are the $(n \times n)$ diagonal matrix of eigenvalues corresponding to the incident modes of the waveguides wg_1 and wg_2, respectively. As we are

considering identical waveguides, we have :

$$\boldsymbol{\mu}_{wg_1} = \boldsymbol{\mu}_{wg_2} = \boldsymbol{\mu} \tag{2.51}$$

Then, we can write:

$$\begin{pmatrix} \mathbf{p}_0 \\ \mathbf{0} \\ \mathbf{0} \\ \mathbf{0} \end{pmatrix} = \begin{pmatrix} {\boldsymbol{\Phi}_{\mathbf{p}}}^{inc} & {\boldsymbol{\Phi}_{\mathbf{p}}}^{ref} & \mathbf{0} & \mathbf{0} \\ -\mathbf{C}_{11}\boldsymbol{\mu}^{N1} & \boldsymbol{\mu}^{-N1} & \mathbf{0} & -\mathbf{C}_{12}\boldsymbol{\mu}^{N2} \\ -\mathbf{C}_{21}\boldsymbol{\mu}^{N1} & \mathbf{0} & \boldsymbol{\mu}^{-N2} & -\mathbf{C}_{22}\boldsymbol{\mu}^{N2} \\ \mathbf{0} & \mathbf{0} & \mathbf{I}_n & -\mathbf{R} \end{pmatrix} \begin{pmatrix} \mathbf{Q}_{wg_1}^{inc(1)} \\ \mathbf{Q}_{wg_1}^{ref(1)} \\ \mathbf{Q}_{wg_2}^{ref(1)} \\ \mathbf{Q}_{wg_2}^{inc(1)} \end{pmatrix} \tag{2.52}$$

Direct inversion of Eq. (2.52) may be prone to ill-conditioning problems. So, after appropriate scaling, we will have:

$$\begin{pmatrix} \mathbf{Q}_{wg_1}^{inc(1)} \\ \mathbf{Q}_{wg_1}^{ref(1)} \\ \mathbf{Q}_{wg_2}^{ref(1)} \\ \mathbf{Q}_{wg_2}^{inc(1)} \end{pmatrix} = \begin{pmatrix} \mathbf{I}_n & \mathbf{0} & \mathbf{0} & \mathbf{0} \\ \mathbf{0} & \boldsymbol{\mu}^{N1} & \mathbf{0} & \mathbf{0} \\ \mathbf{0} & \mathbf{0} & \boldsymbol{\mu}^{N2} & \mathbf{0} \\ \mathbf{0} & \mathbf{0} & \mathbf{0} & \mathbf{I}_n \end{pmatrix} \begin{pmatrix} \mathbf{I}_n & ({\boldsymbol{\Phi}_{\mathbf{p}}}^{inc})^{-1}{\boldsymbol{\Phi}_{\mathbf{p}}}^{ref}\boldsymbol{\mu}^{N1} & \mathbf{0} & \mathbf{0} \\ -\mathbf{C}_{11}\boldsymbol{\mu}^{N1} & \mathbf{I}_n & \mathbf{0} & -\mathbf{C}_{12}\boldsymbol{\mu}^{N2} \\ -\mathbf{C}_{21}\boldsymbol{\mu}^{N1} & \mathbf{0} & \mathbf{I}_n & -\mathbf{C}_{22}\boldsymbol{\mu}^{N2} \\ \mathbf{0} & \mathbf{0} & \boldsymbol{\mu}^{N2} & -\mathbf{R} \end{pmatrix}^{-1} \begin{pmatrix} ({\boldsymbol{\Phi}_{\mathbf{p}}}^{inc})^{-1}\mathbf{p}_0 \\ \mathbf{0} \\ \mathbf{0} \\ \mathbf{0} \end{pmatrix} \tag{2.53}$$

The pressure vector for the k^{th} cross-section is given by:

$$\mathbf{p}^{(k)} = \begin{pmatrix} {\boldsymbol{\Phi}_{\mathbf{p}}}^{inc} & {\boldsymbol{\Phi}_{\mathbf{p}}}^{ref} \end{pmatrix} \begin{pmatrix} \boldsymbol{\mu}^{k-1} & \mathbf{0} \\ \mathbf{0} & \boldsymbol{\mu}^{-(k-1)} \end{pmatrix} \begin{pmatrix} \mathbf{Q}_{wg_{1,2}}^{inc(1)} \\ \mathbf{Q}_{wg_{1,2}}^{ref(1)} \end{pmatrix} \tag{2.54}$$

If the duct was submitted to pressure at both ends, we would have only to replace Eq.(2.50) by Eq.(2.55):

$$({\boldsymbol{\Phi}_{\mathbf{p}}}^{inc})_{wg_2}\mathbf{Q}_{wg_2}^{inc(1)} + ({\boldsymbol{\Phi}_{\mathbf{p}}}^{ref})_{wg_2}\mathbf{Q}_{wg_2}^{ref(1)} = \mathbf{p}_0 \tag{2.55}$$

2.3 Application to the guided acoustical propagation

2.3.1 Rigid duct modes representation

- ***Cylindrical waveguide***

The real parts of the axial wavenumbers of a 0.08 m diameter waveguide are calculated through the WFE method. The ones corresponding to waves travelling in the positive direction of propagation are represented in Fig. 2.3 and compared to the analytical solutions. In this case, the highest frequency at which only plane waves will propagate is ≈ 2500 Hz.

The axial wavenumbers are related to the free field wavenumber and the radial wavenumber

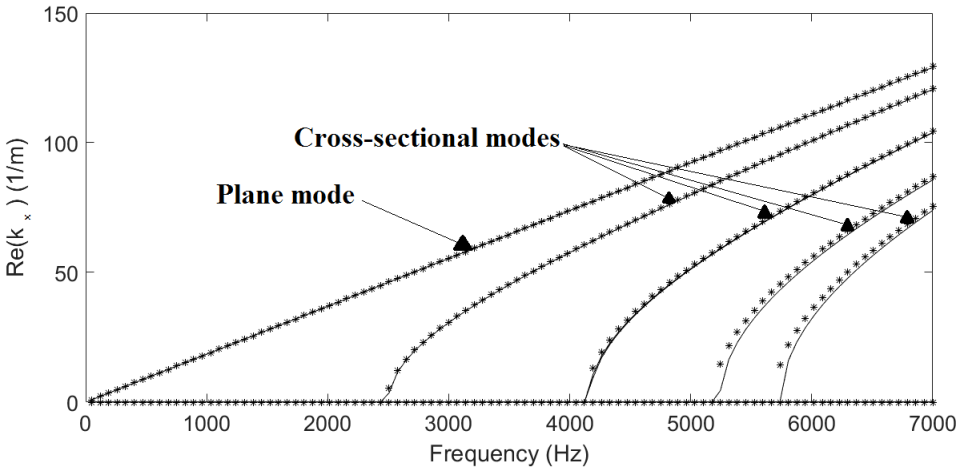

Figure 2.3. *Frequency evolution of the axial wavenumbers real parts corresponding to the forward-going waves for the case of a* 0.08 *m diameter waveguide : (—) WFE method (*) Analytical method.*

by the dispersion relation. For a rigid cylindrical duct, an axial wavenumber will be associated to the i^{th} zero of the derivative of the m^{th} order Bessel function of the first kind as following [81]:

$$k_{mi} = \sqrt{\frac{4\pi^2 f^2}{c^2} - \frac{\chi_{mi}^2}{a^2}} \tag{2.56}$$

where c is the celerity of sound in the air, f is the frequency, χ_{mi} are the Bessel function derivative zeros and a is the radius of the duct.

The axial wave numbers are either real or imaginary. That is to say, for each frequency, there are a finite number of modes with purely real axial wavenumbers which stand for propagating modes and an infinite number of modes with purely imaginary axial wavenumbers which correspond to evanescent ones. Moreover, each mode travels from one end to the other and vice versa. The forward-going (resp. backward-going) waves are such their group velocity c_g^+ (resp. c_g^-) is positive (resp. negative). The group velocity and the phase velocity of a cut-on mode satisfy for each frequency the following relation:

$$c_g^{\pm} c_{ph}^{\pm} = c^2 \quad \text{with } c_{ph}^- \leq -c \leq c_g^- < 0 < c_g^+ \leq c \leq c_{ph}^+ \tag{2.57}$$

Except for the plane wave mode, where $c_{ph} = c_g = \pm c$, the group velocity is smaller than c because the modal wave fronts do not propagate parallel to the x-axis, but rather follow a longer path.

Pressure's real part contours by the ANSYS software and the WFE method are presented in Figs. 2.4 and 2.5 for a cylindrical duct submitted to modes $(0,1)$ and $(1,1)$ respectively and ended by a normalised impedance Z_{end}=2.

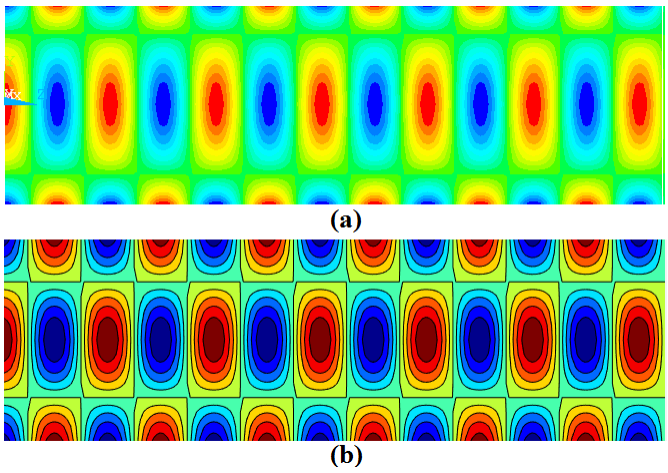

Figure 2.4. *Pressure's real part contours for a cylindrical duct submitted to mode (0,1), f =6000Hz and Z_{end}=2, by (a) ANSYS and (b) WFE.*

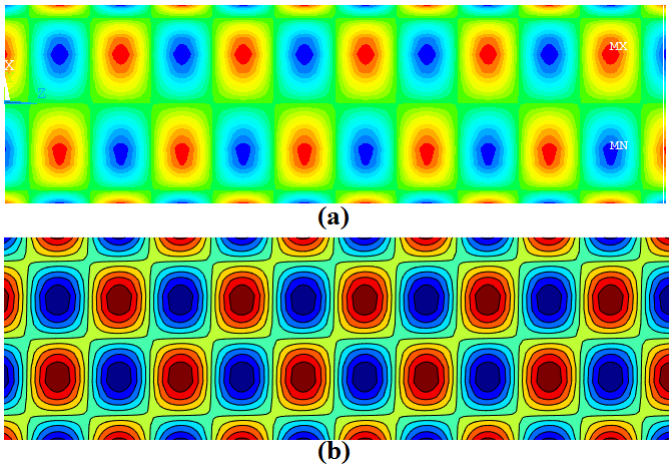

Figure 2.5. *Pressure's real part contours for a cylindrical duct submitted to mode (1,1), f =6000Hz and Z_{end}=2, by (a) ANSYS and (b) WFE.*

- ***Annular waveguide***

The axial wavenumbers of guided acoustical propagation inside an annular duct were calculated. Fig. 2.6 shows the frequency evolution of the axial wavenumbers real parts of forward-going waves by both WFE method and analytical method. Inner and outer radii, a_{inner} and a_{outer}, are equal to 0.04 m and 0.048 m respectively. The axial wavenumbers are calculated analytically by the dispersion relation at each frequency. The transversal wavenumbers α_{mi} in this case satisfy [82, 83]:

$$J_m^{'}(\alpha_{mi}\ a_{inner})\mathcal{Y}_m^{'}(\alpha_{mi}\ a_{outer}) - J_m^{'}(\alpha_{mi}\ a_{outer})\mathcal{Y}_m^{'}(\alpha_{mi}\ a_{inner}) = 0 \tag{2.58}$$

where $J_m^{'}$ and $\mathcal{Y}_m^{'}$ stand here for the derivatives of the m^{th} order Bessel functions of first kind and second kind respectively [45]. m and i are respectively the circumferential order and the radial order of the duct modes. Eq. (2.58) is the result of applying the hard boundary condition at the outer and inner walls of the duct, and solutions were determined using reference [84]. An infinity of solutions exist for each circumferential order m. Solution $\alpha_{00} = 0$ is not included in Eq. (2.58) and corresponds to the plane wave mode. Plane waves always propagate while higher order modes propagate only above the frequency at which they are cut-on [85].

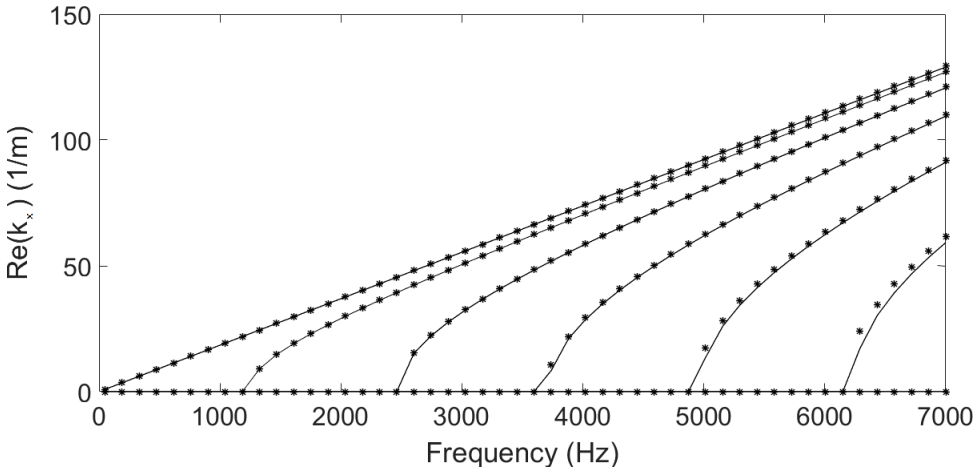

Figure 2.6. *Frequency evolution of the axial wavenumbers real parts corresponding to the forward-going waves for the case of an annular waveguide : (—) WFE method (*) Analytical method.*

2.3.2 Forced response of hard-walled ducts

We consider now a particular example of a rigid duct ended with a real impedance such that it is partially reflective (See Fig. 2.7). There are a variety of acoustic sources that can be applied to excite the system such as a pressure condition or a displacement condition.

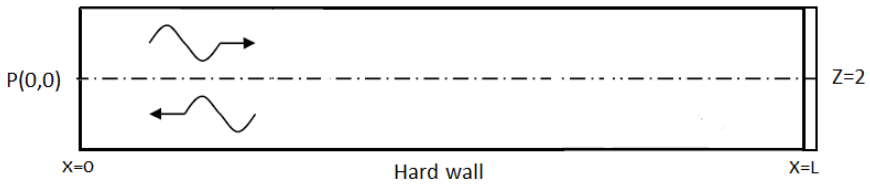

Figure 2.7. *Description of the rigid duct model.*

Here, a pressure condition is applied equally to the end nodes of the duct. This will create a plane wave, and therefore the rigid duct is used under plane wave conditions. The duct was modelled under ANSYS using the 3D element type FLUID30 with a total number of elements equal to 8000.

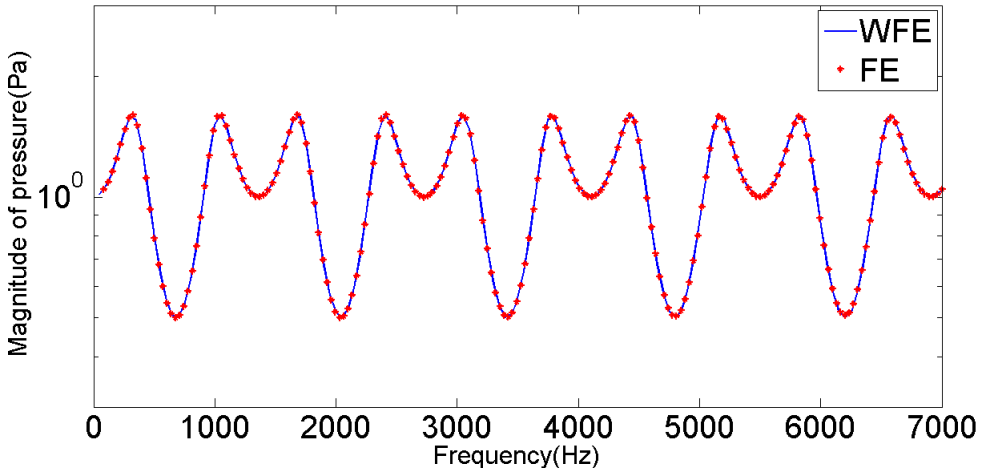

Figure 2.8. *Frequency evolution of the pressure magnitude at $x = L/2$ inside a rigid duct submitted to pressure mode $(0, 0)$ and a normalised impedance $Z = 2$ at its ends.*

This is an entirely acoustic analysis and there are no active displacement degrees of freedom. The real acoustic impedance at the end of the duct may be added using a surface load to the nodes using appropriate APDL commands [86]. The admittance is defined for the elements which have nodes at the end area. A harmonic analysis was considered and post-processing results were compared to the WFE method. The radius of the considered duct is $a = 0.02$ m. The length of the duct is $L = 0.25$ m. The magnitude of the imposed pressure $p(\omega)$ is $p_0 = 1$ Pa and the normalised acoustical impedance at the end is $Z = 2$. The forced response at $x = L/2$ is shown by Fig. 2.8.

Furthermore, the case of a duct submitted to pressures at its both ends was also studied. The same methods were used for modelling, except applying a pressure load at the second end instead of the impedance condition. Here, the acoustic sources generate acoustic plane waves from the ends, and pressures $p(\omega)$ have the same magnitudes $p_0 = 1$ Pa.
The radius of the considered duct is $a = 0.06$ m. The length of the duct is 0.32 m. The cross-sectional areas of the duct were discretised using 177 nodes, and the total number of the FLUID30 elements is 16640. The results given by the WFE in Fig. 2.9 are compared against the results generated using ANSYS.

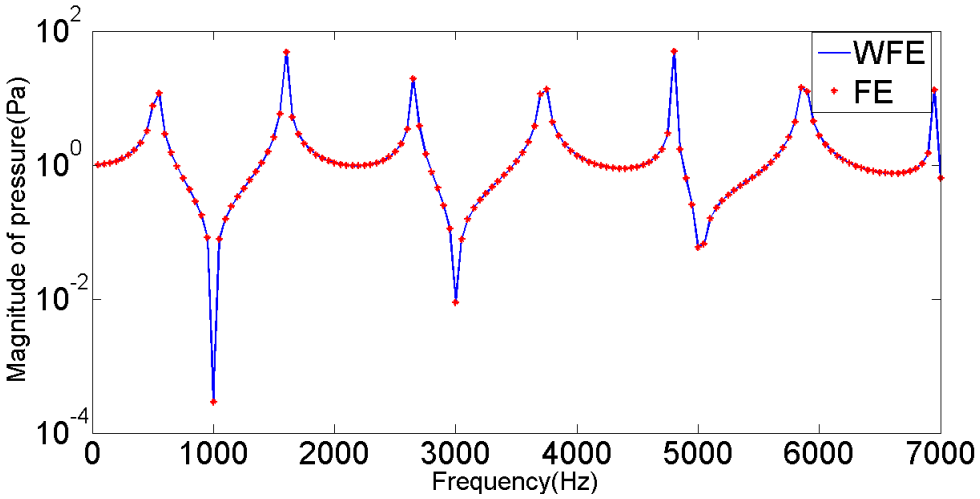

Figure 2.9. *Frequency evolution of the pressure magnitude at $x = L/2$ inside a rigid duct submitted to pressure mode $(0, 0)$ at its both ends.*

2.3.3 Forced response of lined ducts

The case of a duct having a lined part with a complex liner impedance is considered. The element SURF154 [1] is used for the lined area. These are structural elements. Therefore, any fluid elements in contact with these elements must have the displacement degrees of freedom activated.

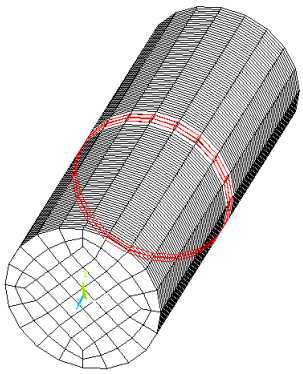

Figure 2.10. *ANSYS Finite Element model of the cylindrical duct.*

[1] This element is a surface effect element. The fluid-structure interaction flag is applied to the selected nodes on which to overlay surface effect elements.

The considered normalised impedance in this example is $Z_l = 2 - 5\mathrm{i}$. The resistance will be defined as the viscosity of the material and the reactance will be introduced within the elastic foundation stiffness with frequency dependence [86]. The element type FLUID30 is used for the internal elements. The duct was submitted to the pressure mode $(0, 0)$ at its both ends. Nevertheless, higher-order propagative modes and evanescent modes can appear due to the discontinuity of impedance. The ANSYS Finite Elements model of the duct is given in Fig. 2.10. The pressure magnitude is $p_0 = 1$ Pa for the both ends. The radius of the duct is $a = 0.06$ m. The WFE method was compared to the FE method as shown in Fig. 2.11.

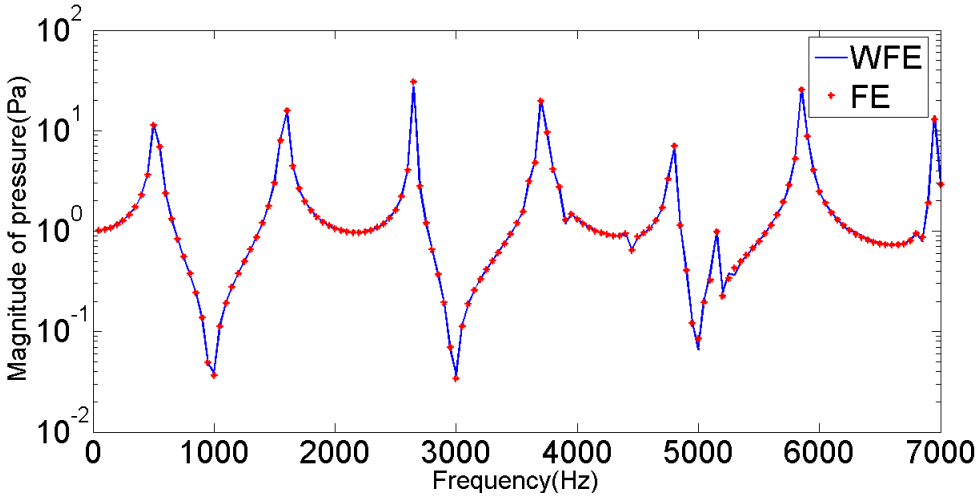

Figure 2.11. *Frequency evolution of the pressure magnitude in one point inside a cylindrical duct with a lined part submitted to pressure mode* $(0, 0)$ *at its both ends.*

The case of a cylindrical lined duct with a real termination impedance is now studied. The other end was submitted to the pressure mode $(0, 0)$ with $(p_0 = 1\mathrm{Pa})$. It is worth noting that, in the frequency domain, p_0 is the magnitude of the harmonic pressure source. The normalised impedance of the liner is $Z_l = 2 - 5\mathrm{i}$, while the normalised impedance at the end is $Z = 2$. The radius of the duct is $a = 0.06$ m. The duct was modelled using 6760 FLUID30 elements respecting the mesh sizing condition given by Eq. (2.38). The forced response using the WFE method is determined after solving Eq. (2.53). The use of the pseudo-inverse when computing the solution is necessary. This uses the singular value decomposition for the

inversion of ill-conditioned matrices [87, 88]. The obtained results are compared to results given by the FE method (See Fig. 2.12).

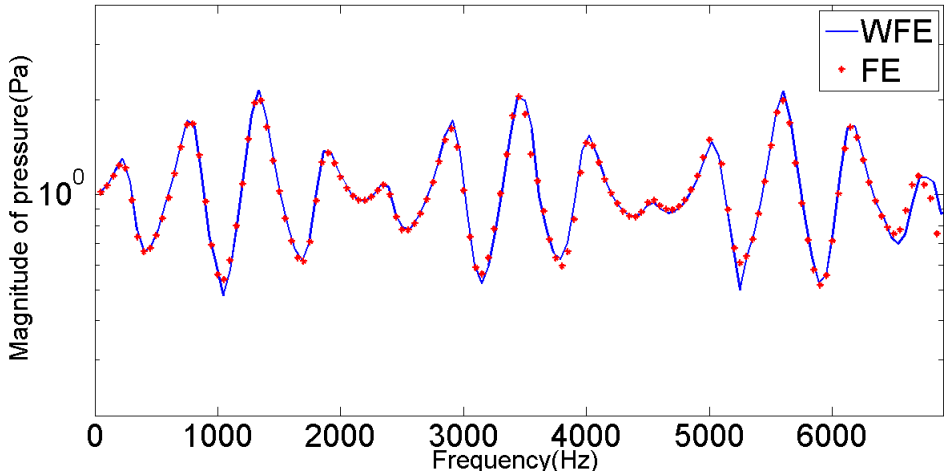

Figure 2.12. *Frequency evolution of the pressure magnitude in one point inside a cylindrical duct with a lined part submitted to pressure mode* $(0, 0)$ *and a normalised impedance* $Z = 2$ *at its ends.*

Let us model at present a duct with a lined part with a rectangular cross-section. The ANSYS Finite Elements model is given in Fig. 2.13. A segment was first modelled under ANSYS using 35 p-only FLUID30 elements.

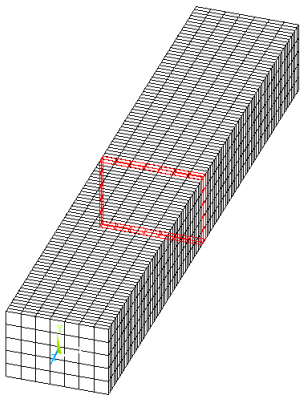

Figure 2.13. *ANSYS Finite Element model of a duct with a rectangular cross-section.*

The mass and stiffness matrices were then exported to MATLAB for post-processing. The scattering matrix was computed as done for the previous examples. A harmonic analysis was then performed under the software ANSYS from 50 Hz to 7 kHz in 50 Hz increments. This was used to calculate the acoustical pressure in a node within the duct using the FE method. The duct was submitted to pressures at its both ends to generate the plane wave mode. The magnitude of pressures $p(\omega)$ is $p_0 = 1$ Pa. The assigned normalised impedance on the lined part of the tube area is $Z_l = 2 - 5\mathrm{i}$. The cross-sectional area is 0.04×0.056 m^2. The forced response in one point inside the duct can be then represented and compared to the WFE method as shows Fig. 2.14.

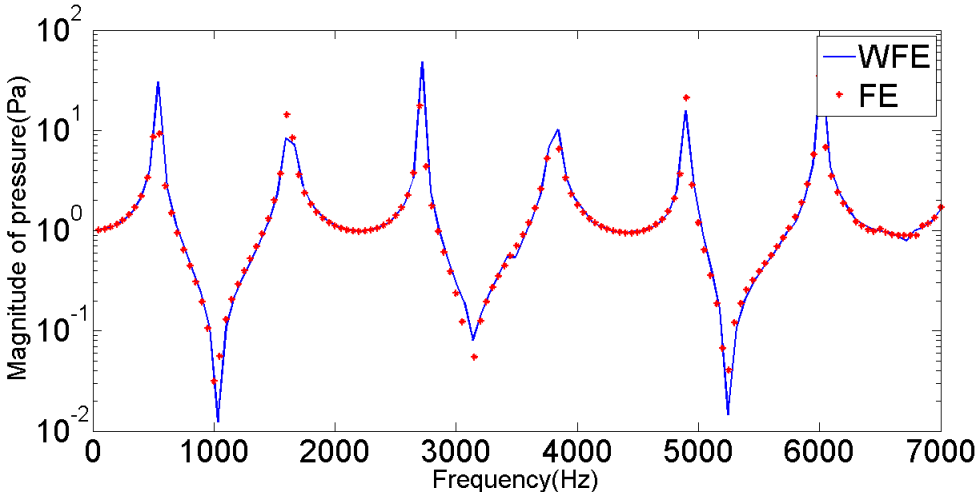

Figure 2.14. *Frequency evolution of the pressure magnitude in one point inside a duct with a lined part submitted to pressure mode* $(0, 0)$ *at its both ends.*

Comparison between the WFE method and the FE method for the forced response shows that the results obtained with the WFE method are accurate compared to the FE method, with considerably lower computational cost as we need to model only a little portion instead of the whole waveguide. Indeed, the CPU time for the WFE method depends only on the mesh density of the cross-sectional area of the duct, while for the FE method it depends also on the length of the modelled duct and increases as the length increases.
As an illustration, the elapsed computing times for the calculation of the forced response of a 0.92 m length rigid duct with both methods are summarised hereafter (Table. 2.1)

Method	CPU time	CPU time reduction percentage
FEM	545.14 s	–
WFEM	65.84 s	87,92 %

Table 2.1. *FE and WFE computing times for a* 0.92 *m length duct and for same machine capacities.*

2.3.4 Scattering coefficients of lined ducts

The scattering matrix depends only on the geometry of the characterised duct regardless of the inputs. Only transmission from one of the two sides to the other side and reflection from the lined part to one of the two sides were studied as the problem is symmetric.

Blocks $\{\mathbf{C}_{ij}\}_{i=1,2,j=1,2}$ of the scattering matrix were computed using the formulation given in 2.2.4. For the formulation given by Eq. (2.36), $\mathbf{C}_{ij}$ is a reflection matrix if $i = j$, and a transmission matrix else.

The 3D fluid elements were used for the WFE discretisation. The WFE method was compared to the analytical method model for axisymmetric waveguides given by [12] with an appropriate truncated modes number.

The following simulations were done for a lined length equal to 0.01 m for a 0.02 m diameter duct, and 0.02 m for a 0.12 m diameter duct. The normalised impedance of the liner is $Z = 2 - 5\mathrm{i}$.

The frequency evolution of the plane wave mode transmission and reflection coefficients for different duct radii is represented in Fig. 2.15 and 2.16.

Designation "of the mode $(0, 0)$" in figures titles stands for the transmission and the reflection of the same mode given by the n th diagonal term of the transmission and the reflection matrices respectively.

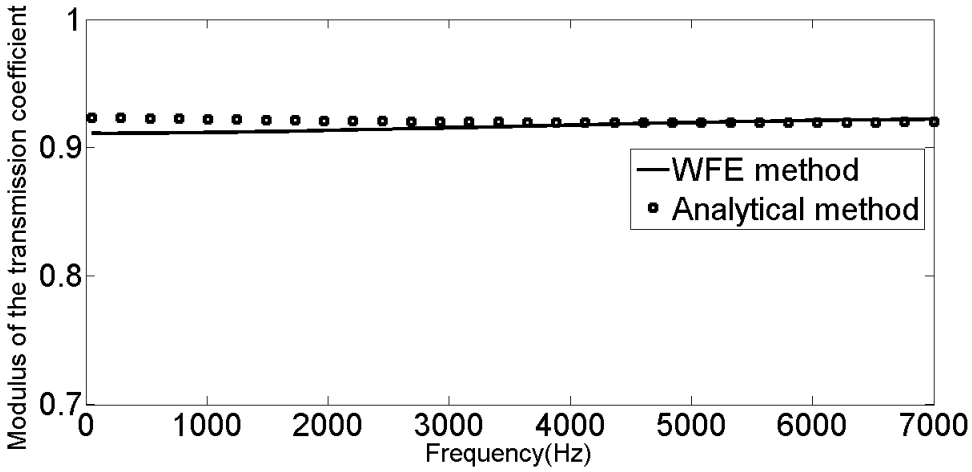

(a)

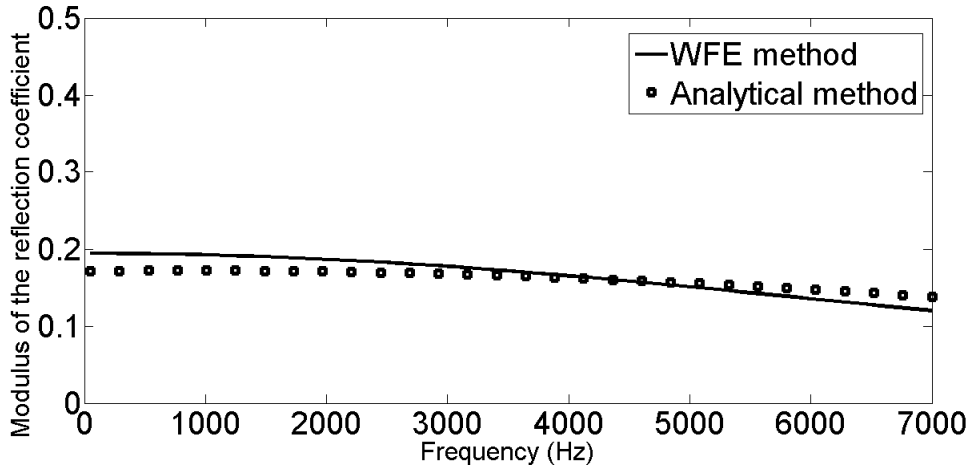

(b)

Figure 2.15. *Modulus of the transmission coefficient (a) and the reflection coefficient (b) of the mode* $(0, 0)$ *for* $Z = 2 - 5\mathrm{i}$ *and a radius* $a = 0.01$ *m.*

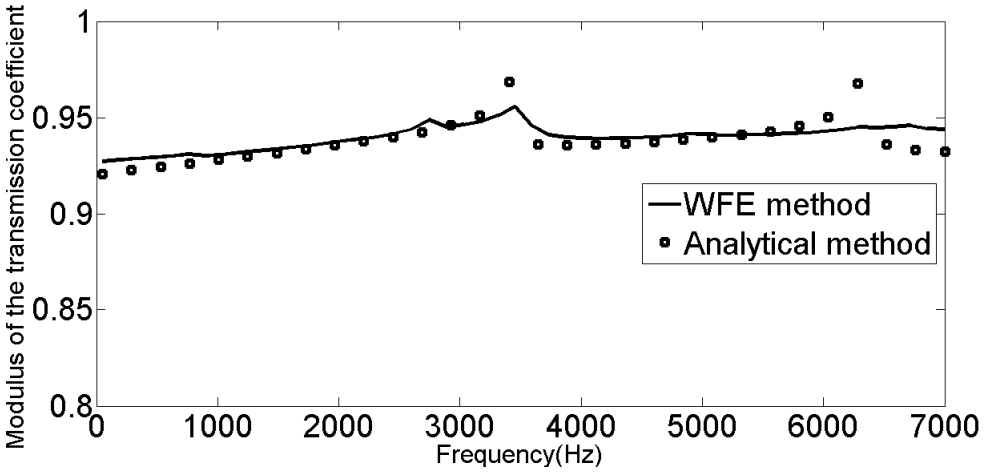

(a)

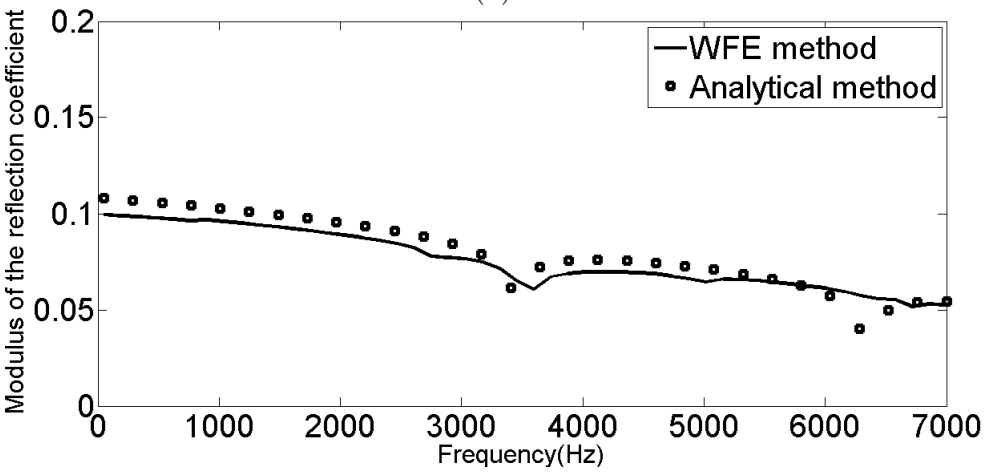

(b)

Figure 2.16. *Modulus of the transmission coefficient (a) and the reflection coefficient (b) of the mode* $(0,0)$ *for* $Z = 2 - 5\mathrm{i}$ *and a radius* $a = 0.06$ *m.*

Furthermore, transmission and reflection coefficients of two high-order modes, $(2,0)$ and $(0,1)$, are represented in Figs. 2.17 and 2.18 from their respective cut-off frequencies. For a radius $a = 0.06$ m, cut-off frequencies of modes $(2,0)$ and $(0,1)$ are 2754 Hz and 3455 Hz respectively.

Conversion between modes $(0,0)$ and $(0,1)$ is represented in Fig. 2.19, while conversion of modes $(0,0)$ and $(2,0)$ gives negligible values.

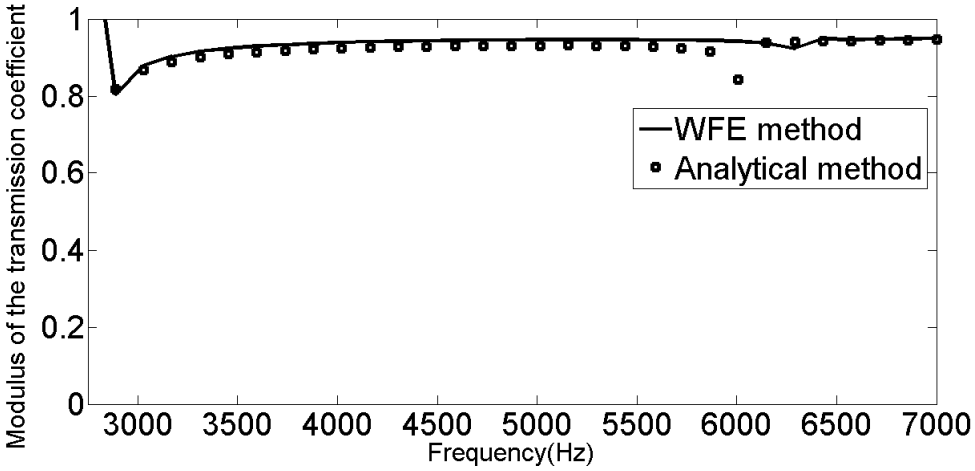

(a)

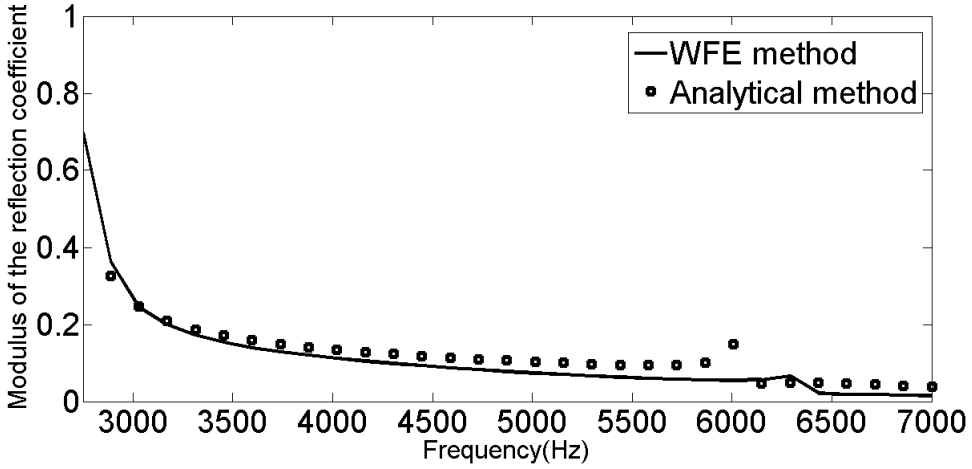

(b)

Figure 2.17. *Modulus of the transmission coefficient (a) and the reflection coefficient (b) of the mode* $(2,0)$ *for* $Z = 2 - 5\mathrm{i}$ *and a radius* $a = 0.06$ *m.*

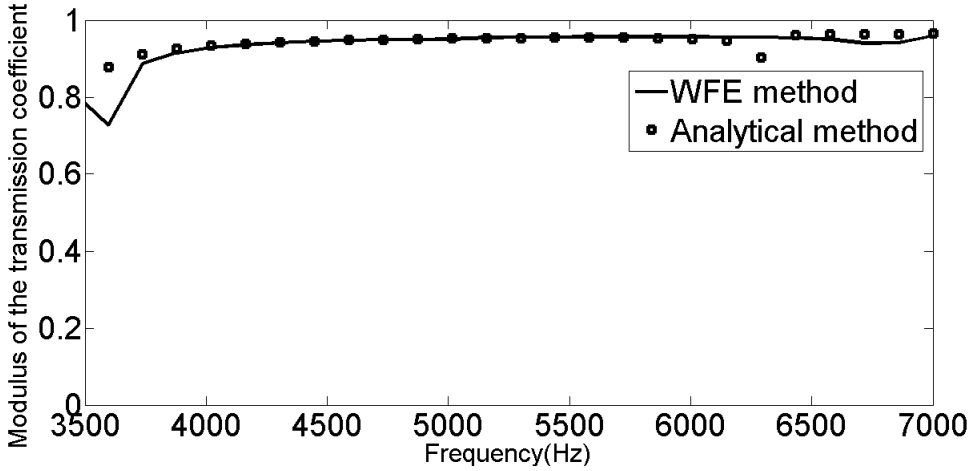

(a)

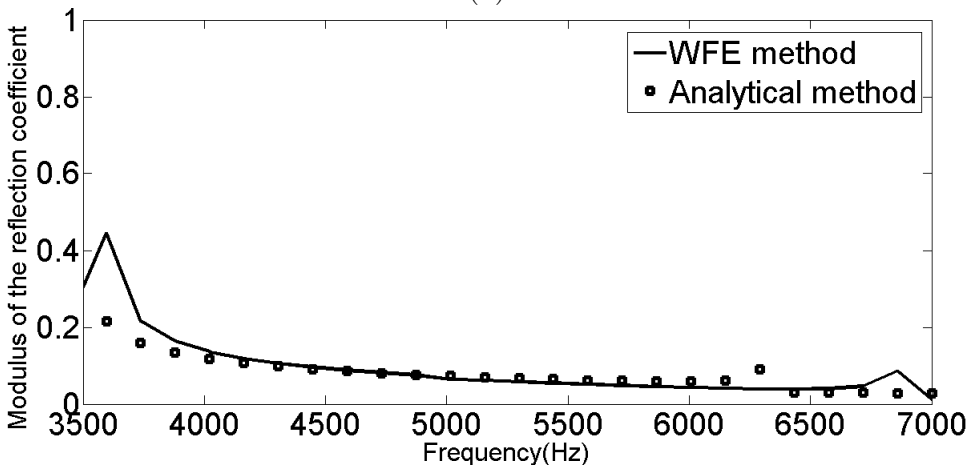

(b)

Figure 2.18. *Modulus of the transmission coefficient (a) and the reflection coefficient (b) of the mode* $(0,1)$ *for* $Z = 2 - 5\mathrm{i}$ *and a radius* $a = 0.06$ *m.*

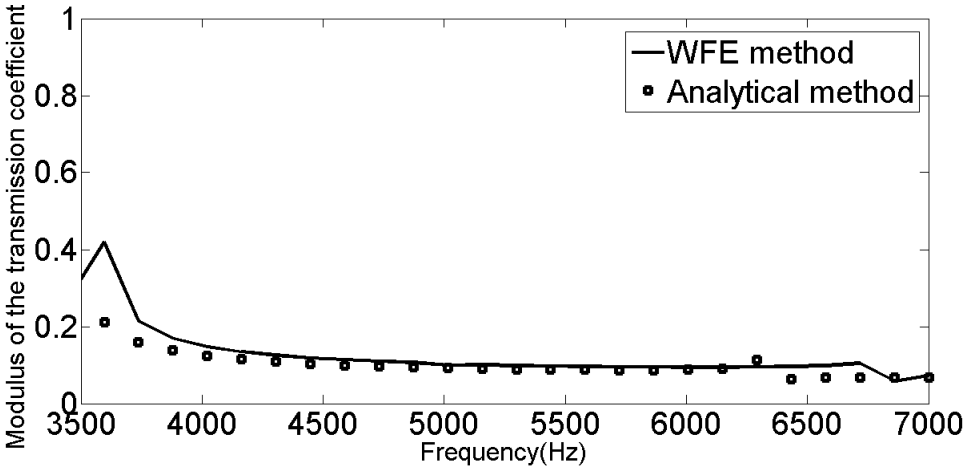

(a)

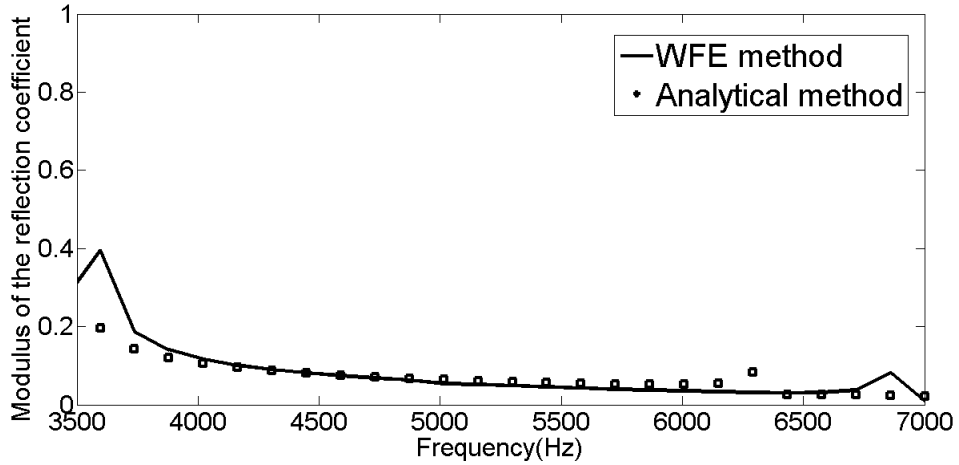

(b)

Figure 2.19. *Modulus of the transmission coefficient (a) and the reflection coefficient (b) for conversion between modes* $(0,0)$ *and* $(0,1)$ *for* $Z = 2 - 5\mathrm{i}$ *and a radius* $a = 0.06$ *m.*

Results of the analytical method and the WFE method for the transmission and reflection coefficients show a good agreement. Each incident mode reflects and transmits into a modal spectrum. However, there is no scattering into other modes with different circumferential orders because of the circumferential symmetry.

It is worth noting that numerical difficulties are more likely to occur for a larger lined length. First, the analytical method becomes prone to numerical issues caused by the evanescent part of the modes inside the lined region in the exponentially diverging terms $\mathrm{e}^{-\mathrm{i}k_j x}$, where k_j are the (complex) axial wavenumbers inside the lined duct part. Secondly, the dynamic

condensation of the matrix $\mathbf{D_c}$ will have a high computational cost since increasing the number of internal degrees of freedom makes inversion of $\tilde{\mathbf{D}}_{ii}$ time consuming.
When the lined length is large, we can consider a cascade of successive elementary scatterers instead [47]. The global scattering matrix of the segmented liner is then obtained by juxtaposition of the elementary segments using a simple composition law [47].

2.4 Conclusion

The study of the guided acoustical propagation through the use of the WFE method has been numerically validated. Eigensolutions are calculated at a particular waveguide section, then pressures and velocities can be determined at any section for the whole waveguide. The use of the Wave Finite Element Method allows the reduction of the number of elements and therefore the computational requirements. Nevertheless, it was shown that some scaling strategies have to be used to overcome numerical difficulties.
Typical configurations of the guided acoustical propagation with and without the introducing of damping due to local impedances have been studied in this chapter. Forced response to imposed boundary conditions at the ends of the waveguide was calculated through the Wave Finite Element approach and validated by the conventional Finite Element approach. The presented results correspond to amplitudes of the resulting wave, sum of the incident and the reflected waves, for different frequencies of excitation. It is shown that the resulting wave can have an amplitude much larger than the amplitude of the incident wave for some frequencies which stand for resonance frequencies, whereas modulus of the impedance imposed at the end of the waveguide determines the amplitude of the reflected wave itself. Constant values of acoustic impedances, including real positive impedances which correspond to a reflection without a change in the the phase (necessarily positive because boundary absorbs energy) and complex impedances, were considered. Until now, simple examples have been dealt with. The main goal was to validate the WFE method. However, a constant liner impedance might be way too far from being sufficiently realistic. In the following chapter, frequency dependent impedances will be rather considered, and acoustic properties of a more complete liner model will be taken into account.

Chapter 3

Numerical modelling of the acoustical multi-modal scattering of ducts with industrial liners

3.1 Introduction

When two duct parts of different properties are linked to each other, a modal representation in each part can be used. However as the modes are different for each region, the expansion of the incident field must be reformulated into an expansion of the transmitted field in the adjacent part and the reflected field using conditions of continuity of pressure and velocity. This is referred to as *mode matching*. This method is used for ducts with discontinuity, typically a change of diameter. When the duct is lined with an absorbing material that allows only sound propagation in the material normal to the wall, the material is considered as locally reacting and may be represented by a wall impedance $Z(\omega)$. The modes in the lined part are calculated using the boundary condition at the wall. Transversal wavenumbers of the lined region have to be found and axial wavenumbers are then calculated using the dispersion relation. Redon *et al.* [42], for instance, used the Newton-Raphson method to compute the roots satisfying the wall impedance boundary condition. Kirby and Denia [89] applied the same method to find roots in a porous region of a circular dissipative silencer. These methods may suffer from missing roots because they depend on initial guesses [89].

Sun *et al.* [90] proposed a method to calculate the solutions for locally and non-locally reacting liners constructing a linear homotopy and solving an ordinary differential equation using a fourth order Runge-Kutta method by varying the homotopy parameter from 0 to 1. When the duct geometry is a little more complex than a circular or a rectangular one, it is not possible to calculate transmission and reflection matrices analytically because the *mode matching* technique requires to express analytically the modes in each part prior to it [91, 92]. Therefore, finite element discretisation is preferred for arbitrary shaped cross-sections.

This chapter is devoted to the study of scattering due to honeycombs and porous liners within periodic waveguides. Locally reacting liners, namely honeycombs, are ones where sound propagation may only occur normal to the surface of the liner, which implies it is characterised only by its local impedance and is completely independent of whatever occurs elsewhere in the liner. The surface impedance of these liners will be calculated. Porous liners are Bulk reacting liners and sound can propagate in all directions. It is not always possible to represent the liner effect by an equivalent impedance, particularly for multi-modal excitation sources. Hence, we will use the three dimensional modelling of the entire porous domain. Scattering due to a change of the boundary at the wall or a change in the medium can be calculated. Acoustic power attenuation and Transmission Loss are computed too. Boundary conditions problems are dealt with and validations by the conventional methods are presented.

3.2 Sound propagation in ducts with locally reacting liners

In this section, the scattering inside ducts due to locally reacting liners is studied. The liner is composed of a micro-perforated plate, a cavity and a rigid backing plate (Fig. 3.1). The dimension of the cavities in the transversal direction is sufficiently little to remain smaller than a wavelength [93]. Waves are then assumed to travel only in the direction normal to the plates. The acoustic impedance of the liner can be calculated independently of the incidence angle. The equivalent surface impedance of the liner is given by the sum of the cavity and micro-perforated plate impedances. The impedance of the cavity can be calculated

by a simple development of the relation between the pressure and velocity inside the cavity . Empirical models are used to determine the micro-perforated plate impedance. Many of them were detailed in literature. Reader may refer to [35, 94, 95, 96, 97]. Here, the linear Guess model will be used. The acoustic velocity and the flow effects are not taken into account. Hence, the linear Guess model is supposed to describe with sufficient accuracy the MPP impedance [98].

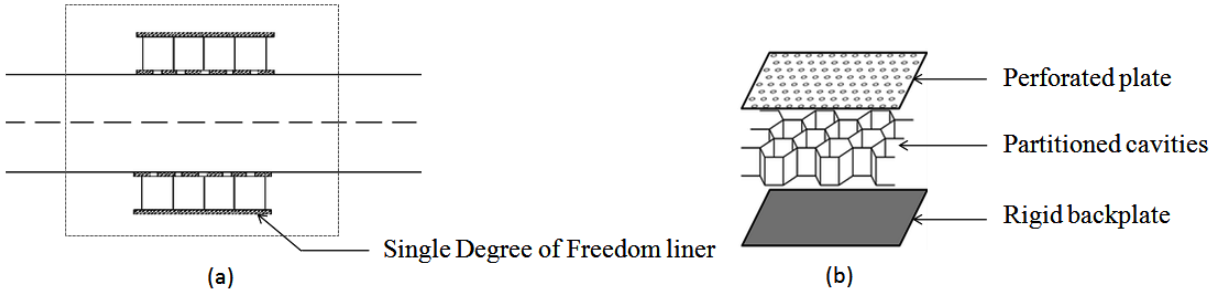

Figure 3.1. *Calculation domain (a) and composition of the liner (b).*

3.2.1 Equivalent impedance computation

- Cavity impedance:

  The pressure inside the cavity can be expressed as follows:

$$p_c(y) = A_c \mathrm{e}^{\mathrm{i}(ky-\omega t)} + B_c \mathrm{e}^{\mathrm{i}(-ky-\omega t)} \tag{3.1}$$

  k is the wavenumber, ω is the angular frequency and y is the axis normal to the plates. The velocity component following y is:

$$v_c(y) = \frac{1}{\rho_0 c}\left(A_c \mathrm{e}^{\mathrm{i}(ky-\omega t)} - B_c \mathrm{e}^{\mathrm{i}(-ky-\omega t)}\right) \tag{3.2}$$

  ρ_0 is the density of the air and c is the celerity of the sound in the air.

  Since the back of the cavity is rigid, $v_c(0) = 0$. Thus, $A_c = B_c$. Then, pressure and

velocity expressions become respectively:

$$p_c(y) = 2A_c \cos(ky)\mathrm{e}^{-\mathrm{i}\omega t} \tag{3.3}$$

$$v_c(y) = 2\mathrm{i}\frac{A_c}{\rho_0 c}\sin(ky)\mathrm{e}^{-\mathrm{i}\omega t} \tag{3.4}$$

The normalised surface impedance of the cavity is finally given by:

$$z_c = \frac{p_c(D)}{\rho_0 c v_c(D)} = -\mathrm{i}\cot(kD) \tag{3.5}$$

where D is the cavity depth.

- Micro-perforated plate impedance:

  We define the following entities:

  Medium properties:

  k: Wavenumber,

  ω: Angular frequency,

  f: Frequency,

  c: Sound celerity,

  ρ_0: Density,

  ν: Kinematic viscosity of the fluid,

  $k_s = (\mathrm{i}\omega/\nu)^{1/2}$: The Stokes wave number.

  Geometric parameters:

  e : Plate thickness,

  d : Orifice diameter,

  φ : Porosity.

  The Guess linear model detailed in [99] is given as following :

  For $ke << 1$, $kd/2 < 1/4$ and $|k_s d/2| > 10$:

$$\mathcal{R} = \frac{\sqrt{8\nu\omega}}{\varphi c}\left(1 + \frac{e}{d}\right) + \frac{1}{8\varphi}(kd)^2 \tag{3.6}$$

$$\chi = \frac{\omega}{\varphi c}\left[e + \frac{8d}{3\pi}(1 - 0.7\sqrt{\varphi}) + \sqrt{\frac{8\nu}{\omega}}\left(1 + \frac{e}{d}\right)\right] \tag{3.7}$$

$\mathcal{R}$ and χ are respectively the resistance and the reactance of the micro-perforated plate. The empirical term $(1 - 0.7\sqrt{\varphi})$ is used as a correction instead of the Fok function to express the holes interaction effect [100].

- Total equivalent impedance:

  The normalised impedance of a perforated plate backed by a cavity is the sum of impedances and is written as following [20]:

$$Z = \mathcal{R} + \mathrm{i}(\chi - \cot(kD)) \tag{3.8}$$

3.2.2 Forced response of a rigid duct ended by perforated plate and backing cavity

This section deals with the prediction of the sound pressure in a hard-walled duct. The studied medium is supposed to be periodic with a plane wave mode excitation at inlet and a perforated plate backed by a cavity at outlet as shown in Fig. 3.2. In this case, the WFE approach is used and compared to the ANSYS post-processing results (the conventional Finite Element method). In order to study the frequency response of the medium using ANSYS,

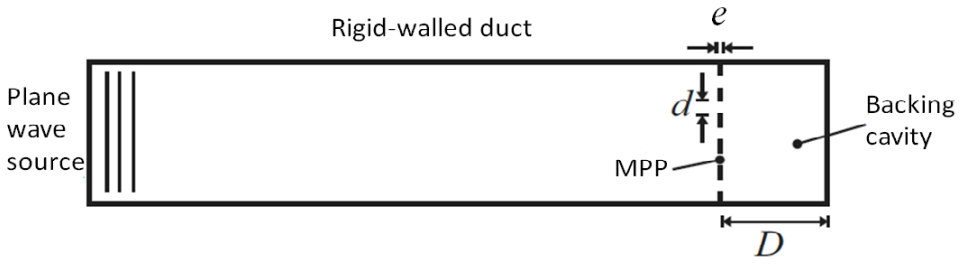

Figure 3.2. *Rigid cylindrical duct ended by a perforated plate and a backing cavity.*

the duct was discretised using the FLUID30 elements in a harmonic analysis. To introduce the termination impedance, the surface effect element SURF154 was used. Since these are

structural elements, every single fluid element in contact with the SURF154 elements must have the displacement degrees of freedom activated. The fluid-structure interaction flag is applied. All other FLUID30 elements have only the pressure degree of freedom. As the impedance is function of the frequency and reactance is less than zero for the low frequencies and greater than zero for high frequencies (Fig. 3.3), one of two ways has to be adopted for introducing the reactance, depending on the sign of the the imaginary part of the impedance. For the frequency range where the reactance is positive, the additional mass per unit area is used. Elsewhere, the elastic foundation stiffness is used. It is not possible to tabulate the real element constants. Thus, an iteration along with the solve command is issued switching between the mass or stiffness definitions following the sign of the imaginary impedance. The pressure magnitudes of the excitation are equal to 1 Pa. Since pressures are applied equally to the the nodes, the plane wave mode was generated.

The radius of the duct is 0.04 m. Length of the duct is $L = 0.24$m. The length of the segments composing the duct used for the WFE method is 0.002 m. Depth of the cavity is $D = 0.01$ m. In this example, a porosity $\varphi = 1\%$, a plate thickness $e = 0.001$ m, and a diameter of the orifices $d = 0.001$ m are considered. 19360 fluid elements were used for the FE model. The frequency evolution of the pressure magnitude in a point at $x = L/2$ is represented in Fig. 3.4.

Parameter	**Value**
Air	
Celerity of sound	340 m/s
Density	1 kg/m^3
Duct	
Radius	0.04 m
Length	0.24 m
Honeycomb	
Porosity	1 %
MPP thickness	0.001 m
Orifices diameter	0.001 m
Cavity depth	0.01 m

Table 3.1. *Summary of the parameters used for the rigid duct ended by a honeycomb structure.*

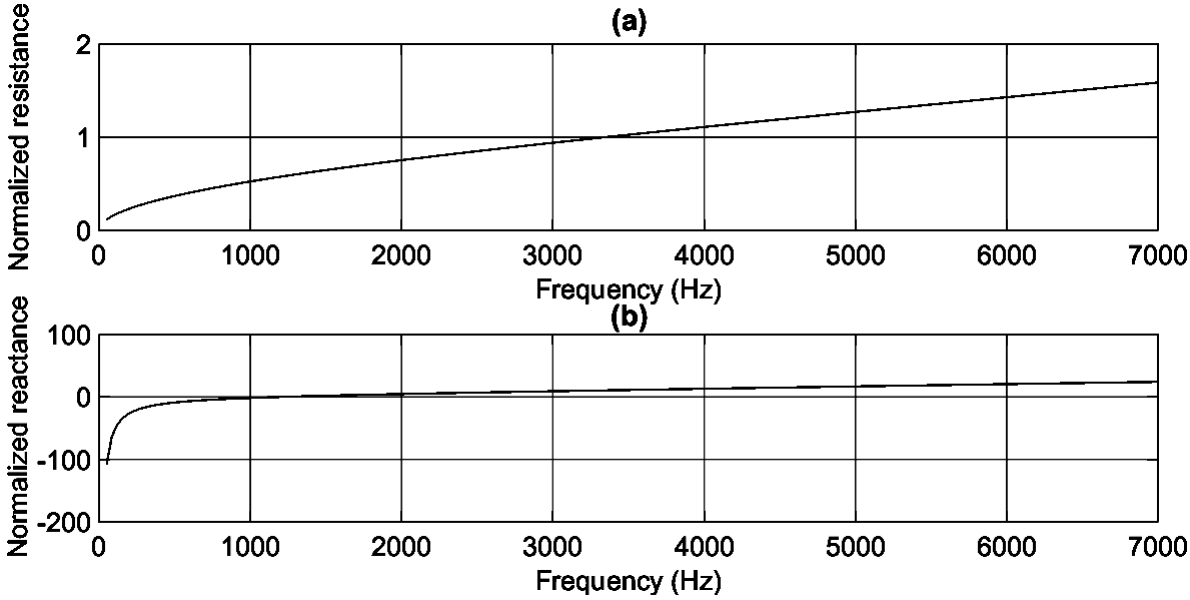

Figure 3.3. *Normalised resistance (a) and normalised reactance (b) at the end of the duct computed using the linear Guess model.*

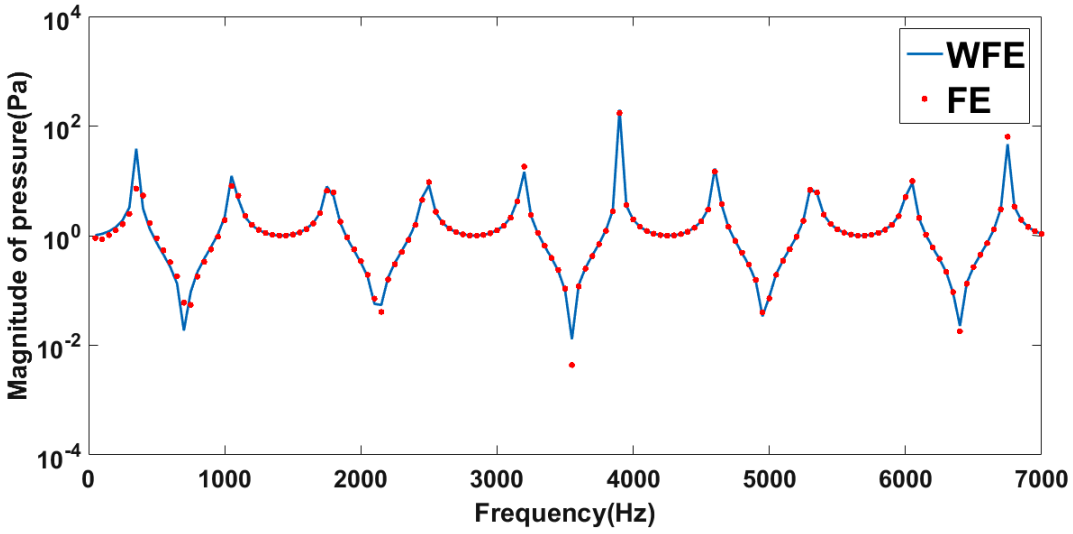

Figure 3.4. *Frequency evolution of the pressure magnitude in one point within a rigid duct submitted to the mode (0,0) and ended by a perforated plate and a backing cavity: (—)WFE method (...)FE method.*

3.2.3 Scattering of lined ducts

- ***Scattering coefficients***

This section deals with the evaluation of scattering coefficients for periodic ducts with impedance discontinuity. We consider a cylindrical duct (see Fig. 3.5). The study was performed up to 8000 Hz for a diameter 0.16 m, and a lined length 0.015 m. 24 modes are cut-on at maximal frequency (See axial wavenumbers in Fig. 3.6), and highest frequency at which only plane wave mode propagates is $\approx$ 1245 Hz. The lined part represents the discontinuity within the duct.

We consider: a porosity φ=3%, a perforated plate thickness $e = 10^{-3}$ m, holes diameter $d = 10^{-3}$ m and a cavity depth $D = 10^{-2}$ m. The frequency evolution of the liner impedance is represented in Fig. 3.7.

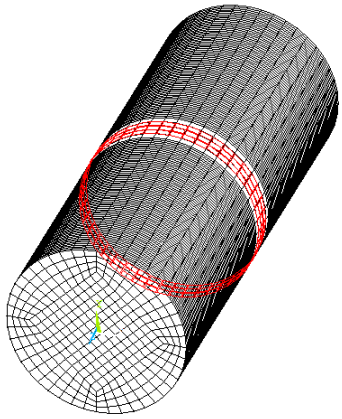

Figure 3.5. *ANSYS Finite Element model of the cylindrical duct with a lined part.*

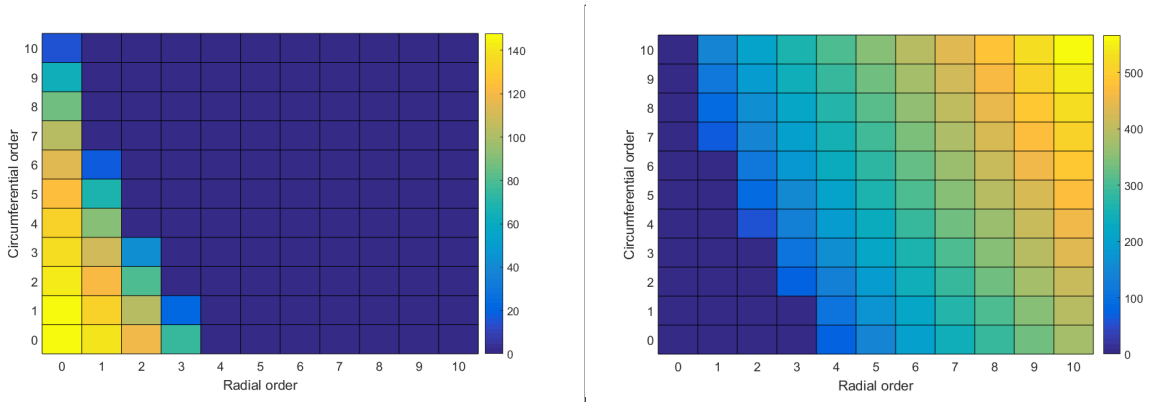

(a) (b)

Figure 3.6. *Axial wavenumbers in the rigid duct part at simulation's maximal frequency: (a)Real part (b)Imaginary part.*

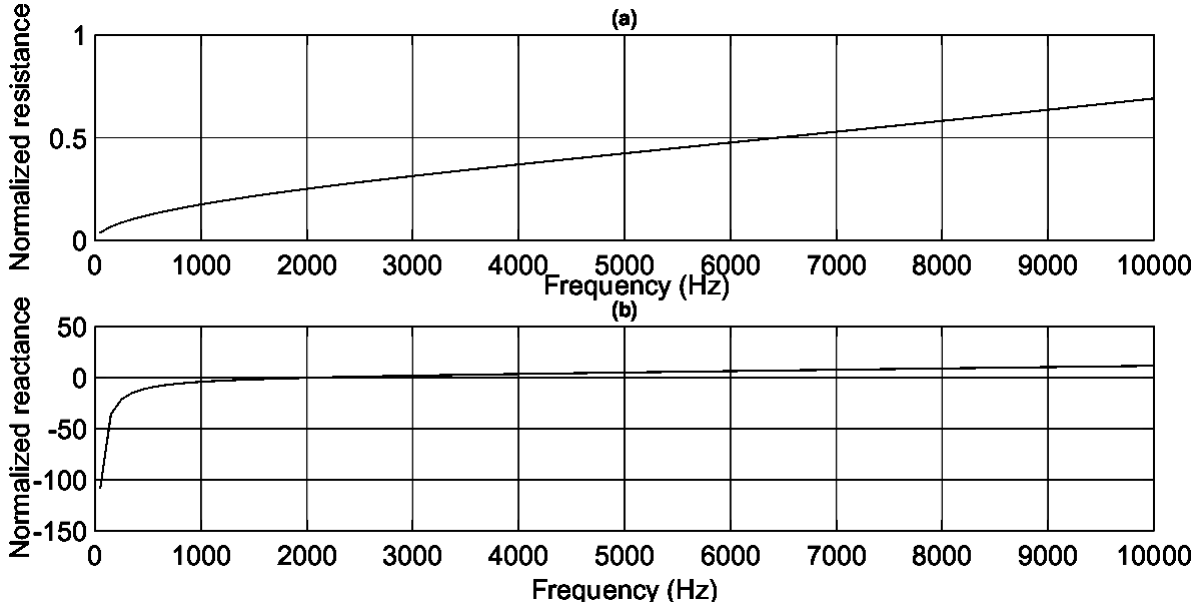

Figure 3.7. *Normalised resistance (a) and normalised reactance (b) of the liner computed using the linear Guess model.*

The cross-section's mesh includes 364 degrees of freedom. The length of segments used for the WFE discretisation is 0.002 m and 3D fluid elements are used. The scattering matrix was also computed for validation using the analytical method as was detailed in [12] with a sufficiently truncated modes number.

Parameter	Value
Air	
Celerity of sound	340 m/s
Density	1 kg/m^3
Duct	
Radius	0.08 m
Lined length	0.015 m
Honeycomb	
Porosity	3 %
MPP thickness	0.001 m
Orifices diameter	0.001 m
Cavity depth	0.01 m

Table 3.2. *Summary of the parameters used for the duct lined with a honeycomb structure.*

Frequency evolution of the scattering coefficients can be then represented for different modes (m, i) by both methods, where m and i stand for the circumferential and radial mode orders respectively. Letters $'T'$ and $'R'$ denote transmission and reflection respectively. Fig. 3.8 shows the transmission and reflection coefficients moduli of the mode (0,0).

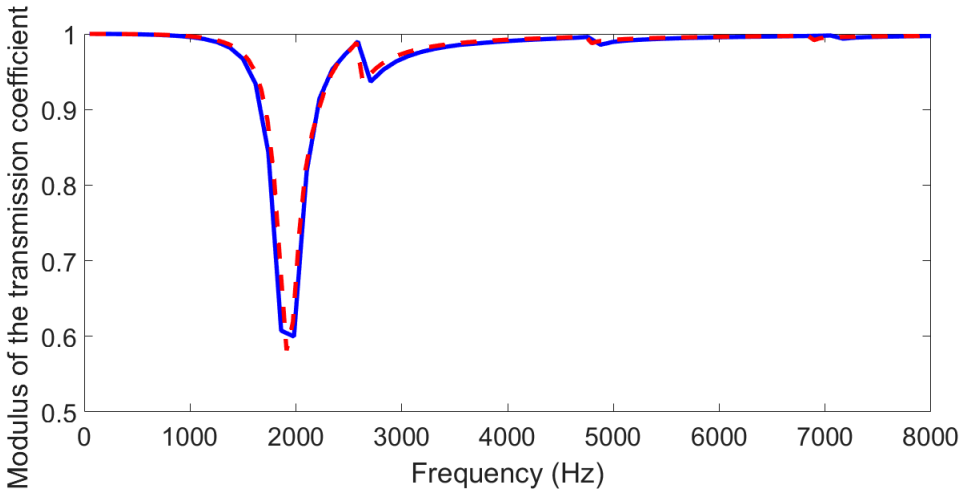

(a)

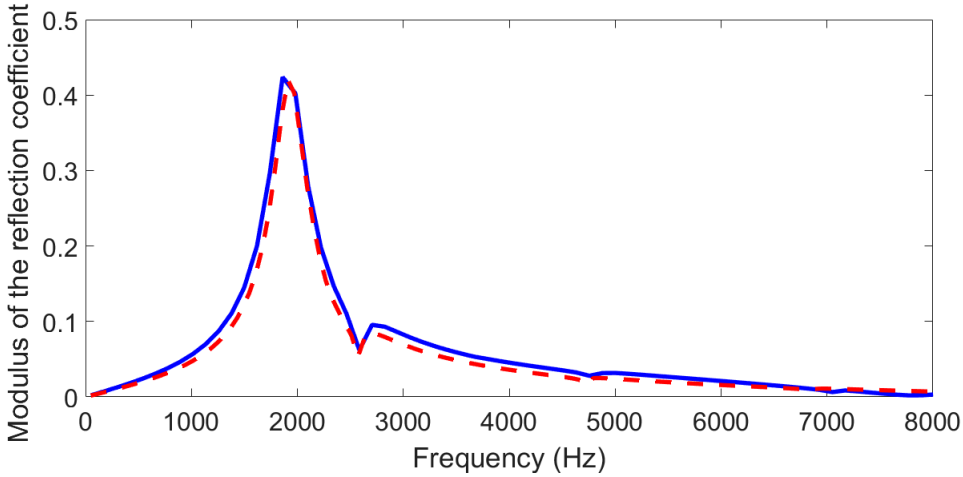

(b)

Figure 3.8. *Frequency evolution of the transmission coefficient* $T((0,0),(0,0))$ *(a) and the reflection coefficient* $R((0,0),(0,0))$ *(b) . (—)WFE method (- - -) Analytical method.*

Scattering of higher orders modes was moreover studied. Fig. 3.9 shows the transmission and reflection coefficients moduli of mode (2,0) from its cut-off frequency. Fig. 3.10 represents the transmission and reflection coefficients moduli of mode (0,1) from its cut-off frequency.

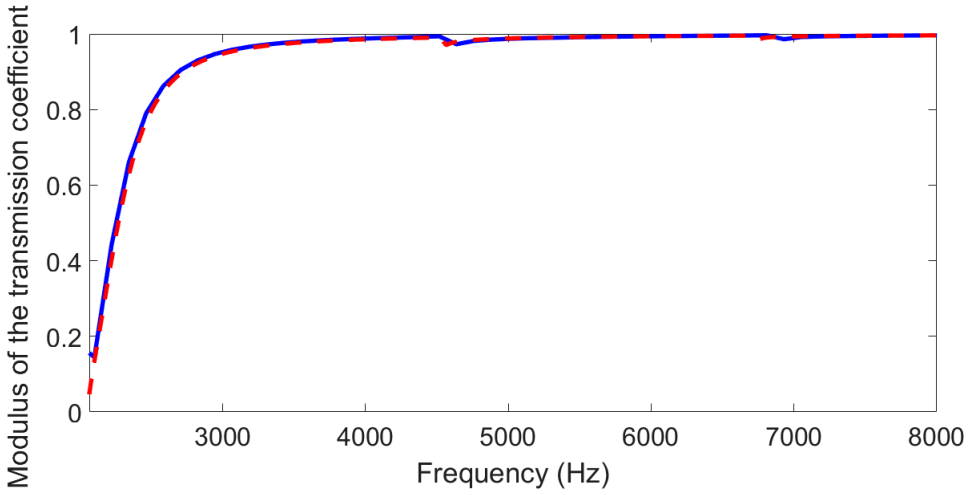

(a)

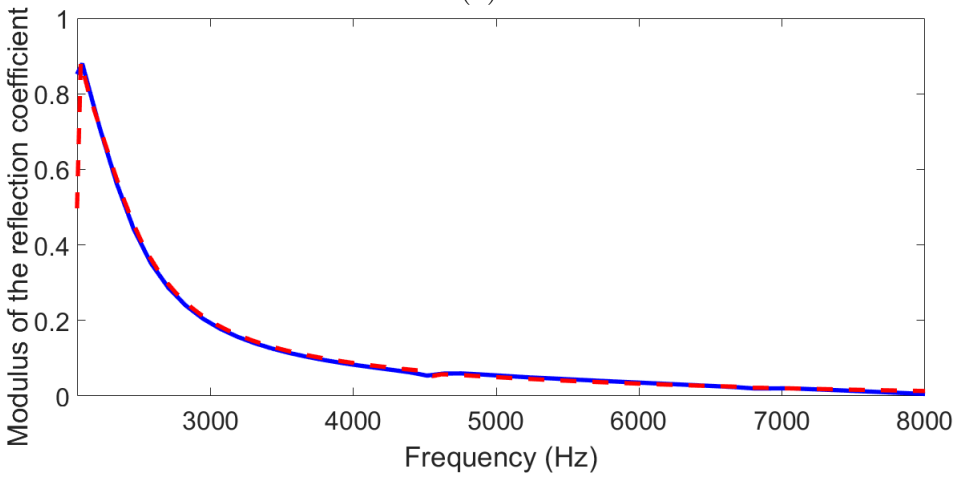

(b)

Figure 3.9. *Frequency evolution of the transmission coefficient* $T((2,0),(2,0))$ *(a) and the reflection coefficient* $R((2,0),(2,0))$ *(b). (—)WFE method (- - -) Analytical method.*

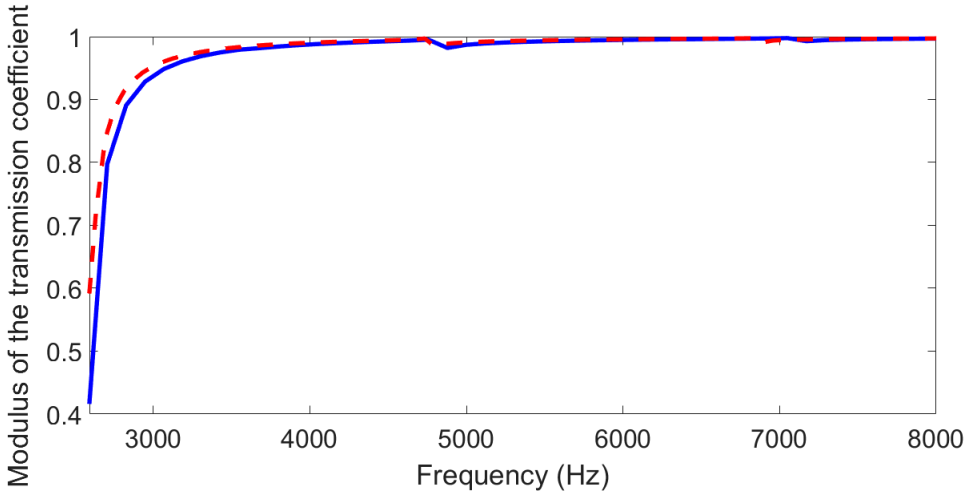

(a)

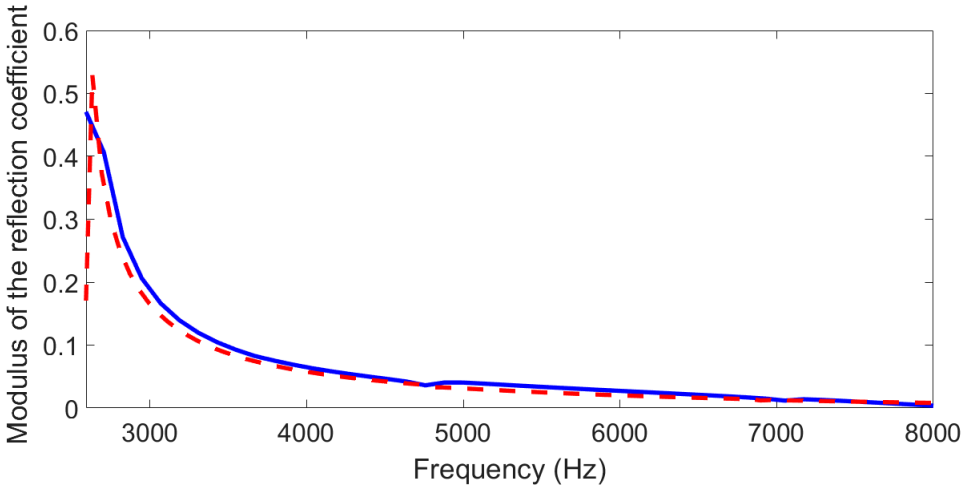

(b)

Figure 3.10. *Frequency evolution of the transmission coefficient* $T((0,1),(0,1))$ *(a) and the reflection coefficient* $R((0,1),(0,1))$ *(b). (—)WFE method (- - -) Analytical method.*

Because of the circumferential symmetry of the duct, there is no scattering from a mode into another mode with different m order. Therefore, only modes with same circumferential order exchange energy.

Conversion coefficients correspond to the off-diagonal terms of the transmission and reflection matrices. Fig. 3.11 represents the conversion of the plane wave mode with mode $(0,1)$. Other validations of the conversion between modes $(2,0)$ and $(2,1)$ are shown in Fig. 3.12.

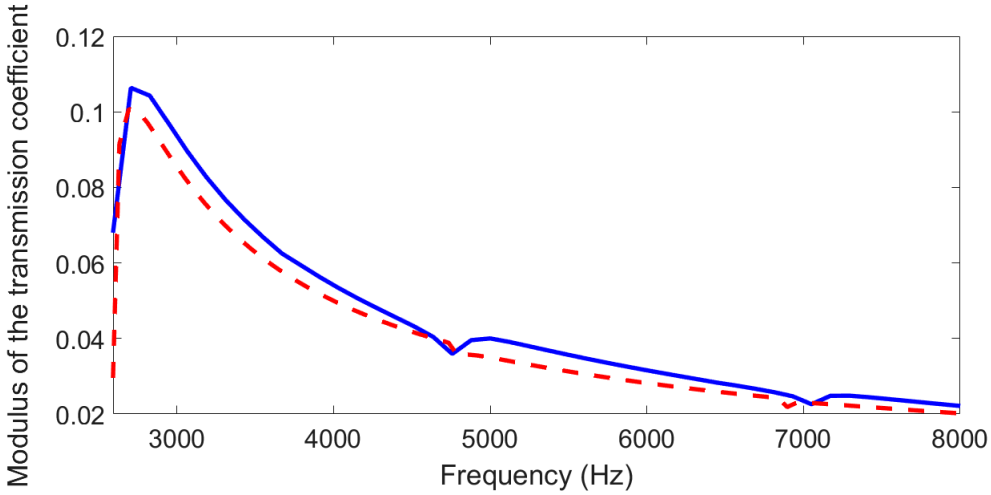

(a)

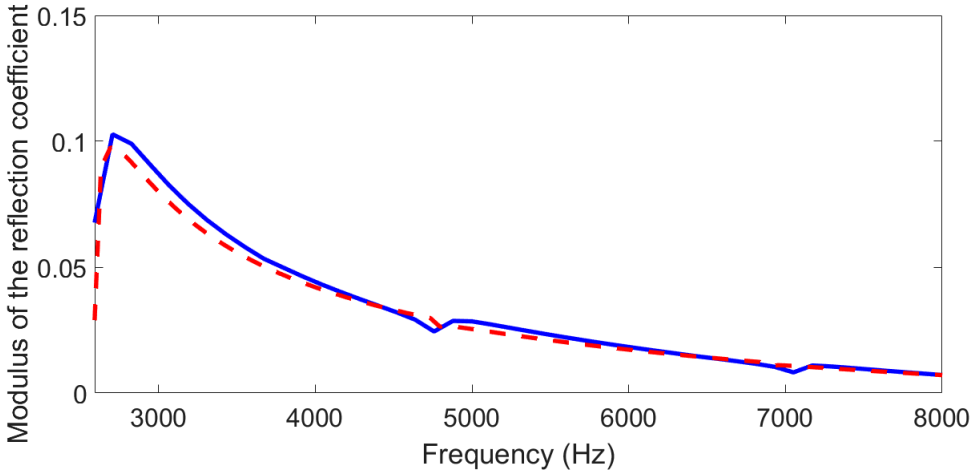

(b)

Figure 3.11. *Frequency evolution of the transmission coefficient* $T((0,0),(0,1))$ *(a) and the reflection coefficient* $R((0,0),(0,1))$ *(b). (—)WFE method (- - -) Analytical method.*

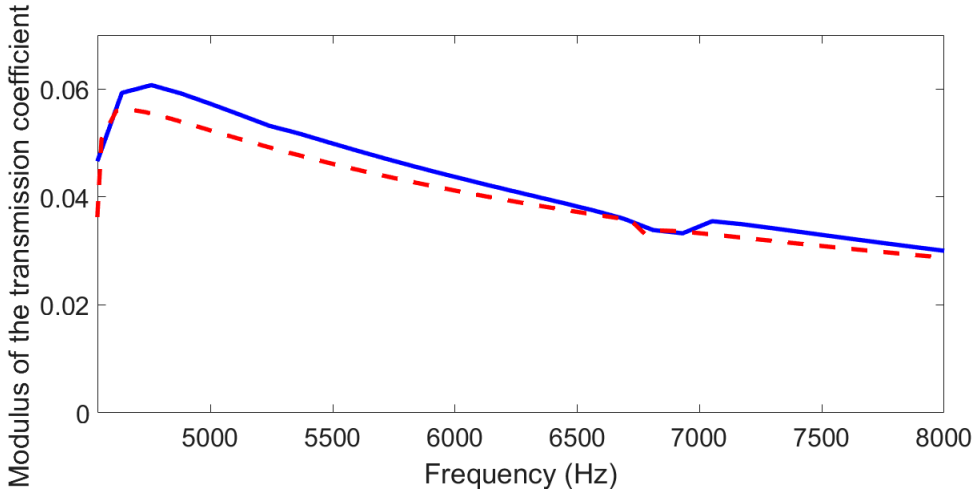

(a)

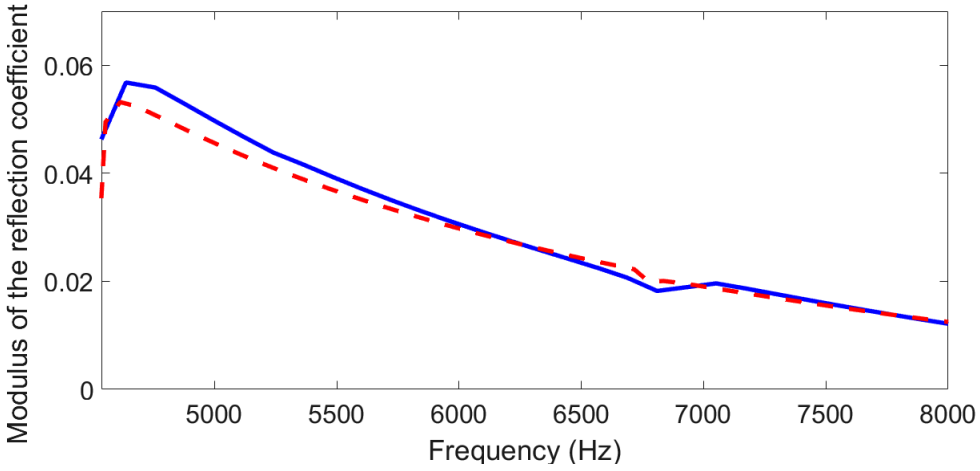

(b)

Figure 3.12. *Frequency evolution of the transmission coefficient* $T((2,0),(2,1))$ *(a) and the reflection coefficient* $R((2,0),(2,1))$ *(b). (—)WFE method (- - -) Analytical method.*

The figures show a fair agreement between the WFE method and the analytical method. It is also noted from Figs. 3.11 and 3.12 that conversion between the m-modes exists and is maximal for the frequencies at which they become cut-on. This result matches well the slight changes of the curves shapes in Figs. 3.8 and 3.9 near the cut-off frequencies of the higher order modes.

It is also shown from the previous results that the scattering coefficients for liners made of honeycombs depend highly on frequency. Maximal reflection is reached when the impedance

is purely resistive . Honeycombs are designed to absorb sound in a particular frequency range. Therefore, variation of the geometric parameters affects the liner performances.

- ***Effect of the geometric parameters on the liner efficiency***

The liner efficiency can be evaluated through the calculation of the acoustic power attenuation. In this section, the effect of the geometric parameters on the liner efficiency is studied by varying one of the parameters at a time and leaving the others unchanged. The effects of the porosity, thickness of the perforated plate and holes diameter are discussed. The acoustic power attenuation W_{att} can be calculated from the scattering matrix as described below [101, 102]:

$$W_{att} = 10\log(\frac{W_{in}}{W_{out}}) \tag{3.9}$$

W_{in} refers to as the incident acoustic power, and is given in this case as follows:

$$W_{in} = (\mathbf{P}^{inc})^h \mathbf{Y} \mathbf{P}^{inc} \tag{3.10}$$

where $\mathbf{P}^{inc} = \left\langle ...P_{mi}^{(1)+}..., ...P_{mi}^{(2)-}... \right\rangle^t$ is the vector of modal pressures incident to the left and right duct sections, h denotes the conjugate transpose and $\mathbf{Y}$ is the diagonal matrix defined such as:

$$\mathbf{Y} = \begin{pmatrix} \mathbf{Y}_{11} & \mathbf{0} \\ \mathbf{0} & \mathbf{Y}_{22} \end{pmatrix} \tag{3.11}$$

with $\mathbf{Y}_{11}$ and $\mathbf{Y}_{22}$ are the diagonal matrices with $(N_{mi}k_{mi})/(2\rho_0\omega)$ on the diagonals. N_{mi} are the coefficients associated with the (m, i) (m stands for the circumferential mode order, and i is the radial mode order) mode defined for a cylindrical duct as [103] :

$$N_{mi} = \pi a^2 J_m^2(\chi_{mi}) \left(1 - \frac{m^2}{\chi_{mi}^2}\right) \tag{3.12}$$

and $N_{00} = 1$, where a is the radius of the duct, J_m is the Bessel function of the first kind of order m and χ_{mi} is the i^{th} root satisfying the hard wall boundary condition: $J_m^{'}(\chi_{mi}) = 0.$. W_{out} corresponds to the outgoing acoustic power from the left and right duct sections. In the present work, the incident modes are assumed to have random initial phases. In this case,

W_{out} is given as following [104]:

$$W_{out} = (\mathbf{P}^{inc})^h diag(\mathbf{C}^h \mathbf{Y} \mathbf{C}) \mathbf{P}^{inc} \tag{3.13}$$

$\mathbf{C}$ is the scattering matrix defined in Eq. (2.37).

When calculating the Transmission Loss, the expression of the the incident acoustic power $W_{in}^{(1)}$ becomes [105]:

$$W_{in}^{(1)} = (\mathbf{P}_1^{inc})^h \mathbf{Y}_{11} \mathbf{P}_1^{inc} \tag{3.14}$$

with $\mathbf{P}_1^{inc} = \left\langle ... P_{mi}^{(1)+} ... \right\rangle^t$ is the vector of modal pressures incident to the left duct section. Taken into consideration the random phases assumption, the transmitted acoustic power $W_{out}^{(2)}$ is given by [104]:

$$W_{out}^{(2)} = (\mathbf{P}_1^{inc})^h diag(\mathbf{T}^h \mathbf{Y}_{11} \mathbf{T}) \mathbf{P}_1^{inc} \tag{3.15}$$

Here, $\mathbf{T}$ stands for the transmission matrix. The Transmission Loss TL is finally given by:

$$TL = 10 \log \left(\frac{W_{in}^{(1)}}{W_{out}^{(2)}} \right) \tag{3.16}$$

Figs. 3.13, 3.14 and 3.15 show the effect of the porosity, plate thickness and holes diameter on the acoustic power attenuation, respectively. Figs. 3.16, 3.17 and 3.18 show the effect of the porosity, plate thickness and holes diameter on the Transmission Loss, respectively.

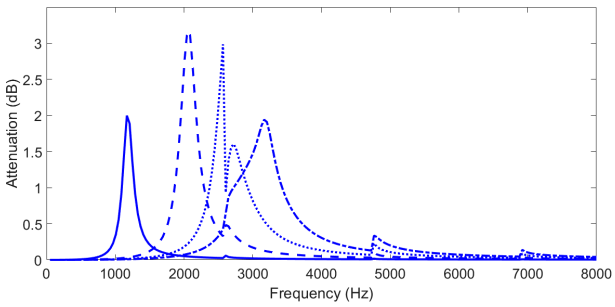

Figure 3.13. *Effect of the porosity φ of the perforated plate on the acoustic power attenuation of the lined duct part (–):$\varphi = 1\%$; (- -):$\varphi = 3\%$; (. . .):$\varphi = 5\%$; (- . -):$\varphi = 7\%$.*

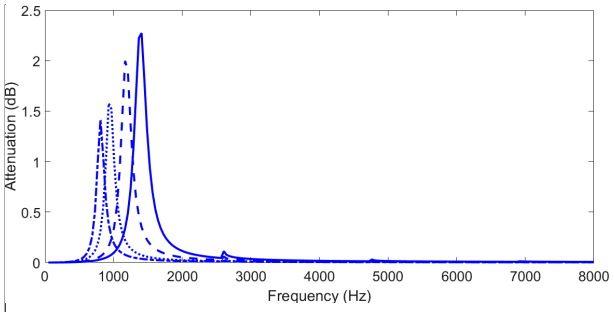

Figure 3.14. *Effect of the thickness e of the perforated plate on the acoustic power attenuation of the lined duct part (–): $e = 0.5.10^{-3}$ m ; (- -):$e = 1.10^{-3}$ m ; (. . .):$e = 2.10^{-3}$ m ; (- . -):$e = 3.10^{-3}$ m.*

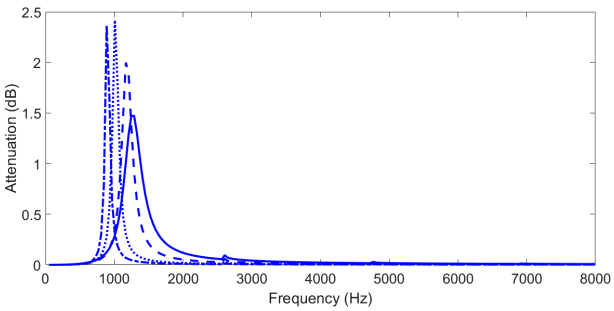

Figure 3.15. *Effect of the diameter d of orifices of the perforated plate on the acoustic power attenuation of the lined duct part (–): $d = 0.5.10^{-3}m$; (- -):$d = 1.10^{-3}$ m ; (. . .):$d = 2.10^{-3}m$; (- . -):$d = 3.10^{-3}$ m.*

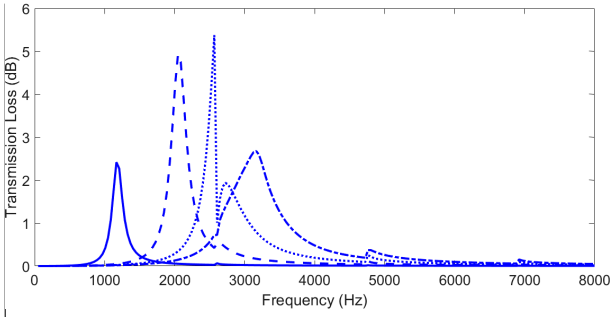

Figure 3.16. *Effect of the porosity φ of the perforated plate on the Transmission Loss of the lined duct part (–):$\varphi = 1\%$; (- -):$\varphi = 3\%$; (. . .):$\varphi = 5\%$; (- . -):$\varphi = 7\%$.*

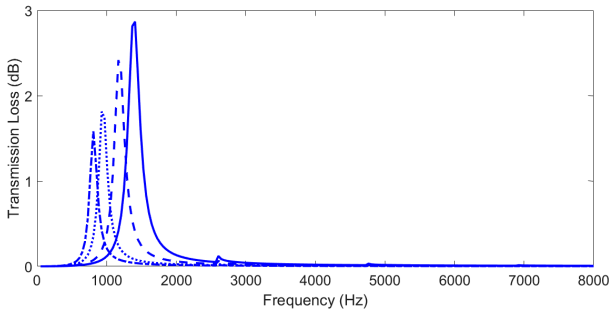

Figure 3.17. *Effect of the thickness e of the perforated plate on the Transmission Loss of the lined duct part (–): $e = 0.5.10^{-3}$ m ; (- -):$e = 1.10^{-3}$ m ; (. . .):$e = 2.10^{-3}$ m ; (- . -):$e = 3.10^{-3}$ m.*

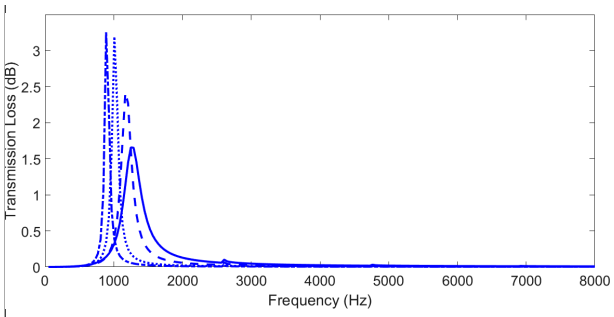

Figure 3.18. *Effect of the diameter d of orifices of the perforated plate on the Transmission Loss of the lined duct part (–): $d = 0.5.10^{-3}m$; (- -):$d = 1.10^{-3}$ m ; (. . .):$d = 2.10^{-3}m$; (- . -):$d = 3.10^{-3}$ m.*

It has been already shown that the frequency of maximal attenuation and maximal attenuation itself depend on the geometric parameters of the liner. The attenuation is maximal when the liner's impedance is purely resistive. Decreasing the perforated plate thickness and increasing the orifices diameter lead to an increase of the maximal attenuation. The frequency of maximal attenuation is shifted to the higher frequencies when porosity increases, and decreases when plate thickness and orifices diameter increase. Furthermore, as expected, it is noted that Transmission Losses are greater than attenuations. This is a predictable consequence as Transmission Loss of the acoustic power includes reflection as well as absorption,

contrarily to the attenuation which only characterises the absorption by the liner.

3.3 Sound propagation in ducts with porous lining

This section deals with the porous liners case. The surface impedance of a porous material is dependent on the mode incidence angle, and an expression of the impedance can be only calculated per mode of propagation [106]. Thus, it is more convenient to use the three dimensional modelling of the entire porous domain rather than using the equivalent surface impedance of the wall. The frame of the porous medium is assumed to be rigid, and the Johnson-Champoux-Allard equivalent fluid model is therefore used.

3.3.1 Equivalent fluid model of porous materials

Assuming that the frame of the porous medium is rigid, the porous material can be defined using the Johnson-Champoux-Allard equivalent fluid model, which uses the complex effective density and velocity. The wave equation is written as following [107]:

$$\boldsymbol{\nabla}^2 p + \omega^2 \frac{\tilde{\rho}}{\tilde{K}} p = 0 \tag{3.17}$$

where $\tilde{\rho}$ and $\tilde{K}$ are respectively the effective density and effective bulk modulus and are given as:

$$\tilde{\rho}(\omega) = \frac{\sigma\varphi}{\mathrm{i}\omega}\left[1 + \frac{4\mathrm{i}\alpha_\infty^2 \eta\omega\rho_0}{\varphi^2\Lambda^2\sigma^2}\right]^{1/2} + \rho_0\alpha_\infty \tag{3.18}$$

and

$$\tilde{K}(\omega) = \frac{P_0\gamma}{\gamma - (\gamma-1)\left[\dfrac{8\eta}{\mathrm{i}\omega\rho_0 P_r \Lambda'^2}\left(1 + \dfrac{\Lambda'^2 \mathrm{i}\omega\rho_0 P_r}{16\eta}\right)^{1/2} + 1\right]^{-1}} \tag{3.19}$$

where σ is the fluid resistivity (ratio of the static pressure difference to the product of the velocity and the thickness of the porous sample), φ is the porosity (ratio of the volume of fluid contained in the pores to the total volume of the material), α_∞ is the tortuosity (ratio of the

length of the pore path to the distance between two pore points), η is the dynamic viscosity, ρ_0 is the density of the fluid, Λ is the viscous characteristic length (high frequency viscous and inertial effects introduced by Johnson [108]), $\Lambda^{'}$ is the thermal characteristic length (thermal exchanges between the material frame and the pore saturating fluid introduced by Champoux and Allard [109]), P_0 is the static reference pressure, γ is the ratio of specific heats at respectively constant pressures and volumes defined as $\gamma = C_p/C_v$, and P_r is the Prandtl number [110].

It is worth noting that $\tilde{\rho}$ and $\tilde{K}$ are complex and frequency dependent. The equivalent density and equivalent bulk modulus are related to the effective density and effective bulk modulus respectively by:

$$\rho_e = \frac{\tilde{\rho}}{\varphi} \tag{3.20}$$

$$K_e = \frac{\tilde{K}}{\varphi} \tag{3.21}$$

The sound celerity in the equivalent fluid c_e is given by:

$$c_e = \sqrt{\frac{K_e}{\rho_e}} \tag{3.22}$$

The complex wavenumber in the equivalent fluid model k_e is then expressed as follows[111]:

$$k_e = \frac{\omega}{c_e} = \omega\sqrt{\frac{\tilde{\rho}}{\tilde{K}}} \tag{3.23}$$

Further, the mass and stiffness elementary matrices $\mathbf{M^e}$ and $\mathbf{K^e}$ are respectively given by:

$$\mathbf{M^e} = \int\int\int_{\Omega^e} \frac{1}{\tilde{\rho}c_e^2}\mathbf{N}\mathbf{N^t}\mathrm{d}v \tag{3.24}$$

$$\mathbf{K^e} = \int\int\int_{\Omega^e} \frac{1}{\tilde{\rho}}[\boldsymbol{\nabla}\mathbf{N}]^\mathbf{t}[\boldsymbol{\nabla}\mathbf{N}]\mathrm{d}v \tag{3.25}$$

where $\mathbf{N}$ is the column vector of shape functions N_i, $[\boldsymbol{\nabla}\mathbf{N}]$ is the matrix of vectors $\boldsymbol{\nabla}N_i$ and Ω^e is the volume domain of a single element.

The surface impedance $Z_s(\theta_j)$ of the equivalent fluid is given as follows [112]:

$$Z_s(\theta_j) = -\mathrm{i}Z_c \frac{k_e}{k_{e,n}} \cot(k_{e,n} d_e) \tag{3.26}$$

where $Z_c = (1/\varphi)\tilde{\rho} c_e$ is the characteristic impedance of the equivalent fluid, d_e is the thickness of the equivalent fluid, and $k_{e,n}$ is the component of wavenumber k_e in the direction normal to the walls and is given by:

$$k_{e,n} = \sqrt{k_e^2 - \left(\frac{\omega}{c} \sin\theta_j\right)^2} \tag{3.27}$$

with θ_j is the incidence angle of the jth mode and is expressed as:

$$\theta_j = \arccos\left(\sqrt{1 - \left(\frac{f_j^c}{f}\right)^2}\right) \tag{3.28}$$

f_j^c is the cut-off frequency of the mode. The reflection coefficient from the porous layer to the medium is further given by:

$$R_j = \frac{Z_s \cos\theta_j - \rho_0 c}{Z_s \cos\theta_j + \rho_0 c} \tag{3.29}$$

3.3.2 Forced response of rigid ducts with a porous layer termination

In the current section, response of guided waves incident to porous interfaces is explored. Let us consider a rigid duct ended by a porous material layer. The porous material layer is backed by a rigid wall. The pressure amplitudes were first computed by the WFE method. Two alternatives are here used:

(1) Replacing the porous layer by an equivalent acoustic impedance as in Eq. (3.26). The reflection is calculated, and therefore a reflection condition is defined as a boundary condition at the end of the duct.

(2) Three dimensional modelling of the porous domain, i.e. solution provided by the full FE model of the lining using Eqs. (3.24) and (3.25) (See Fig. 3.19).

- ***FE modelling of the porous material***

The porous domain was discretised using cubic elements and linear interpolation functions. The differentials of the shape functions with respect to x, y and z are expressed using differentials with respect to the natural coordinates [77], and elementary mass and stiffness matrices of the equivalent fluid are calculated. The matrices are finally assembled.

- ***Boundary conditions expression***

The continuity of pressures and velocities at the interface air-equivalent fluid leads to:

$$\begin{pmatrix} \mathbf{\Phi_p}^{inc}\mathbf{Q}^{inc(N+1)} + \mathbf{\Phi_p}^{ref}\mathbf{Q}^{ref(N+1)} \\ \mathbf{\Phi_v}^{inc}\mathbf{Q}^{inc(N+1)} + \mathbf{\Phi_v}^{ref}\mathbf{Q}^{ref(N+1)} \end{pmatrix} = \begin{pmatrix} \mathbf{p}_l \\ -\mathbf{v}_l \end{pmatrix} \tag{3.30}$$

where superscript (i) refers to the i^{th} cross section of the rigid duct part, N is the number of segments composing the air-filled waveguide, $\mathbf{\Phi_p}$ and $\mathbf{\Phi_v}$ refer respectively to the pressure and velocity block components of the matrix of eigenvectors calculated by the WFE eigenproblem, $\mathbf{p}_l$ and $\mathbf{v}_l$ are pressures and velocities vectors corresponding to the left surface of the equivalent fluid.
The boundary conditions expressions finally yield the following system allowing the calculation of amplitudes $\mathbf{Q}^{inc(1)}$ and $\mathbf{Q}^{ref(1)}$:

$$\begin{cases} \boldsymbol{\mu}^{-N}\mathbf{Q}^{ref(1)} = -(\mathbf{D^{e*}}\mathbf{\Phi_p}^{ref} + \mathbf{\Phi_v}^{ref})^{-1}(\mathbf{D^{e*}}\mathbf{\Phi_p}^{inc} + \mathbf{\Phi_v}^{inc})\boldsymbol{\mu}^{N}\mathbf{Q}^{inc(1)} \\ \\ \mathbf{\Phi_p}^{inc}\mathbf{Q}^{inc(1)} + \mathbf{\Phi_p}^{ref}\mathbf{Q}^{ref(1)} = \mathbf{p}_0 \end{cases} \tag{3.31}$$

where $\mathbf{D^{e*}}$ is the dynamic stiffness matrix of the equivalent fluid condensed onto its left side (See Appendix C), $\mathbf{p}_0$ is the vector of imposed pressure and $\boldsymbol{\mu}$ is the diagonal matrix of eigenvalues corresponding to the incident modes.

- ***Validation by FEM***

The WFE results were then compared to the FE solution of the harmonic analysis for the entire duct model carried out by ANSYS. The Johnson-Champoux-Allard model is activated for the porous material and the physical constants are input. It is worth noting that implementation in the ANSYS 14.5 release uses the effective terms as defined in Eqs. (3.18) and

(3.19) and is not what a user would expect, as one should normally solve for the equivalent terms (divided by porosity) [86].

A hard-walled duct with a 0.056 m×0.04 m rectangular cross section was considered. Thickness of the porous layer is 0.01m. The properties of the porous material are: $\sigma = 10000$ N.s/m^4, $\varphi = 0.88$, $\alpha_\infty = 1$, $\Lambda = 129.10^{-6}$ m and $\Lambda' = 198.10^{-6}$ m. Figs. 3.20 and 3.21 show the frequency evolution of the pressure amplitude in one point inside the duct submitted to the (0,0) and (1,1) modes respectively. For the case of excitation by the mode (1,1), the forced response was presented from 5000 Hz, since the wave is evanescent for the lower frequencies.

Parameter	**Value**
Air	
Celerity of sound	340 m/s
Density	1 kg/m^3
Duct	
Width	0.056 m
Height	0.04 m
Porous	
Layer depth	0.01 m
Resistivity	10000 N.s/m^4
Porosity	0.88
Tortuosity	1
Viscous characteristic length	129.10^{-6} m
Thermal characteristic length	198.10^{-6} m

Table 3.3. *Summary of the parameters used for the rigid duct ended by the porous layer.*

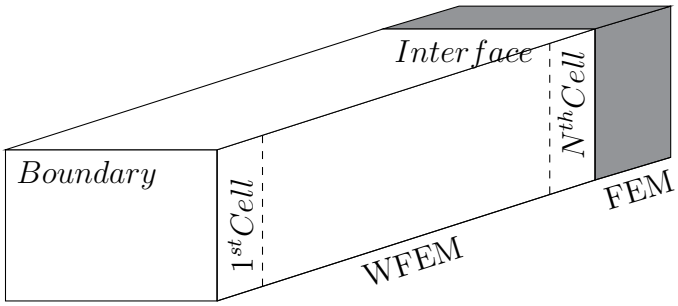

Figure 3.19. *Description of the Boundary Conditions problem.*

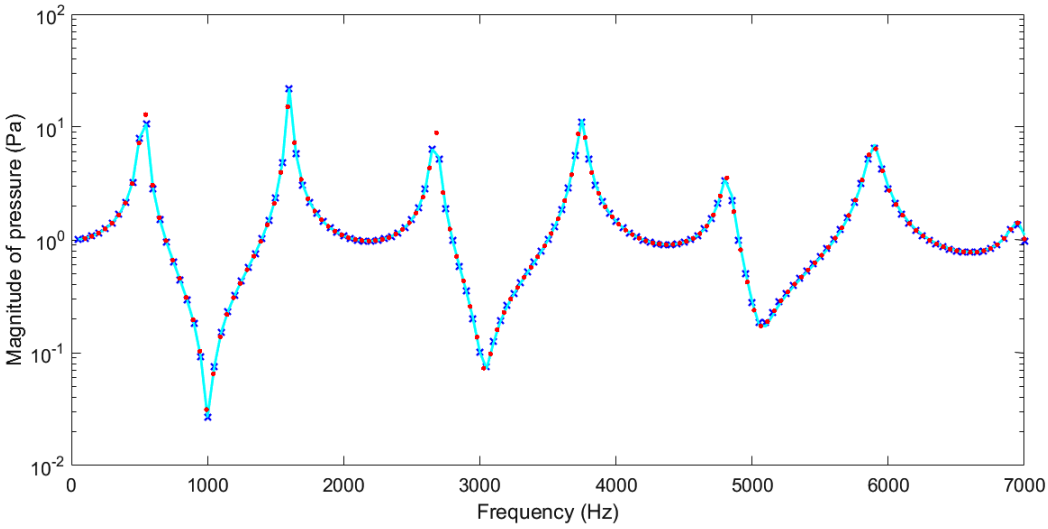

Figure 3.20. *Frequency evolution of the pressure magnitude in one point within a rigid duct submitted to the mode (0,0) and ended by a porous layer : (×) WFE method+equivalent impedance; (—) WFE method+FE boundary; (.) FE method.*

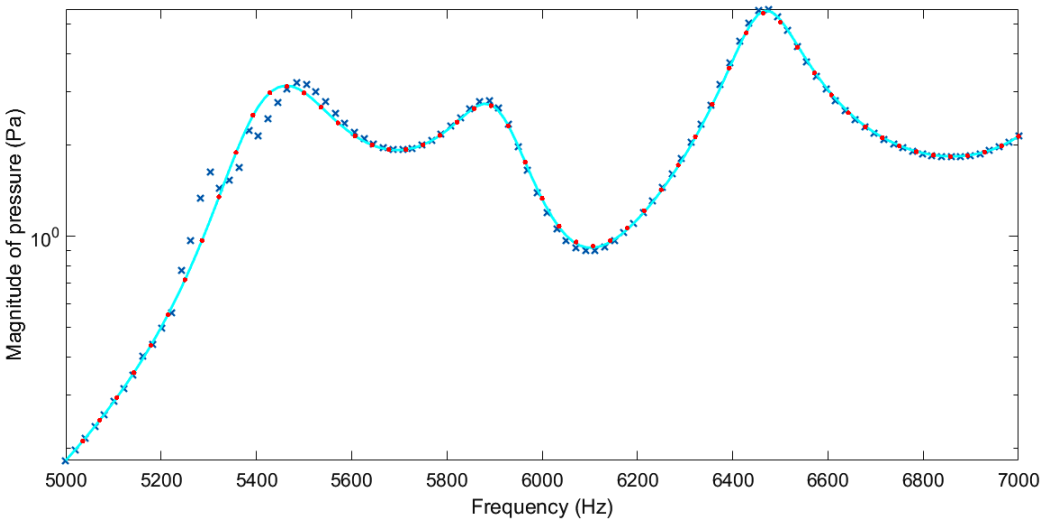

Figure 3.21. *Frequency evolution of the pressure magnitude (from cut-off frequency) in one point within a rigid duct submitted to the mode (1,1) and ended by a porous layer : (×) WFE method+equivalent impedance ; (—) WFE method+FE boundary ; (.) FE method.*

The above presented figures show a good agreement between the FE results provided by the commercial software ANSYS and the proposed method. Furthermore, Fig. 3.21 shows that some numerical issues could occur at particular frequencies when using the condition of reflection by the equivalent impedance as defined in Eq. (2.40). Use of the FE model of the porous material through the system (3.31) is beneficial to avoid the numerical singularities.

3.3.3 Acoustic scattering of a hard walled-porous domain transition in ducts

In this section, the scattering from a porous layer inside a duct is studied. Let us consider the waveguide presented in Fig. 3.22. The porous medium is defined using the Johnson-Champoux-Allard model. The elementary mass and stiffness matrices are assembled to obtain the matrices of the porous part. The dynamic stiffness matrix of the porous domain is calculated and condensed onto its left and right ends. Then, the scattering matrix is expressed as in Eq. (2.37). The forced response is first calculated through the equations provided by the WFE method [30]. The results are then compared to the full FE analysis by ANSYS.

Dimensions of the cross section of the above-mentioned waveguide are 0.056 m×0.04 m. Depth of the porous layer is 0.015 m. Same constants of the porous material equivalent fluid model considered in the previous section were used. Figs. 3.23 and 3.24 show the pressure magnitudes for a duct submitted to the pressure mode (0,0) at both ends, and a duct submitted to the pressure mode (0,0) and ended by rigid wall, respectively.

Parameter	**Value**
Air	
Celerity of sound	340 m/s
Density	1 kg/m^3
Duct	
Width	0.056 m
Height	0.04 m
Porous	
Layer depth	0.015 m
Resistivity	10000 N.s/m^4
Porosity	0.88
Tortuosity	1
Viscous characteristic length	129.10^{-6} m
Thermal characteristic length	198.10^{-6} m

Table 3.4. *Summary of the parameters used for the duct with a hard walled-porous domain transition.*

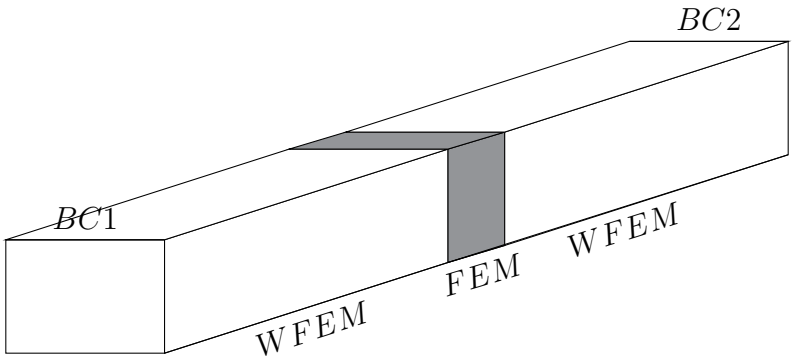

Figure 3.22. *Description of the approach used to the study of the scattering by a porous medium inside the duct.*

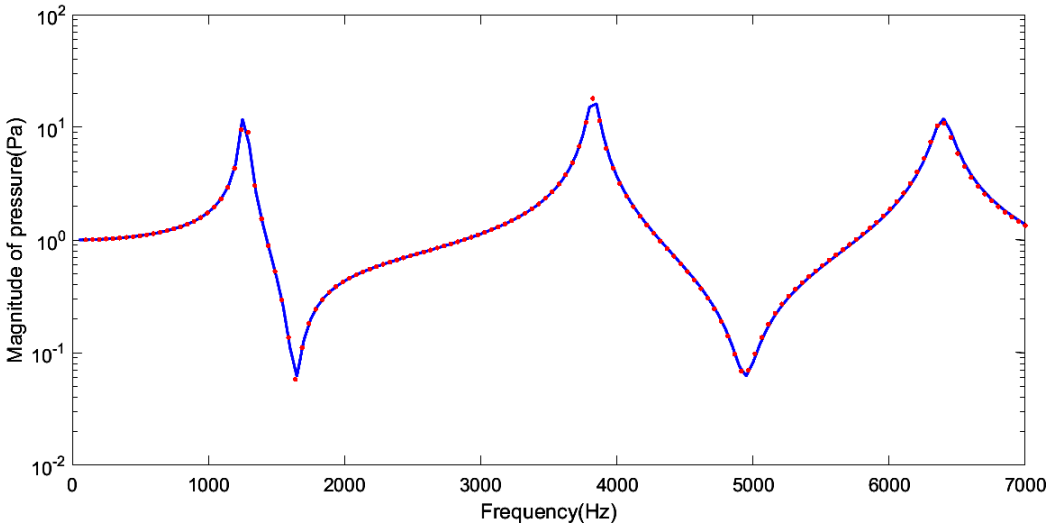

Figure 3.23. *Frequency evolution of the pressure magnitude in one point within a duct submitted to the mode (0,0) at both ends : (—) WFE method; (.) FE method.*

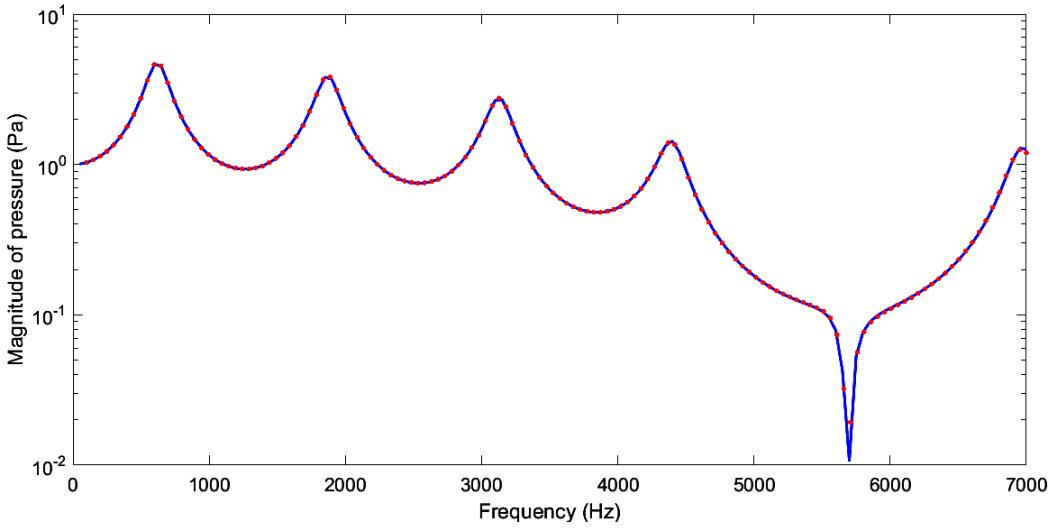

Figure 3.24. *Frequency evolution of the pressure magnitude in one point within a duct submitted to the mode (0,0) and ended by a rigid wall : (—) WFE method; (.) FE method.*

3.4 Conclusion

In this chapter, the acoustical scattering of honeycombs liners was first studied using an equivalent surface impedance representation at the walls. An empirical frequency-dependent

impedance model was used. Damping due to the acoustic impedance was added for the lined duct walls. Then, the scattering of porous materials was studied through a hybrid WFE/FE method. An equivalent fluid model was used for the FE discretisation of the scatterer. The proposed approach benefits from the coupling of the WFE method for the rigid parts and the FE method for the lined parts. This allows the study of the scattering due to heterogeneity of the media when it can not be represented by a local impedance. At this stage, propagation in the presence of fluid flow has not yet been studied. In the next chapter, the acoustical propagation inside periodic waveguides with uniform mean flow will be investigated.

Chapter 4

Characterisation of guided acoustical propagation with mean flow

4.1 Introduction

Ducts are usually lined with sound absorbing materials to reduce noise levels. A practical example is the inlet of an aircraft engine [2, 46]. The impedance boundary condition allows the determination of the modes travelling in the lined duct. However, mean flow effects in ducts can not be neglected (Fig. 4.1). Duct modes are in this case obtained by resolution of the convected Helmholtz equation with respect to the boundary condition.

This chapter is devoted to the study of the guided acoustical propagation with a uniform mean flow. The convected Helmholtz equation is solved. The boundary conditions of the lined duct are expressed, and the acoustic fields are derived. The weak variational formulation of the problem is presented. Results of applying the WFE method to the convected acoustical propagation inside periodic waveguides are compared to the analytical ones. Although following is a simplification because a uniform flow is supposed, it can still be an important model of a real lined duct .

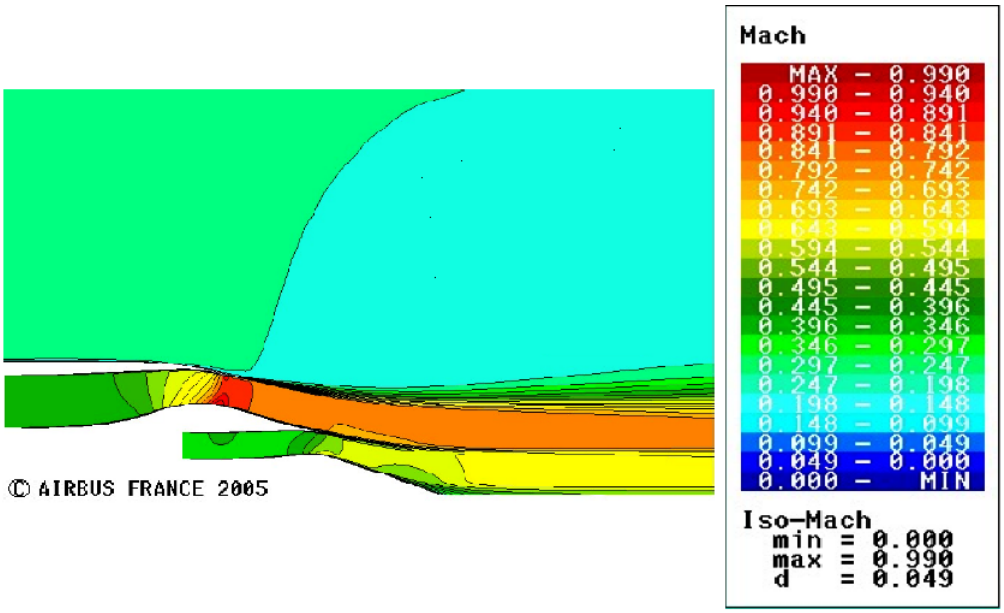

Figure 4.1. *Mach number field near the exhaust duct's jet of an aircraft engine at a particular engine regime[8].*

4.2 Assumptions

To describe the propagation of the guided acoustical waves with flow, it is assumed that the following approximations are valid:

- The perturbations are small and equations are linear in the acoustic quantities.
- The fluid is homogeneous, non-viscous and thermally non-conductive.
- The flow is subsonic and uniform (i.e. Mach number remains sufficiently small and flow velocity components do not depend on the spatial coordinates).
- A harmonic time dependence ($e^{-i\omega t}$) is supposed.

Furthermore, we suppose hereafter that the waveguides are periodic and do not present a change in the cross-sectional dimension.

4.3 Governing equations

4.3.1 Convected Helmholtz equation

Let $\mathbf{U}$ be the vector given by $\mathbf{U} = U\mathbf{x}$ with U is the flow velocity and $\mathbf{x}$ is the direction of the flow. This flow consists of a uniform mean flow with small perturbations given by:

$$\bar{\mathbf{v}} = U\mathbf{x} + \mathbf{v} \tag{4.1}$$

$$\bar{p} = p_0 + p \tag{4.2}$$

$$\bar{\rho} = \rho_0 + \rho \tag{4.3}$$

Under the above mentioned conditions, linearisation leads to the following equations [8]

$$\left(\frac{\partial}{\partial t} + U\frac{\partial}{\partial x}\right)\rho + \rho_0 \boldsymbol{\nabla}\mathbf{v} = 0 \tag{4.4}$$

$$\rho_0\left(\frac{\partial}{\partial t} + U\frac{\partial}{\partial x}\right)\mathbf{v} + \boldsymbol{\nabla}p = 0 \tag{4.5}$$

$$\left(\frac{\partial}{\partial t} + U\frac{\partial}{\partial x}\right)(p - c^2\rho) = 0 \tag{4.6}$$

where p, $\mathbf{v}$ and ρ_0 stand for the pressure, velocity and density of the fluid. Combining Eqs. (4.4), (4.5) and (4.6) yields to the convected Helmholtz equation (in dimensional form):

$$\left(\frac{\partial}{\partial t} + U\frac{\partial}{\partial x}\right)^2 p - c^2\boldsymbol{\nabla}^2 p = 0 \tag{4.7}$$

The Mach number M is defined as:

$$M = \frac{U}{c} \tag{4.8}$$

where c is the sound celerity in the air.

We consider a two-dimensional channel, with x-axis being the axis parallel to the walls of the duct, and the y-axis the normal to the walls. A flow in the $\mathbf{x}$ direction is assumed. Dividing by c^2 and supposing a harmonic time dependence, Eq. (4.7) is rewritten in this case as follows [113]:

$$(1-M^2)\frac{\partial^2 p}{\partial x^2}+\frac{\partial^2 p}{\partial y^2}+2\mathrm{i}kM\frac{\partial p}{\partial x}+k^2 p=0 \tag{4.9}$$

4.3.2 Rigid duct modes

The pressure satisfies the Neumann boundary condition on the two rigid walls of the duct:

$$\frac{\partial p}{\partial y}=0 \tag{4.10}$$

Mathematically, the duct is defined by the unbounded domain $\Omega=\mathbb{R}\times[0,h]$, where h is the dimension of the duct in the y direction. Solutions of Eqs. (4.9) and (4.10) are:

$$p_j^{\pm}(x,y)=\mathrm{e}^{\mathrm{i}k_j^{\pm}x}\psi_j(y) \tag{4.11}$$

where: $\psi_0(y)=\sqrt{\dfrac{1}{h}}$; and $\psi_j(y)=\sqrt{\dfrac{2}{h}}\cos\left(\dfrac{j\pi y}{h}\right)$ for $j\in\mathbb{N}^*$ (Details of resolution were given in section 1.2.3).

The axial wave numbers associated to the mode j are defined as following:

$$k_j^{\pm}=\frac{-kM\pm\sqrt{k^2-\dfrac{j^2\pi^2}{h^2}(1-M^2)}}{1-M^2} \tag{4.12}$$

The sign + means that the axial wave number is computed in the flow direction, while the sign − means that the axial wave number is computed in the opposite direction of the flow. Introducing

$$E=\frac{kh}{\pi\sqrt{1-M^2}} \tag{4.13}$$

and $E_0=[E]$ the integer part of E, it is shown that when $j\leq E_0$, $k_j^{\pm}$ is real and the mode

is called propagative. The number of propagative modes is also an increasing function of the Mach number M. When $j > E_0$, the axial wave number is complex (purely imaginary only if M=0 i.e. non convective case):

$$k_j^{\pm} = \frac{-kM \pm \mathrm{i}\sqrt{\frac{j^2\pi^2}{h^2}(1-M^2) - k^2}}{1-M^2} \tag{4.14}$$

In this case, $p_j^{\pm}$ is exponentially decreasing when $x \longrightarrow +\infty$ and is called an evanescent mode.

Fig. 4.2 shows the pressure's real part contours of a rigid channel submitted to the mode j=2 at 8000 Hz and ended by a normalised impedance Z_{end}=2 for $M = 0$ and $M = 0.3$.

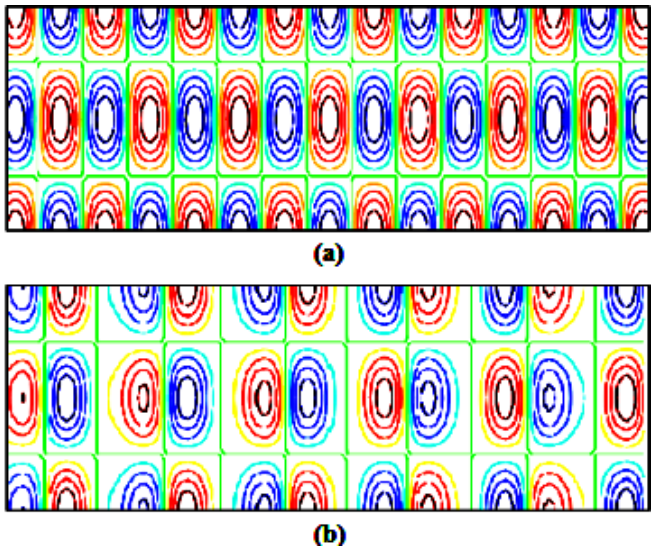

Figure 4.2. *Pressure's real part contours for j =2, f =8000Hz, Z_{end} =2, and (a): M =0 and (b):M =0.3 (Solution by the WFE method).*

It is clearly noted from Fig. 4.2 that, for a rigid duct, flow does not have an effect on the mode shape but on the axial pattern of wave propagation. Moreover, the cut-off frequency is lowered from $jc/(2h)$ without flow to $\sqrt{1-M^2}jc/(2h)$ with flow. Therefore, more modes are likely to be cut-on with flow than without.

The group velocity $\partial\omega/\partial k_j$ is positive for the p_j^+ modes and negative for the p_j^- modes.

Another effect of the presence of flow is the existence, when $k \in]\sqrt{1-M^2}j\pi/h, j\pi/h[$, of modes p_j^+ which have a negative phase velocity ω/k_j and a positive group velocity.

4.3.3 Ingard-Myers boundary condition

We propose to describe the general formulation of acoustic propagation in a two-dimensional lined duct with uniform flow parallel to the x-axis with a constant velocity denoted U and we suppose that the liner is locally reacting. With a grazing uniform mean flow, the lined wall impedance is not defined directly at the wall but at a distance ϑ_y such that:

$$Z = \lim_{\vartheta_y \to 0} \frac{p(x, \vartheta_y)}{v_y(x, \vartheta_y)} \tag{4.15}$$

where ϑ_y is the thickness of a boundary layer much smaller than the acoustic wavelength and much smaller than the transverse size of the duct h (See Fig. 4.3).

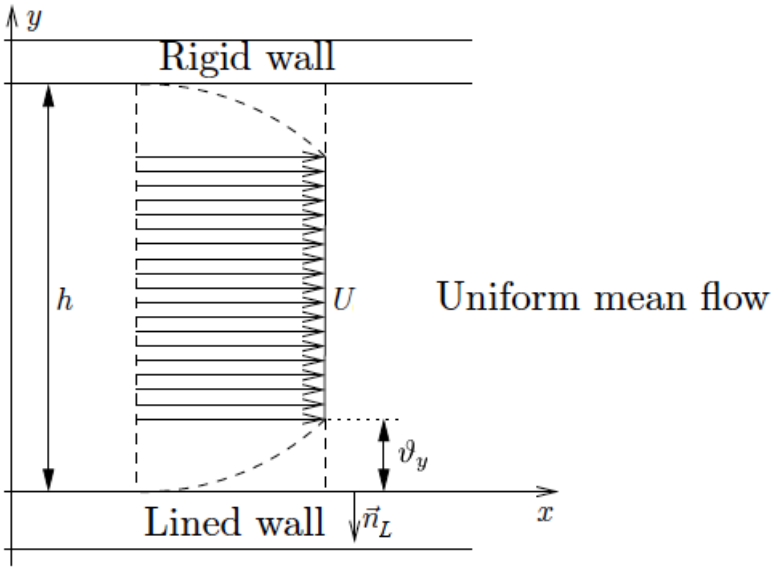

Figure 4.3. *Illustration of the duct with notations for the uniform mean flow formulation.*

The acoustic velocity v_y normal to the wall may be given by means of the the normal acoustic displacement ξ_y in the core of the flow (for $y \geq \vartheta_y$ in uniform mean flow) and at the

lined wall ($y = 0$) as following:

$$v_y = \left(-\mathrm{i}\omega + U\frac{\partial}{\partial x} \right) \xi_y \quad \text{for } y \geq \vartheta_y \tag{4.16}$$

$$v_y = \mathrm{i}\omega\xi_y \quad \text{for } y = 0 \tag{4.17}$$

When ϑ_y tends to 0, the normal acoustic displacement ξ_y is continuous across the boundary layer. Continuity of ξ_y and Eq. (4.5) lead to:

$$Z\frac{\partial p}{\partial n_L} = \frac{\rho_0}{\mathrm{i}\omega}\left(-\mathrm{i}\omega + U\frac{\partial}{\partial x} \right)^2 p \tag{4.18}$$

where Z is the acoustic impedance of the absorbing boundary.

This is the boundary condition for an absorbing boundary Γ_L in presence of mean flow and is called the Ingard-Myers condition [114, 115]. Ingard-Myers boundary condition was widely used in engineering applications for lined duct with uniform flow. Nevertheless, this boundary condition does not take into consideration the viscothermal effects near the wall. Some authors discussed the validity of the Ingard-Myers boundary condition and proposed a modified boundary condition taking into account the viscosity near the lined walls [116, 117, 118]. Renou and Auregan [117] introduced an additional parameter ϵ in the wall boundary condition accounting for the viscous losses at the treated wall so that a modified Ingard-Myers boundary condition is written as:

$$\frac{\partial p}{\partial n_L} = \frac{\rho_0}{\mathrm{i}Z\omega}\left(-\mathrm{i}\omega + (1+\epsilon)U\frac{\partial}{\partial x} \right)\left(-\mathrm{i}\omega + U\frac{\partial}{\partial x} \right) p \tag{4.19}$$

ϵ is determined experimentally. Note that for $\epsilon = 0$ the Ingard-Myers boundary condition is re-obtained.

Use of the Ingard-Myers boundary condition hereafter is justified since we made the non viscous fluid assumption [119].

4.4 Variational formulation

We define the coordinate system $(x_1, ..., x_n)$, and Ω a subset of $\mathbb{R}^n$. We suppose that the mean flow is in the $\mathbf{x}_1$ direction and that the duct is periodic and infinite in the same direction. If we multiply the convected Helmholtz equation by a test function q and apply the Green formula, then the weak variational formulation of the n-dimensional problem is written as following [120, 121, 122]:

$$\begin{aligned}&\int_\Omega -\boldsymbol{\nabla} q \boldsymbol{\nabla} p \mathrm{d}x + \frac{1}{c^2}\int_\Omega (\mathrm{i}\omega q + \mathbf{U}\boldsymbol{\nabla} q)(-\mathrm{i}\omega p + \mathbf{U}\boldsymbol{\nabla} p)\mathrm{d}x \\ &+ \int_{\partial\Omega}\left[q\frac{\partial p}{\partial n} - \frac{1}{c^2}\mathbf{U}\mathbf{n}q\left(-\mathrm{i}\omega + U\frac{\partial}{\partial n}\right)p\right]\mathrm{d}\sigma = 0\end{aligned} \tag{4.20}$$

where

$$\boldsymbol{\nabla} = \left(\begin{array}{ccc}\dfrac{\partial}{\partial x_1}, & \cdots & , \dfrac{\partial}{\partial x_n}\end{array}\right)^t$$

and $\partial\Omega$ is the boundary of the domain Ω.

The third integration term can be reduced to $\displaystyle\int_{\Gamma_L} q\frac{\partial p}{\partial n_L}\mathrm{d}\sigma$ as the lined walls are normal to the flow direction, with Γ_L is the lined boundary and $\mathbf{n}_L$ is the outward normal to the lined boundary. This term can be expressed using the Ingard-Myers boundary condition followed by an integration by parts as:

$$\begin{aligned}&\int_{\Gamma_L} q\frac{\partial p}{\partial n_L}\mathrm{d}\sigma = -\rho_0\omega^2\int_{\Gamma_L} q\frac{p}{\mathrm{i}\omega Z}\mathrm{d}\sigma - 2\mathrm{i}\omega\rho_0 U\int_{\Gamma_L} q\frac{\partial}{\partial x_1}\left(\frac{p}{\mathrm{i}\omega Z}\right)\mathrm{d}\sigma \\ &-\rho_0 U^2\int_{\Gamma_L}\frac{\partial q}{\partial x_1}\frac{\partial}{\partial x_1}\left(\frac{p}{\mathrm{i}\omega Z}\right)\mathrm{d}\sigma + \rho_0 U^2\left[q\frac{\partial}{\partial x_1}\left(\frac{p}{\mathrm{i}\omega Z}\right)\right]_{\Gamma_L}\end{aligned} \tag{4.21}$$

4.5 Discrete problem

The WFE method starts from modelling one segment of a waveguide with fluid elements and extracting its mass and stiffness matrices. With mean flow, matrices can not be extracted

directly from ANSYS's Mechanical APDL as fluid elements do not support mean flow. The dynamic stiffness matrix of the segment needs to be calculated to apply the WFE method.

4.5.1 Dynamic stiffness matrix of the rigid duct

When considering the free wave propagation with flow, terms of the dynamic stiffness matrix $\mathbf{D} = \mathbf{K} - \omega^2\mathbf{M}$ of the rigid duct part can be calculated using Eq. (4.22) :

$$D_{ij}^e = \int_{\Omega^e} -\boldsymbol{\nabla} N_i \boldsymbol{\nabla} N_j \mathrm{d}x + \frac{1}{c^2}\int_{\Omega^e} (\mathrm{i}\omega N_i + \mathbf{U}\boldsymbol{\nabla} N_i)(-\mathrm{i}\omega N_j + \mathbf{U}\boldsymbol{\nabla} N_j)\mathrm{d}x \tag{4.22}$$

with:

D_{ij}^e: are the elementary dynamic stiffness matrix terms; $1 \leq i \leq 2^n$ and $1 \leq j \leq 2^n$ where n is the dimension of the problem,

N_i: are the shape functions [123],

$$\boldsymbol{\nabla} N_i = \boldsymbol{\mathcal{J}}^{-1}\boldsymbol{\nabla}_\perp N_i \tag{4.23}$$

with $\boldsymbol{\mathcal{J}}$ is the Jacobian matrix [77] and $\boldsymbol{\nabla}_\perp$ stands for the derivatives with respect to the natural coordinates [124].

The matrix $\mathbf{D^e}$ is the contribution from the element to the global assembled matrix $\mathbf{D}$. The elementary matrices are then assembled and the global matrix is obtained. The transfer matrix $\mathbf{S}$ is then calculated using the square blocks of the matrix $\mathbf{D}$.

4.5.2 Dynamic stiffness matrix of the lined duct

The elementary dynamic stiffness matrices corresponding the lined duct part are calculated by adding the damping term for the nodes belonging to the lined boundary.

$$\begin{aligned}(D_c^e)_{ij} = D_{ij}^e &- \rho_0\omega^2 \int_{\Gamma_L^e} N_i \frac{N_j}{\mathrm{i}\omega Z}\mathrm{d}\sigma - 2\mathrm{i}\omega\rho_0 U \int_{\Gamma_L^e} N_i \frac{\partial}{\partial x_1}\left(\frac{N_j}{\mathrm{i}\omega Z}\right)\mathrm{d}\sigma \\ &-\rho_0 U^2 \int_{\Gamma_L^e} \frac{\partial N_i}{\partial x_1}\frac{\partial}{\partial x_1}\left(\frac{N_j}{\mathrm{i}\omega Z}\right)\mathrm{d}\sigma + \rho_0 U^2 \left[N_i \frac{\partial}{\partial x_1}\left(\frac{N_j}{\mathrm{i}\omega Z}\right)\right]_{\Gamma_L^e}\end{aligned} \tag{4.24}$$

The dynamic stiffness matrix of the liner is then calculated through the assembly of the elementary matrices and condensed onto its left and right edges. The scattering matrix is to be calculated as was detailed in chapter 2.

4.6 Analytical computation of the scattering matrix

We consider the problem of the acoustical propagation in an infinite 2D lined duct with uniform flow, and we make dimensionless as following:

$$p' = p/(\rho_0 c^2) \quad , \quad k_j'^{\pm} = k_j^{\pm} h$$

$$\omega' = \omega h/c \quad , \quad Z' = Z/(\rho_0 c)$$

$$x' = x/h \quad , \quad y' = y/h$$

h is the transverse dimension of the duct, ρ_0 is the density of the fluid and c is the celerity of the sound in the fluid.

In what follows, $'$ is dropped for the sake of convenience. We consider a 2D channel with a rigid upper wall and an acoustic lining on its lower wall as shown in Fig. 4.4. The x-axis is the axis parallel to the walls of the duct and the flow direction, and the y-axis is the normal to the walls.

The displacement potential ϕ is defined such as:

$$p = -\left(\mathrm{i}\omega + M\frac{\partial}{\partial x}\right)^2 \phi \tag{4.25}$$

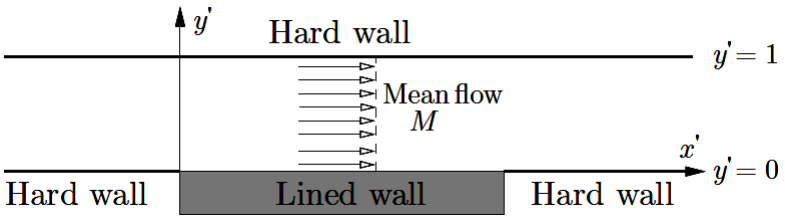

Figure 4.4. *Illustration of the lined channel.*

The displacement potential obeys to a convective wave equation (in dimensionless form):

$$\left(\mathrm{i}\omega + M\frac{\partial}{\partial x}\right)^2 \phi - \boldsymbol{\nabla}^2\phi = 0 \tag{4.26}$$

Solution of Eq. (4.26) in the rigid duct can be written by means of orthogonal eigenfunctions ψ_j as follows:

$$\phi(x,y) = \sum_{j=0}^{\infty} \psi_j(y) X_j(x) \tag{4.27}$$

$$\psi_j = \begin{cases} 1 & \text{if } j = 0 \\ \sqrt{2}\cos(\alpha_j y) & \text{if } j \neq 0 \end{cases} \tag{4.28}$$

$\alpha_j = j\pi$ are the transversal wavenumbers, and:

$$\int_0^1 \psi_i(y)\psi_j(y)\mathrm{d}y = \delta_{i,j} \tag{4.29}$$

where $\delta_{i,j}$ is the Kronecker index [1].

On the lined wall the boundary condition is:

$$\frac{\partial\phi}{\partial n_L} = \frac{1}{\mathrm{i}Z\omega}\left(\mathrm{i}\omega + M\frac{\partial}{\partial x}\right)^2 \phi \tag{4.30}$$

Note that Eq. (4.30) is the Ingard-Myers boundary condition with dimensionless convention of the variables.

We note $D_t = \left(\mathrm{i}\omega + M\frac{\partial}{\partial x}\right)$.

Eq. (4.26) is projected over the basis of orthogonal functions $\psi_j(y)$:

$$\int_0^1 D_t^2\phi\psi_j(y)\mathrm{d}y - \int_0^1 \frac{\partial^2\phi}{\partial x^2}\psi_j(y)\mathrm{d}y - \int_0^1 \frac{\partial^2\phi}{\partial y^2}\psi_j(y)\mathrm{d}y = 0 \tag{4.31}$$

We aim to reduce the order of derivation of the third term of Eq. (4.31) from 2 to 1 in order to use the Ingard-Myers boundary condition. Rewriting the third term of Eq. (4.31) using

[1] $\delta_{i,j} = 1$ if $i = j$ and $\delta_{i,j} = 0$ if $i \neq j$

an integration by parts gives:

$$-\int_0^1 \frac{\partial^2\phi}{\partial y^2}\psi_j(y)\mathrm{d}y = -\left[\psi_j(y)\frac{\partial\phi}{\partial y}\right]_0^1 + \int_0^1 \frac{\partial\phi}{\partial y}\frac{\partial\psi_j(y)}{\partial y}\mathrm{d}y \tag{4.32}$$

The first term of Eq. (4.32) is given by the boundary conditions:

$$\frac{\partial\phi}{\partial y}|_{y=1} = 0 \tag{4.33}$$

$$\psi_j\frac{\partial\phi}{\partial y}|_{y=0} = \psi_j(0)\frac{\partial\phi}{\partial y}(0) \tag{4.34}$$

The second term of Eq. (4.32) is calculated using an integration by parts:

$$\int_0^1 \frac{\partial\phi}{\partial y}\frac{\partial\psi_j(y)}{\partial y}\mathrm{d}y = \left[\frac{\partial\psi_j(y)}{\partial y}\phi\right]_0^1 - \int_0^1 \frac{\partial^2\psi_j(y)}{\partial y^2}\phi\mathrm{d}y \tag{4.35}$$

The first derivative of ψ_j is:

$$\frac{\partial\psi_j(y)}{\partial y} = -\alpha_j\sin(\alpha_j y) \tag{4.36}$$

Hence:

$$\left[\frac{\partial\psi_j(y)}{\partial y}\phi\right]_0^1 = 0 \tag{4.37}$$

The second derivative of ψ_j is:

$$\frac{\partial^2\psi_j(y)}{\partial y^2} = -\alpha_j^2\psi_j(y) \tag{4.38}$$

Eq. (4.31) becomes:

$$\int_0^1 D_t^2\phi\psi_j(y)\mathrm{d}y - \int_0^1 \frac{\partial^2\phi}{\partial x^2}\psi_j(y)\mathrm{d}y + \int_0^1 \alpha_j^2\psi_j(y)\phi\mathrm{d}y + \psi_j(0)\frac{\partial\phi}{\partial y}(0) = 0 \tag{4.39}$$

where

$$\begin{aligned}&\psi_j(0)\frac{\partial\phi}{\partial y}(0) = \psi_j(0)\frac{1}{\mathrm{i}Z\omega}D_t^2\phi(0) = \\ &\psi_j(0)\frac{1}{\mathrm{i}Z\omega}\left[-\omega^2\phi(0) + 2\mathrm{i}\omega M\frac{\partial\phi}{\partial x}(0) + M^2\frac{\partial^2\phi}{\partial x^2}(0)\right]\end{aligned} \tag{4.40}$$

Finally, projection of (4.26) on the basis of rigid eigenfunctions leads to (in vectorial notation):

$$D_t^2\mathbf{X} + \frac{1}{\mathrm{i}Z\omega}\mathbf{C_L}D_t^2\mathbf{X} - \frac{\mathrm{d}^2\mathbf{X}}{\mathrm{d}x^2} + \mathbf{A_R}\mathbf{X} = \mathbf{0} \tag{4.41}$$

where

$$\mathbf{C_L} = \begin{pmatrix} 1 & \sqrt{2} & \cdots \\ \sqrt{2} & 2 & \cdots \\ \vdots & \vdots & \ddots \end{pmatrix} \text{ and } \mathbf{A_R} = \begin{pmatrix} \alpha_0^2 & 0 & \cdot \\ 0 & \alpha_1^2 & \\ \vdots & & \ddots \end{pmatrix}.$$

In the lined part, Eq. (4.41) is arranged as following:

$$\mathbf{M}_1\frac{\mathrm{d}^2\mathbf{X}}{\mathrm{d}x^2} = \mathbf{M}_2\frac{\mathrm{d}\mathbf{X}}{\mathrm{d}x} + \mathbf{M}_3\mathbf{X} \tag{4.42}$$

with

$$\mathbf{M}_1 = (1-M^2)\mathbf{I} - \frac{M^2}{\mathrm{i}Z\omega}\mathbf{C_L}$$

$$\mathbf{M}_2 = 2\mathrm{i}\omega M\mathbf{I} + \frac{2M}{Z}\mathbf{C_L}$$

$$\mathbf{M}_3 = \mathbf{A_R} - \omega^2\mathbf{I} + \frac{\mathrm{i}\omega}{Z}\mathbf{C_L}.$$

Eq. (4.42) can be rewritten as follows :

$$\frac{\mathrm{d}}{\mathrm{d}x}\begin{pmatrix} \mathbf{X} \\ \mathbf{\Pi} \end{pmatrix} = \begin{pmatrix} \mathbf{0} & \mathbf{I} \\ \mathbf{M}_1^{-1}\mathbf{M}_3 & \mathbf{M}_1^{-1}\mathbf{M}_2 \end{pmatrix}\begin{pmatrix} \mathbf{X} \\ \mathbf{\Pi} \end{pmatrix} \tag{4.43}$$

where $\mathbf{\Pi} = \mathrm{d}\mathbf{X}/\mathrm{d}x$. The wavenumbers K_{Lm} of the lined duct part are calculated by means of the eigenvalues λ_m of the Eq. (4.43) matrix as $K_{Lm} = \mathrm{i}\lambda_m$. The associated eigenvectors are split in two sets following the sign of $\Im(K_{Lm})$ and regrouped in matrices ($\mathbf{V}^+$ and $\mathbf{V}^-$) [5]: $\mathbf{V}^+$ for $\Im(K_{Lm}) < 0$ and $\mathbf{V}^-$ for $\Im(K_{Lm}) > 0$. Vectors $\mathbf{X}$ and $\mathbf{\Pi}$ can be then calculated anywhere inside the lined part, and particularly, at the edges of the lining.

$$\mathbf{X}(x) = \mathbf{V}_1^+\mathbf{E}^+(x)\mathbf{B}_1 + \mathbf{V}_1^-\mathbf{E}^-(x)\mathbf{B}_2 \tag{4.44}$$

where $\mathbf{V}_1^+$ and $\mathbf{V}_1^-$ are the first n rows of $\mathbf{V}^+$ and $\mathbf{V}^-$respectively, $\mathbf{E}^{\pm}(x)$ are the matrices with $\exp(-\mathrm{i}K_{Lm}^{\pm}x)$ on the diagonal, and $\mathbf{B}_1$ and $\mathbf{B}_2$ are waves amplitudes [5].

The continuity of $\mathbf{X}$ and $\mathbf{\Pi}$ at the lined part edges (interfaces with rigid parts) allows the calculation of the scattering matrix [5, 125] by expressing the relation between the amplitude of out-coming and incoming waves.
The acoustic displacement potential was used rather than the acoustic pressure because of the regularity of ϕ near a sudden change in wall impedance contrarily to the pressure [5, 126]. Blocks of the scattering matrix in terms of acoustic pressure are easily given by means of blocks of the scattering matrix in terms of displacement potential as mentioned by Renou and Auregan [126].

4.7 Numerical validations

4.7.1 Rigid ducts

- ***Two dimensional case***

An infinite rigid duct carrying a mean uniform fluid flow is considered. The problem is two-dimensional, set in the xy-plane, where the x- (resp., y-) axis is parallel (resp., normal) to the walls of the duct. Dimension of the duct following y is $h = 0.08$ m. A 0.003 m length reduced two dimensional FE model was used for the WFE method. Frequency evolution of the axial wavenumbers of forward going waves calculated by the WFE method and analytical method is represented in Fig. 4.5 for a Mach number $M = +0.2$.

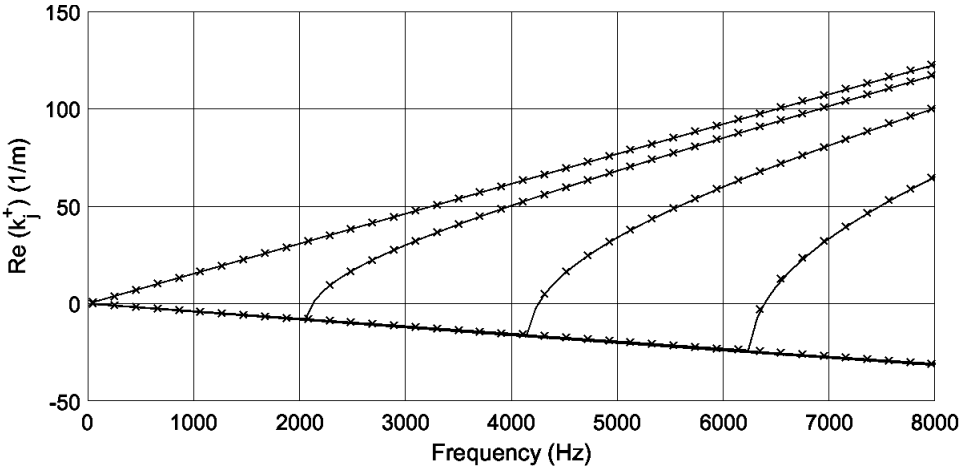

Figure 4.5. *Frequency evolution of the axial wavenumbers real parts corresponding to the forward going waves for $h = 0.08$ m and $M = 0.2$: (-) WFE method (×) Analytical method.*

- ***Three dimensional case***

Acoustical propagation inside an infinite rigid duct with a rectangular cross-section is studied in this section. A subsonic uniform mean flow in the **x** direction is assumed. Width of the duct is 0.056 m and height is 0.04 m (See Fig. 4.6). A 0.003 m length reduced FE model of the duct is used for the WFE discretisation. Frequency evolution of the axial wavenumbers calculated by the WFE method and analytical method is represented in Fig. 4.7 for a Mach number $M = +0.2$. Fig. 4.8 shows the evolution of the axial wavenumber of the first order mode along the width of the duct in the complex plan for a frequency varying from 50 Hz to 8000 Hz.

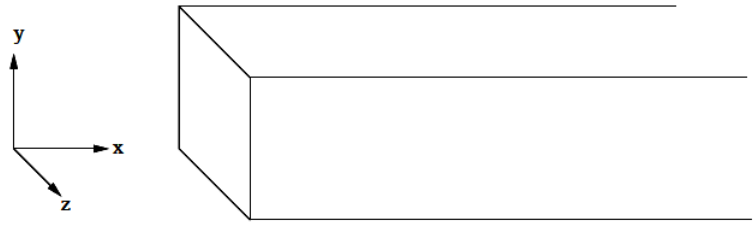

Figure 4.6. *Illustration of the acoustical waveguide carrying the mean flow.*

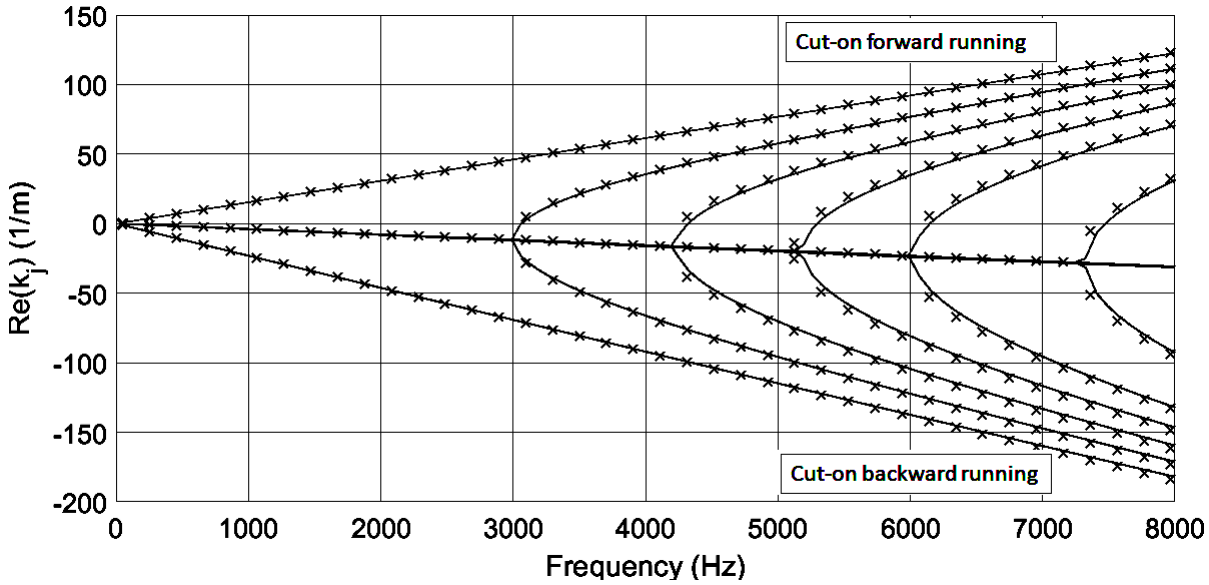

Figure 4.7. *Frequency evolution of the axial wavenumbers real parts for a* $0.056 \times 0.04\ m^2$ *rectangular cross-section and* $M = 0.2$*: (—) WFE method (×) Analytical method.*

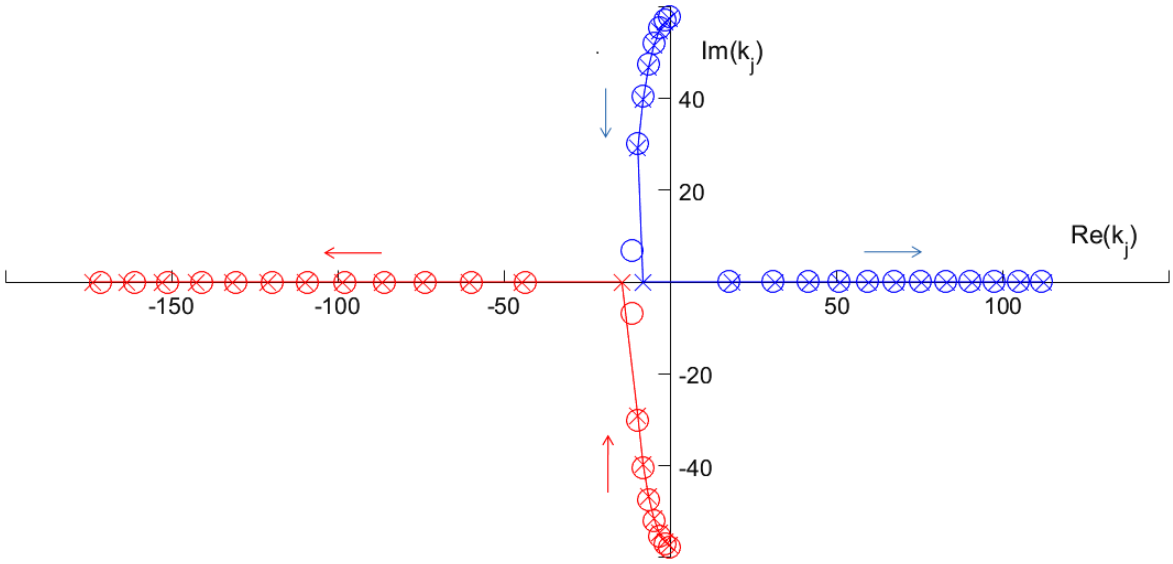

Figure 4.8. *Evolution of the axial wavenumber of the first order mode along the width of the duct in the complex plan when varying the frequency from* 50 *Hz to* 8000 *Hz* (O)*: WFE solutions* (×)*: Analytical solutions "Blue" forward running wave "Red" backward running wave.*

For $M = 0$ (absence of flow), the axial wavenumbers are purely imaginary when the modes are cut-off. That is to say that below a given frequency the wave vanishes after some travelled distance along the x-axis.

For $M > 0$, below the cut-off frequency, the axial wavenumbers are complex and have, in addition to the imaginary part corresponding to the decaying component of the wave, a negative real part which corresponds to an oscillating component of the wave (Eq. (4.14) and Fig. 4.8). When they become cut-on ($f > jc/(2h)\sqrt{1-M^2}$), the forward running waves, in particular and only these, will have a positive group velocity $\partial\omega/\partial k_j$ and a negative phase velocity ω/k_j as long as the frequency remains lower than $jc/(2h)$ (which is the cut-off frequency without flow) i.e. $k \in]\sqrt{1-M^2}j\pi/h, j\pi/h[$ (branches in the yellow section in Fig. 4.9).

If $M < 0$, the same applies for the backward running modes with opposite signs for the axial wavenumber real part, the group velocity and the phase velocity.

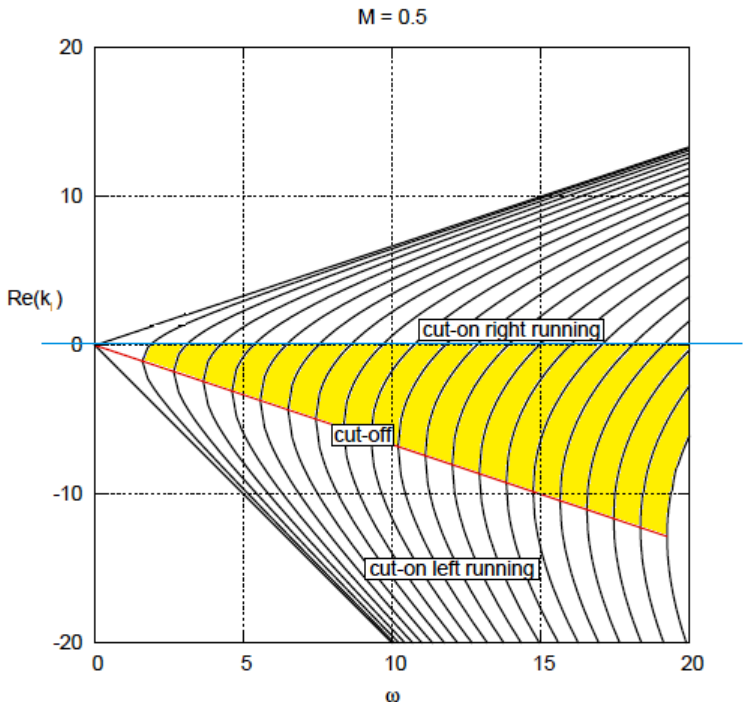

Figure 4.9. *Evolution of the axial wavenumbers real parts for a duct carrying a mean uniform flow with* $M = +0.5$.

Altogether, it is shown that it is not the sign of k_j but its radical in Eq. (4.12) that corresponds to the direction of propagation. Furthermore, it is noted that when the flow velocity increases, the wave length becomes larger (Eq. (4.12) and Fig. 4.2) and the cut-off frequency decreases. This means that for a given frequency more modes are likely to be cut-on as the flow velocity is more important. A raise of the transversal dimension h (dimension following y) of the waveguide will lead also to increasing the number of the cut-on modes. Although the axial pattern of the waves changes in presence of flow, the mode shapes remain the same as without flow for a rigid waveguide (Fig. 4.2). Indeed , the same boundary condition given in Eq. (4.10) applies whether or not the flow exists. This is not true for a lined wall though, because the Ingard-Myers boundary condition defined in Eq. (4.18) is used in this case.

4.7.2 Lined ducts

- ***Validation by the analytical method***

We consider an infinite two dimensional channel with a rigid upper wall and a lined lower wall (same problem as presented in Fig. 4.4) [127]. A subsonic uniform mean flow is assumed in the direction parallel to the walls. The Mach number is equal to $M = +0.1$. A relatively small Mach number is chosen to ensure pushing away hydrodynamic surface waves mentioned by Rienstra in [128] to the high frequencies. Turbulence effects are assumed to be absent. Dimension of the channel is $h = 0.08$ m. Lined length is 0.009 m and normalised impedance of the acoustic lining is taken equal to Z =0.2. The fluid is supposed to be non-viscous so that use of the Ingard-Myers boundary condition is justified for the study of the scattering by the lined part of duct.

2D fluid elements with linear interpolation were used to model the WFE segments. Damping due to the lining on the lower part was introduced. Assembled dynamic stiffness matrix of the lined channel portion was calculated and condensed onto its left and right edges to find an expression of the scattering matrix. The calculation of the scattering through the use of the WFE method was compared to the analytical method. Figs. 4.10, 4.11 and 4.12 show the scattering coefficients evolution of the same incident and scattered modes.

For all the following results, the Mach number is $M = +0.1$ (direction of flow from the left side to the right side of the waveguide) and the scattering is calculated for waves incident to the lined part following the same direction (incident waves coming from the left, transmission from the left to the right and reflection of waves from the lined part to the left side).

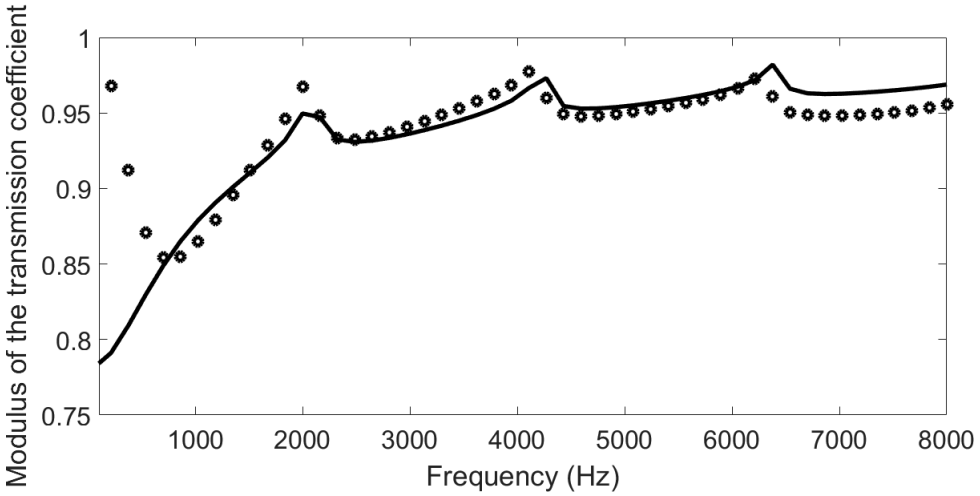

(a)

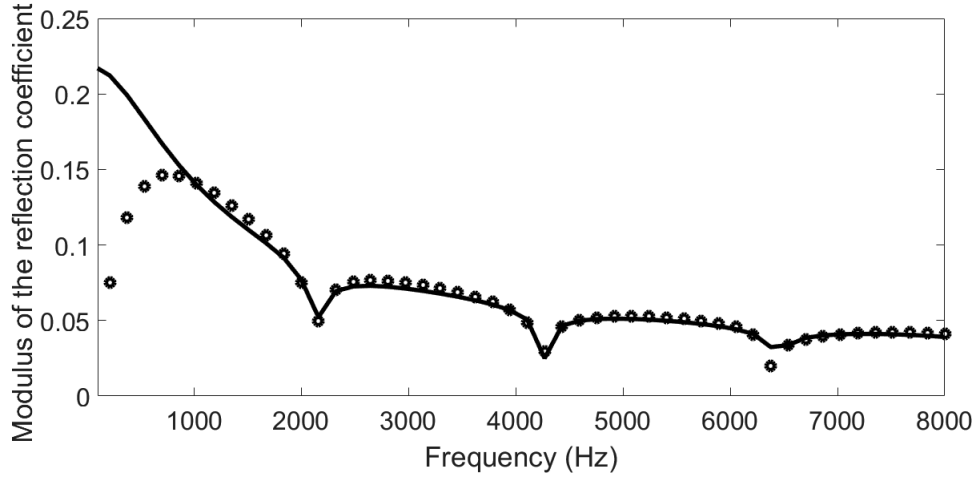

(b)

Figure 4.10. *Frequency evolution of the transmission coefficient (a) and the reflection coefficient (b): incident mode order: $j = 0$, transmitted/reflected mode order: $j' = 0$. (—)WFE method (o) Analytical method.*

Conversion between the modes is shown in Figs. 4.13 and 4.14 . Modes are represented from their cut-off frequencies (See Table 4.1).

Mode order	0	1	2	3
Cut-off frequency	0 Hz	2115 Hz	4229 Hz	6343 Hz

Table 4.1. *Cut-off frequencies of the first modes for a 2D channel height equal to 0.08 m and a Mach number $M = 0.1$.*

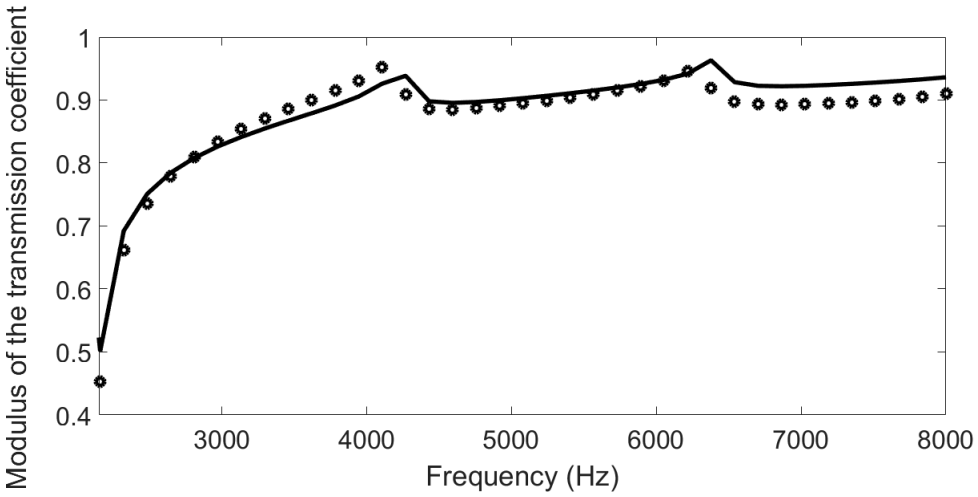

(a)

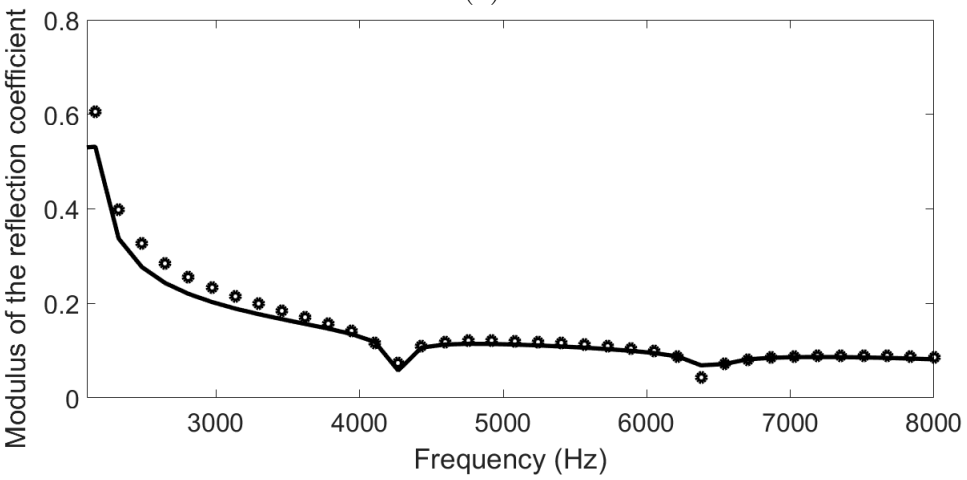

(b)

Figure 4.11. *Frequency evolution of the transmission coefficient (a) and the reflection coefficient (b): incident mode order: $j = 1$, transmitted/reflected mode order: $j' = 1$. (—)WFE method (o) Analytical method.*

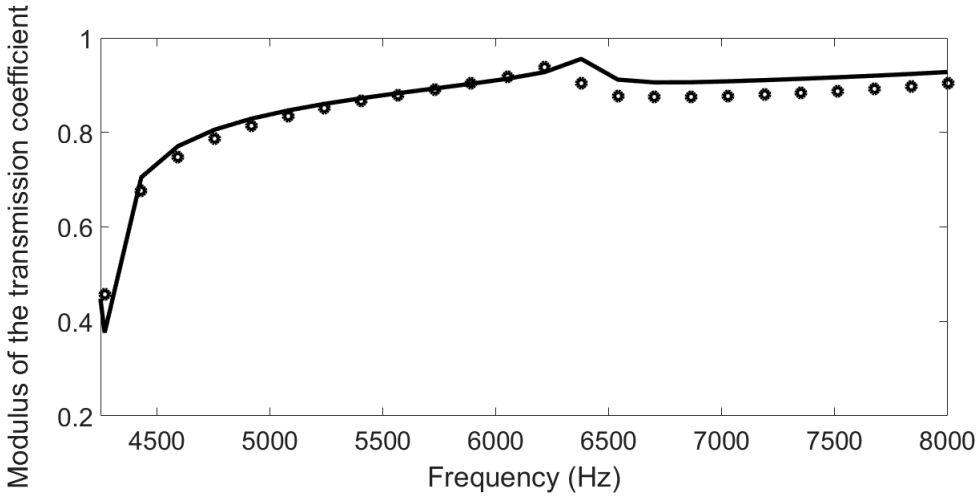

(a)

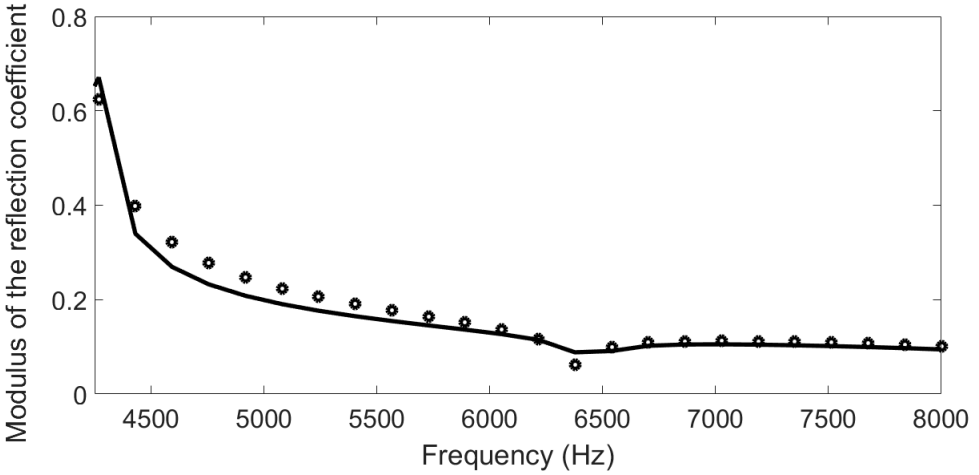

(b)

Figure 4.12. *Frequency evolution of the transmission coefficient (a) and the reflection coefficient (b): incident mode order:* $j = 2$*, transmitted/reflected mode order:* $j' = 2$*. (—)WFE method (o) Analytical method.*

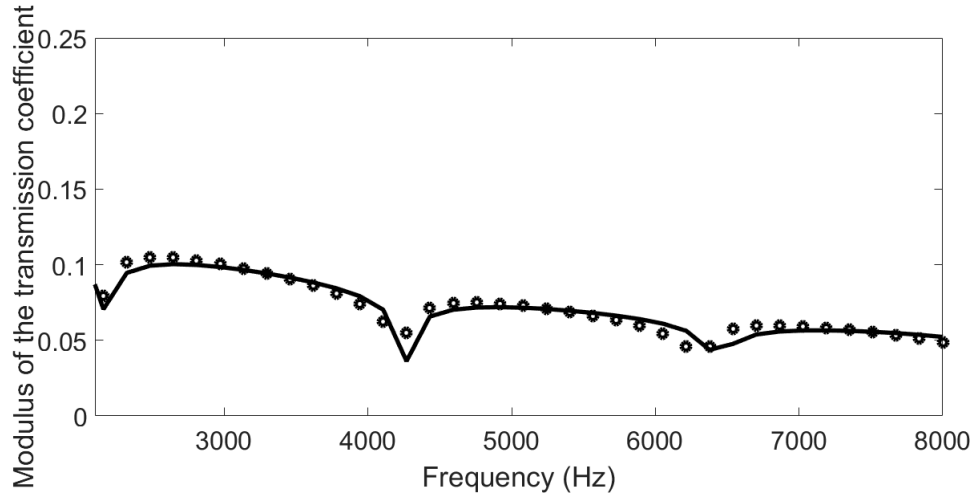

(a)

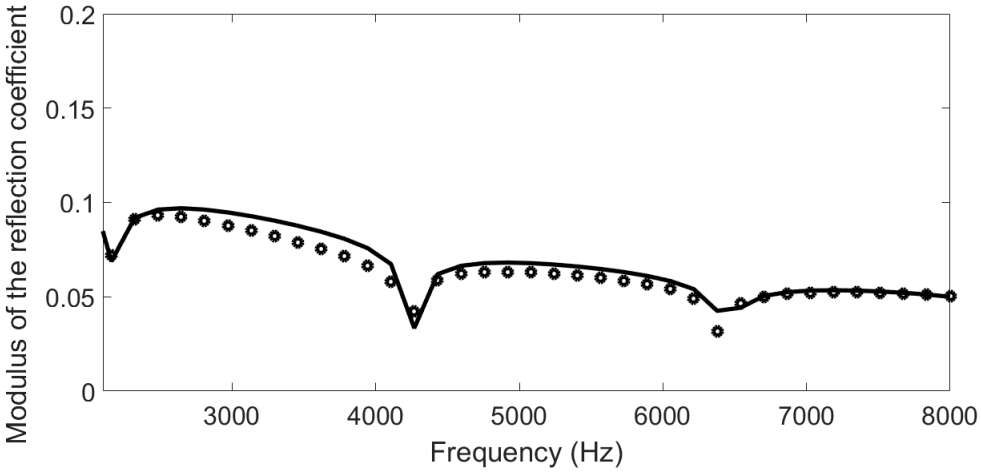

(b)

Figure 4.13. *Frequency evolution of the transmission coefficient (a) and the reflection coefficient (b): incident mode order:* $j = 1$*, transmitted/reflected mode order:* $j' = 0$*. (—)WFE method (o) Analytical method.*

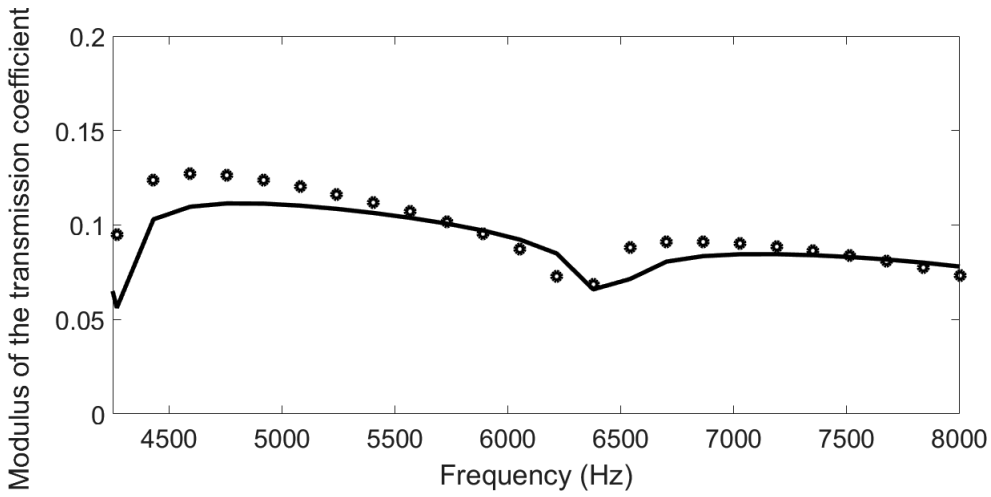

(a)

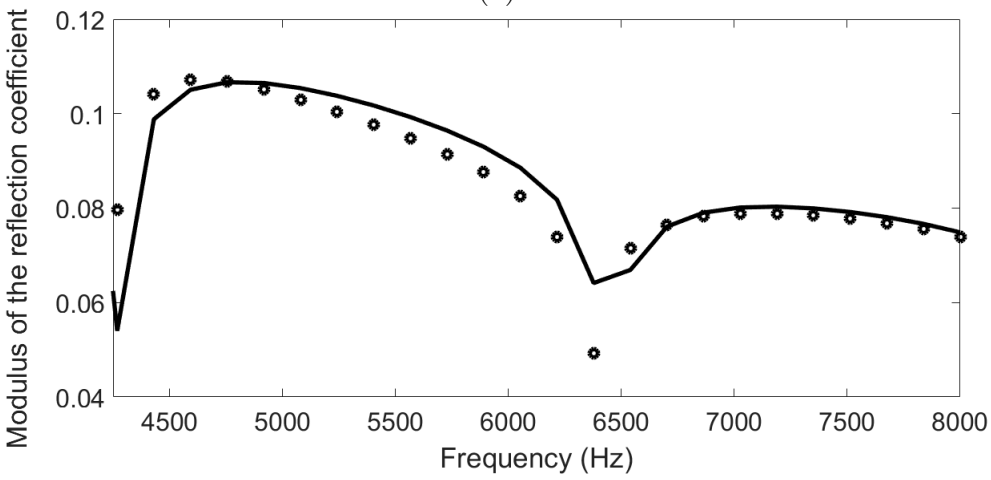

(b)

Figure 4.14. *Frequency evolution of the transmission coefficient (a) and the reflection coefficient (b): incident mode order: $j = 2$, transmitted/reflected mode order: $j' = 1$. (—)WFE method (o) Analytical method.*

Each mode transmits and reflects into the same mode, and all the other modes but in lower proportion. What is more, in presence of a uniform mean flow the reflection from the lined part to one end is not any more the same as the reflection from the lined part to the other end despite the symmetry of the geometry. This implies that the reflection matrices and the transmission matrices corresponding to the square blocks of the scattering matrix are calculated in the convective case depending on the direction of incidence being in the same direction of the mean flow or opposite to it.

It should be noted that the number of truncated modes affects the solution. An appropriate choice of truncation is to include same number of modes for both methods. The number of truncated modes is identical in each duct region and is chosen according to the number of cut-on modes in the rigid-walled duct at the maximal frequency [92]. The effect of the evanescent modes on the scattering for the low frequencies is therefore taken into account.

- ***Effect of the flow on the acoustical scattering and attenuation***

The flow effect on the scattering coefficients is investigated in the current section. To this end, a two dimensional waveguide lined on its lower wall is considered with same dimensions as presented in the previous section. The normalised impedance of the liner is $Z = 0.2$. The scattering coefficients are computed for different Mach numbers and both in the downstream and the upstream directions (See Fig. 4.15 for the notations and Figs. 4.16 and 4.17 for the transmission and the reflection coefficients respectively).

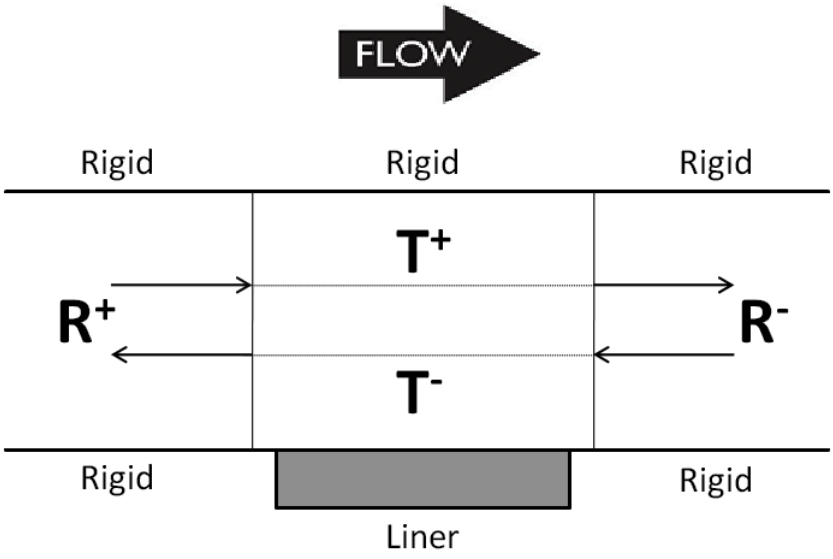

Figure 4.15. *Illustration of the lined channel with notations for the transmission and reflection matrices.*

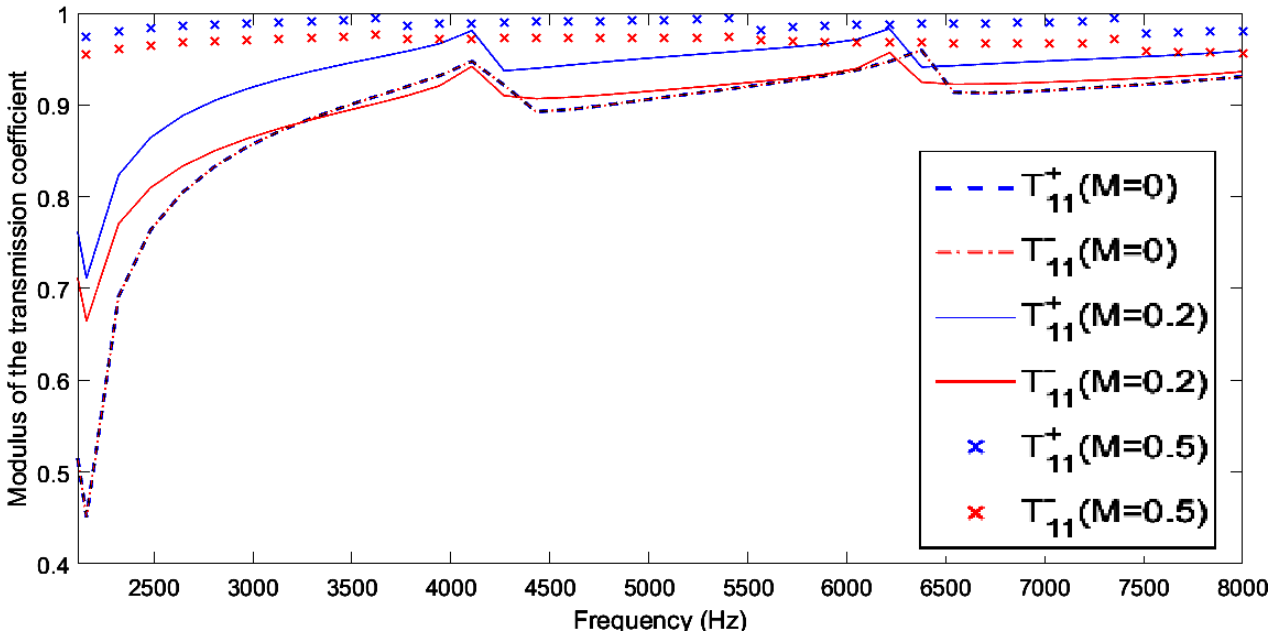

Figure 4.16. *Effect of the flow on downstream and upstream transmissions: incident mode order: $j = 1$; transmitted mode order: $j' = 1$.*

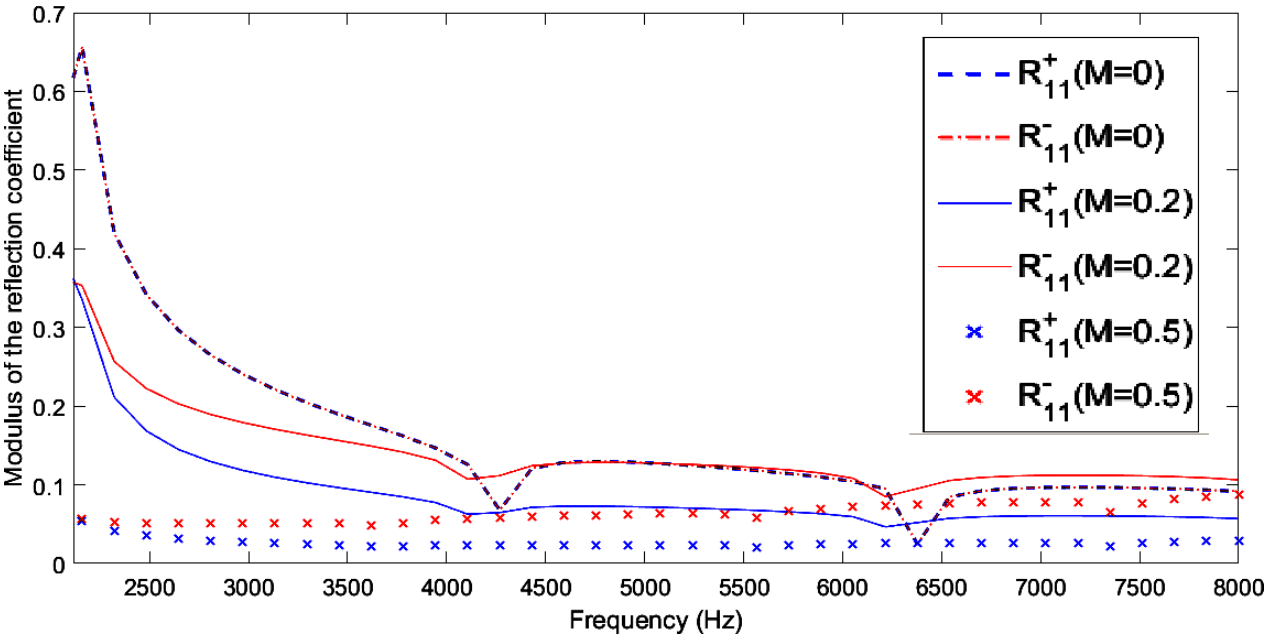

Figure 4.17. *Effect of the flow on downstream and upstream reflections: incident mode order: $j = 1$; reflected mode order: $j' = 1$.*

First, it is noted that in the absence of flow the scattering coefficients are same whether calculated in the downstream or upstream direction since the duct's geometry is symmetric. This is no more true in the presence of flow. Transmission in the downstream direction (same as flow direction) is more important than transmission in the upstream direction (opposite to the flow direction) while the downstream reflection coefficients are greater than the upstream reflection coefficients. Furthermore, a raise of the flow velocity leads to an increase of the transmission in the direction of flow and a decrease of the upstream reflection coefficients. Transmission and reflection in the opposite directions are less affected by the raise of flow velocity unless important Mach numbers are reached.

Efficiency of the liner can be evaluated through the acoustic power attenuation. The attenuation is obtained by calculating the incoming and outgoing acoustic powers from both duct sides as follows:

$$W_{att} = 10\log_{10}\left(\frac{(\mathbf{P}^{inc})^h\mathbf{Y_e}\mathbf{P}^{inc}}{(\mathbf{P}^{inc})^h(\mathbf{C}^h\mathbf{Y_s}\mathbf{C})\mathbf{P}^{inc}}\right) \tag{4.45}$$

where $\mathbf{P}^{inc} = \left\langle ...P_j^{(1)+}..., ...P_j^{(2)-}... \right\rangle^t$ is the vector of modal pressures incident to the left and right duct sections, h denotes the conjugate transpose, $\mathbf{C}$ is the scattering matrix defined in Eq. (2.37) and $\mathbf{Y_e}$ is the diagonal matrix defined as:

$$\mathbf{Y_e} = \begin{pmatrix} \frac{(1+M^2)N_0k_0^+}{2\rho c(k-Mk_0^+)} & & & & & \\ & \ddots & & & & \\ & & \frac{(1+M^2)N_{n-1}k_{n-1}^+}{2\rho c(k-Mk_{n-1}^+)} & & & \\ & & & \frac{(1+M^2)N_0k_0^-}{2\rho c(k-Mk_0^-)} & & \\ & & & & \ddots & \\ & & & & & \frac{(1+M^2)N_{n-1}k_{n-1}^-}{2\rho c(k-Mk_{n-1}^-)} \end{pmatrix}$$

$\mathbf{Y_s}$ is the diagonal matrix given by:

$$\mathbf{Y_s} = \begin{pmatrix} \frac{(1+M^2)N_0 k_0^-}{2\rho c(k - Mk_0^-)} & & & & & \\ & \ddots & & & & \\ & & \frac{(1+M^2)N_{n-1} k_{n-1}^-}{2\rho c(k - Mk_{n-1}^-)} & & & \\ & & & \frac{(1+M^2)N_0 k_0^+}{2\rho c(k - Mk_0^+)} & & \\ & & & & \ddots & \\ & & & & & \frac{(1+M^2)N_{n-1} k_{n-1}^+}{2\rho c(k - Mk_{n-1}^+)} \end{pmatrix}$$

where N_j are the normalisation coefficients.

The acoustic power attenuation calculated for different Mach numbers is presented in Fig. 4.18 .

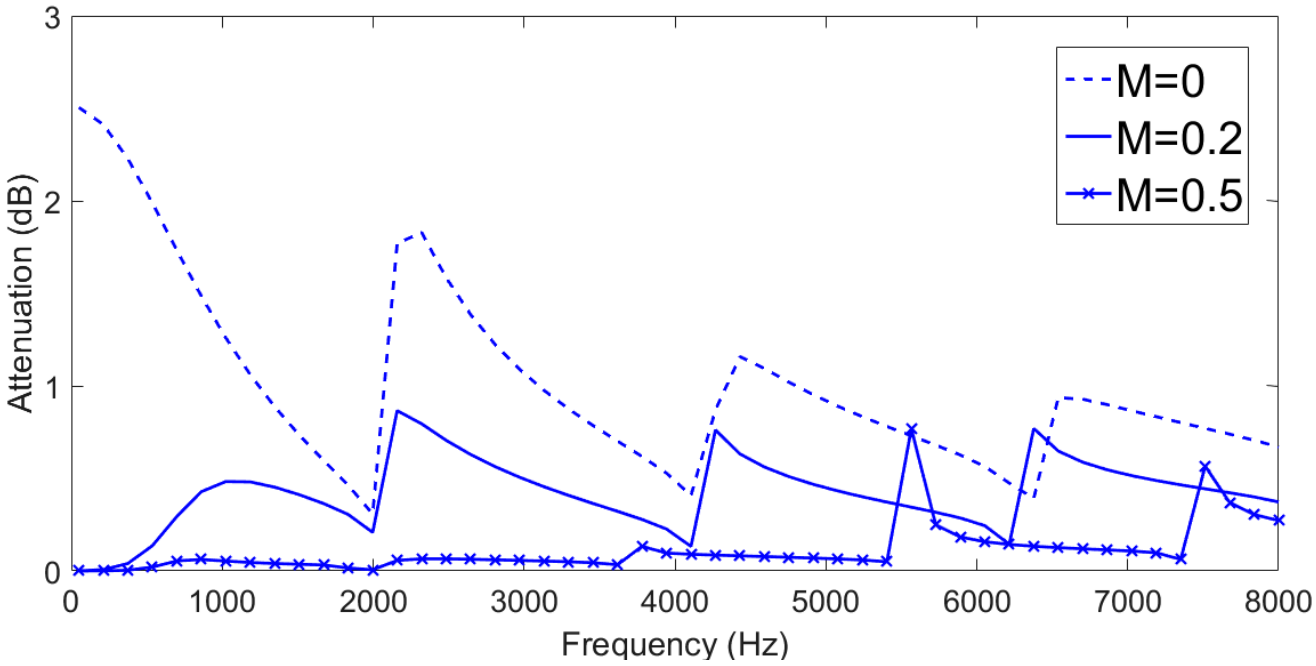

Figure 4.18. *Effect of the flow on the acoustic power attenuation.*

It is shown that the attenuation decreases for larger Mach numbers. All modes cut-on at 8000 Hz were included in the calculation of the total acoustic attenuation. This means that overall acoustic scattering effect becomes less important when the Mach number increases. Attenuation peaks are also observed when a higher mode is cut-on. However, a homogenised constant surface impedance is not representative of a realistic surface impedance equivalent to a locally reacting acoustic treatment on the duct wall as it depends on the flow as well as frequency. Therefore, combined effects of flow and impedance must be taken into account when calculating the acoustic attenuation. Grazing air flow effect on the acoustic impedance was emphasised through empirical formulas in literature [94, 99, 129, 130]. Most of the empirical models show that a grazing air flow at one hole surface increases acoustic resistance and decreases acoustic reactance. Kirby and Cummings model [94] representing a perforated plate impedance and accounting for the flow effect will be used here. The total impedance of a perforated plate backed by a cavity in the presence of flow can be then calculated. Following Kirby and Cummings empirical model [94], the resistance and reactance of a perforated plate are respectively given as following:
While $20\% < \varphi < 27\%$, $e = 10^{-3}$m or $e = 1.5.10^{-3}$m, $d = 3.10^{-3}$m , 1000Hz $< f <$ 7000Hz, pressure amplitude is very low and flow velocity does not exceed 70 m/s :

$$\mathcal{R} = \frac{\sqrt{8\nu\omega}}{\varphi c}\frac{e}{d} + \left[26.16\left(\frac{e}{d}\right)^{-0.169} - 20\right]\frac{v^*}{\varphi c} - 4.055\frac{fe}{\varphi c} \tag{4.46}$$

$$\chi = \frac{\omega}{\varphi c}\left[e + \epsilon\frac{8d}{3\pi}\right] \tag{4.47}$$

with:

$$\epsilon = 1 \qquad \text{if } \frac{v^*}{fe} \leq 0.18\frac{d}{e}$$

$$\epsilon = \left(1 + 0.6\frac{e}{d}\right)\mathrm{e}^{\left(\frac{\frac{v^*}{fe} - 0.18\frac{d}{e}}{1.8 + \frac{e}{d}}\right)} - 0.6\frac{e}{d} \qquad \text{if } \frac{v^*}{fe} > 0.18\frac{d}{e}$$

where v^* is the friction velocity characteristic of the inner viscous boundary layer of the fluid.

The remaining parameters are used with same notations as in chapter 3. Fig. 4.19 shows the acoustic power attenuation calculated for $M = 0.2$ and a duct geometry same as was presented above.

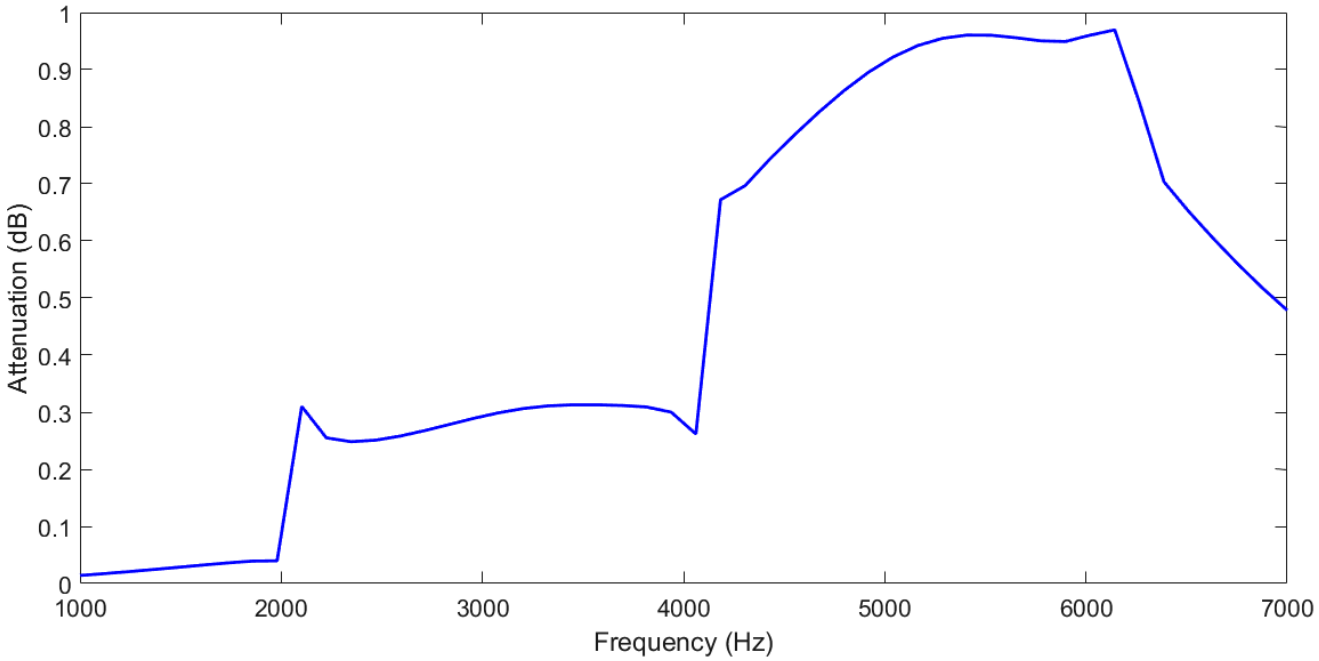

Figure 4.19. *Acoustic power attenuation with application to the Kirby and Cummings empirical impedance model integrating flow effect for* $M = 0.2$, $\varphi = 20\%$, $e = 10^{-3}m$, $d = 3.10^{-3}$ *and* $D = 10^{-2}m$.

It should be noted that previous results apply only for a mean uniform flow and would not be valid for particular flow velocity profiles [131].

4.8 Conclusion

A good agreement of results provided by the Wave Finite Element Method and the analytical approach has been reached for the study of the acoustical propagation inside rigid ducts. Some important outcomes of adding a uniform flow arise such as the raise of the wave length and the number of the cut-on modes. Modes behaviours were completely described for a rigid waveguide and duct modes concept was shown to be the same as for the non-convective case.

Furthermore, the multi-modal reflection and transmission inside acoustical waveguides due to a change in the impedance of the wall were also successfully predicted through the Wave Finite Element Method. It was shown that flow has an effect on transmission and reflection. Effects of flow velocity and orientation were therefore discussed. When the wall impedance is not infinite, mode shapes are determined with respect to the boundary condition at the wall which depends on the flow, namely the Ingard-Myers boundary condition for an inviscid model. In this case, differences between the modes shapes for the convective and the non-convective cases are to crop up particularly near the walls. A damping term should be added to the cell matrices used in the Wave Finite Element approach to be able to study the duct modes inside a lined region. Besides, as the WFE Method was successfully validated with the analytical calculations for a two dimensional convective problem, a next aim would be studying the scattering for three dimensional and more complex cross-sectional geometries.

General conclusion

This work dealt with the guided acoustical propagation. The announced goal was to characterise a waveguide in a way that the upstream and downstream transmissions and reflections and acoustic attenuation could be predicted regardless of the inputs.

Generally, these problems are dealt with by a modal approach. The basic principle is to define a set of functions (the modal basis) that satisfy Helmholtz equation. Each mode or a combination of modes is a solution to the propagation problem. However, the solutions have to satisfy the boundary condition at the wall. The boundary condition does not correspond to a rigid wall condition anywhere since ducts could be modelled as waveguides with three regions, two of them are hard-walled, with an impedance-walled region in between. Applying an analytical mode matching technique requires expressing these solutions in each duct region. One must keep in mind that, aside from the geometrical limitation, calculation of the transversal wavenumbers satisfying a non rigid boundary condition is generally done through an iterative method which could lead to results with missing roots. Another approach was proposed in this thesis and was to resort to a discrete problem. This took into account the damping by the liner and its dissipative character to predict the acoustic quantities scattered to the rigid parts whatever liner's nature is and without the need of representing explicitly the modes inside the lined region. The method proposed in this work did it well, since it combined a Finite Element Method modelling of the scatterer with a Wave Finite Element approach for the rigid parts allowing the computation of the pressure anywhere inside the rigid waveguide parts with the least computational requirements. Admittedly, a well known undesired issue arises when using the Wave Finite Element Method. That is the necessity of inversion of ill-conditioned matrices in the computation procedure. The use of a Singular Value Decomposition, and even a truncated one, could still be not sufficient to ensure

reliability. It was shown in the framework of this work that some scaling strategies had to be performed, certainly not a direct inversion of the matrices at their very first forms. This was proved to give good results when compared to results by the conventional approaches. Mechanical APDL acoustic analyses were used for the forced responses with various imposed conditions at the ends of a lined waveguide as a validation , while the analytical approach was used for the validation of the scattering coefficients themselves. Each incident mode reflects and transmits into a modal spectrum in different proportions. Significance of the conversion between the modes was highlighted and therefore the dependency of the the scattering coefficients solutions on the modes truncation was shown to be not an artefact of the method but a natural outcome.

It was shown that the proposed approach allows all modes orders to be fully studied being a 3D and multi-modal approach. Some of the geometries treated in this thesis were maybe too much simple but merely validation with the analytical approaches was intended. The study was extended to the study of the acoustical propagation with flow though. The modes behaviours were completely described for the rigid waveguides, particularly their physically most distinctive property, the axial wavenumber. For rigid walls, we have a finite number of cut-on modes, with the possibility of being more numerous with flow than without, and infinitely many cut-off (axially exponentially decaying) modes. For a wall with a finite impedance, the study was not completely performed within this work. Obviously, differences are much more likely to appear with flow than without. All modes decay exponentially but some strongly are while others less. Apart from this difference in axial direction, there is also a conspicuous difference in the radial direction. Most modes are present throughout the duct, but some exist only near the wall. They decay exponentially in the radial direction away from the wall. These modes are called surface waves. Some exist both in the convective and non-convective cases, but some only with mean flow, called hydrodynamic surface waves. These are likely to exist as Mach number becomes larger. Moreover, The Ingard-Myers boundary condition was used in this work for the lined walls in presence of flow as the model was assumed to be inviscid, but many researchers have already been working on it, and its validity is still controversial. It has been shown indeed that it is not very accurate in the case of a propagation in the opposite direction to the flow. Furthermore, literature

has provided several empirical models integrating the grazing air flow effect on the acoustic impedance. It has been shown that a grazing air flow at one hole surface of a resistive layer increases acoustic resistance and decreases acoustic reactance. Nevertheless, the remarkable discrepancies between models have to be mentioned. This is explained by the fact that the experimental studies and accompanying empirical models were performed using experimental techniques differing among their authors and with different imposed conditions such as exclusive validity for particular Mach numbers, pressures amplitudes and limited frequency ranges. The use of these empirical formulas preferring a model over another is too restricted for limited conditions to be used in a general theoretical context unless tolerating errors for wider intervals.

There are still some cases which could be studied as a recommended future work:

- Representation of wave shapes and wavenumbers for a wall with a finite impedance. A comparison can be drawn with the rigid duct modes with a possible study of the effect of variation of the impedance. Moreover, the above mentioned observations for propagation with flow inside lined sections can be further investigated.

- Extension to the 3D cases for propagation with flow.

- Study of more complex liner configurations. This may include spliced liners, for which scattering into different azimuthal mode orders and less attenuation than uniform liners with same impedance are expected, and liners with arbitrarily varying impedance through the circumference or impedance strips in the axial direction.

- Study of the scattering for ducts with a sudden change in diameter: Mode matching must be used at these sections as radial wavenumbers depend on the duct diameter.

Appendix A

Expression of the symplectic transfer matrix S

A waveguide segment is assumed to be discretised using the same nodal distribution at its left and right edges, say n nodes for each edge, with no internal nodes inside the segment. Then, relations between pressures and velocities vectors of a waveguide segment provide:

$$\mathbf{v}_l = \mathbf{D}_{ll}\mathbf{p}_l + \mathbf{D}_{lr}\mathbf{p}_r \tag{A.1}$$

$$\mathbf{v}_r = \mathbf{D}_{rl}\mathbf{p}_l + \mathbf{D}_{rr}\mathbf{p}_r \tag{A.2}$$

where subscripts l and r stand for the left and the right edges of the segment respectively, $\mathbf{p}$ and $\mathbf{v}$ are the pressures and velocities vectors and $\mathbf{D}_{ll}$,$\mathbf{D}_{lr}$,$\mathbf{D}_{rl}$ and $\mathbf{D}_{rr}$ are the square $(n \times n)$ blocks of the dynamic stiffness matrix of the segment.
Following developments aim to find a relation between the left and right state vectors $\mathbf{u}_l^t = [(\mathbf{p}_l)^t(-\mathbf{v}_l)^t]$ and $\mathbf{u}_r^t = [(\mathbf{p}_r)^t(\mathbf{v}_r)^t]$. Eq. (A.1) can be re-written as following:

$$\mathbf{p}_r = -\mathbf{D}_{lr}^{-1}\mathbf{D}_{ll}\mathbf{p}_l + \mathbf{D}_{lr}^{-1}\mathbf{v}_l \tag{A.3}$$

Replacing $\mathbf{p}_r$ by its expression in Eq. (A.3) into Eq. (A.2) leads to write:

$$\mathbf{v}_r = (\mathbf{D}_{rl} - \mathbf{D}_{rr}\mathbf{D}_{lr}^{-1}\mathbf{D}_{ll})\mathbf{p}_l + \mathbf{D}_{rr}\mathbf{D}_{lr}^{-1}\mathbf{v}_l \tag{A.4}$$

From Eqs. (A.3) and (A.4), we have:

$$\begin{pmatrix} \mathbf{p}_r \\ \mathbf{v}_r \end{pmatrix} = \mathbf{S} \begin{pmatrix} \mathbf{p}_l \\ -\mathbf{v}_l \end{pmatrix} \tag{A.5}$$

where

$$\mathbf{S} = \begin{pmatrix} -\mathbf{D}_{lr}^{-1}\mathbf{D}_{ll} & -\mathbf{D}_{lr}^{-1} \\ \mathbf{D}_{rl} - \mathbf{D}_{rr}\mathbf{D}_{lr}^{-1}\mathbf{D}_{ll} & -\mathbf{D}_{rr}\mathbf{D}_{lr}^{-1} \end{pmatrix} \tag{A.6}$$

Appendix B

Reflection from an acoustic impedance at the end of a waveguide under a higher order mode propagation condition

Calculation of the reflection from a termination impedance is detailed hereafter.
Let us suppose that one pressure mode propagates inside a rigid waveguide and that L is its length . The waveguide is ended at $x = L$ by an acoustic impedance Z_L. The pressure wave will be the sum of two waves travelling in the positive and negative x-directions:

$$p(x, y, z, t) = \left(A\mathrm{e}^{-\mathrm{i}k_x x} + B\mathrm{e}^{\mathrm{i}k_x x}\right) \psi(y, z)\mathrm{e}^{-\mathrm{i}\omega t} \tag{B.1}$$

where A is the amplitude of the left running wave and B is the amplitude of the right running wave.
To simplify the maths, we will use then the variable $(L - x)$ rather than x. Eq. (B.1) becomes:

$$p(x, y, z, t) = \left(A\mathrm{e}^{-\mathrm{i}k_x (L-x)} + B\mathrm{e}^{\mathrm{i}k_x (L-x)}\right) \psi(y, z)\mathrm{e}^{-\mathrm{i}\omega t} \tag{B.2}$$

The axial wavenumber k_x is given by:

$$k_x = k\cos\theta \tag{B.3}$$

where k is the free-field wavenumber and θ is the mode incidence angle.
Using Euler's equation $[\rho_0 \partial v/\partial t = -\partial p/\partial x]$, one may obtain the particle velocity:

$$v(x,y,z,t) = \frac{\cos\theta}{\rho_0 c}\left(A\mathrm{e}^{-\mathrm{i}k\cos\theta(L-x)} - B\mathrm{e}^{\mathrm{i}k\cos\theta(L-x)}\right)\psi(y,z)\mathrm{e}^{-\mathrm{i}\omega t} \tag{B.4}$$

where k is the free-field wavenumber, θ is the mode incidence angle, ρ_0 is the density of the fluid, c is the celerity of the sound in the air and L is the length of the waveguide.
The impedance of the wave can be then expressed as:

$$Z(x) = \frac{\rho_0 c}{\cos\theta}\frac{A\mathrm{e}^{-\mathrm{i}k\cos\theta(L-x)} + B\mathrm{e}^{\mathrm{i}k\cos\theta(L-x)}}{A\mathrm{e}^{-\mathrm{i}k\cos\theta(L-x)} - B\mathrm{e}^{\mathrm{i}k\cos\theta(L-x)}} \tag{B.5}$$

The wave impedance at $x = L$ must be equal to the impedance of the termination:

$$\begin{aligned} Z_L &= \frac{\rho_0 c}{\cos\theta}\frac{(A+B)}{(A-B)} \\ &= \frac{\rho_0 c}{\cos\theta}\frac{(1+B/A)}{(1-B/A)} \end{aligned} \tag{B.6}$$

The reflection coefficient $R_j = (B/A)$ is expressed as:

$$R_j = \frac{Z_L\cos\theta - \rho_0 c}{Z_L\cos\theta + \rho_0 c} \tag{B.7}$$

When using the non-dimensional variables convention,

$$Z_L^{normalised} = \frac{Z_L}{\rho_0 c} \tag{B.8}$$

Eq. (B.7) is rewritten as following:

$$R_j = \frac{Z_L^{normalised}\cos\theta - 1}{Z_L^{normalised}\cos\theta + 1} \tag{B.9}$$

Given the reflection coefficient, the absorption coefficient can be further calculated. In several previous works, the absorption coefficient was used to characterise and evaluate acoustic performance of absorbing materials [132, 133, 134]. The absorption coefficient ζ_j is given by :

$$\zeta_j = 1 - |R_j|^2 \tag{B.10}$$

$$\zeta_j = \frac{4\Re(Z_L^{normalised})}{(1 + \Re(Z_L^{normalised}))^2 + (\Im(Z_L^{normalised}))^2} \tag{B.11}$$

Appendix C

Boundary condition expression for porous terminations

Let us consider a periodic rigid duct filled with air with a porous layer termination at its right end. The porous material layer is backed by a rigid wall. The rigid duct part is divided into N segments. An equivalent fluid is used for modelling the porous material. The continuity of pressures and velocities vectors at the interface air-equivalent fluid provides the following relation:

$$\begin{pmatrix} {\boldsymbol{\Phi}_{\mathbf{p}}}^{inc}\mathbf{Q}^{inc(N+1)} + {\boldsymbol{\Phi}_{\mathbf{p}}}^{ref}\mathbf{Q}^{ref(N+1)} \\ {\boldsymbol{\Phi}_{\mathbf{v}}}^{inc}\mathbf{Q}^{inc(N+1)} + {\boldsymbol{\Phi}_{\mathbf{v}}}^{ref}\mathbf{Q}^{ref(N+1)} \end{pmatrix} = \begin{pmatrix} \mathbf{p}_l \\ -\mathbf{v}_l \end{pmatrix} \tag{C.1}$$

where superscript (i) refers to the i^{th} cross section of the rigid duct part, and $\mathbf{p}_l$ and $\mathbf{v}_l$ are pressures and velocities vectors corresponding to the left surface of the equivalent fluid. The following equation can be then written:

$$\mathbf{D^*}({\boldsymbol{\Phi}_{\mathbf{p}}}^{inc}\mathbf{Q}^{inc(N+1)} + {\boldsymbol{\Phi}_{\mathbf{p}}}^{ref}\mathbf{Q}^{ref(N+1)}) = -({\boldsymbol{\Phi}_{\mathbf{v}}}^{inc}\mathbf{Q}^{inc(N+1)} + {\boldsymbol{\Phi}_{\mathbf{v}}}^{ref}\mathbf{Q}^{ref(N+1)}) \tag{C.2}$$

where $\mathbf{D^*}$ is the dynamic stiffness matrix of the equivalent fluid condensed onto its left side.

$$\mathbf{D^*} = \mathbf{D}_{ll} - \mathbf{D}_{lr}\mathbf{D}_{rr}^{-1}\mathbf{D}_{rl} \tag{C.3}$$

with $\mathbf{D}_{ll}$, $\mathbf{D}_{lr}$, $\mathbf{D}_{rr}$ and $\mathbf{D}_{rl}$ are the square blocks of the dynamic stiffness matrix of the equivalent fluid.

A relation between amplitudes $\mathbf{Q}^{ref(1)}$ and $\mathbf{Q}^{inc(1)}$ can be then expressed:

$$\boldsymbol{\mu}^{-N}\mathbf{Q}^{ref(1)} = -(\mathbf{D}^{*}{\boldsymbol{\Phi}_{\mathbf{p}}}^{ref} + {\boldsymbol{\Phi}_{\mathbf{v}}}^{ref})^{-1}(\mathbf{D}^{*}{\boldsymbol{\Phi}_{\mathbf{p}}}^{inc} + {\boldsymbol{\Phi}_{\mathbf{v}}}^{inc})\boldsymbol{\mu}^{N}\mathbf{Q}^{inc(1)} \tag{C.4}$$

with $\boldsymbol{\mu}$ is the diagonal matrix of eigenvalues corresponding to the incident modes.
Eq. (C.4) is combined with an equation resulting from the expression of the boundary condition at the left end of the duct so that $\mathbf{Q}^{inc(1)}$ and $\mathbf{Q}^{ref(1)}$ can be then easily determined.

Bibliography

[1] R.J. Astley, R. Sugimoto, and P. Mustafi. Computational aero-acoustics for fan duct propagation and radiation. current status and application to turbofan liner optimisation. *J Sound Vib*, 330:3832–3845, 2011.

[2] J.M. Roche. *Simulation numérique de l'absorption acoustique de matériaux résonants en présence d'écoulement*. PhD thesis, Université du Maine, LeMans, 2011.

[3] R. Visser. *A Boundary Element Approach to Acoustic Radiation and Source Identification*. PhD thesis, Université de Twente, Enschede, 2004.

[4] M. Taktak, J.M. Ville, M. Haddar, and F. Foucart. Evaluation of a lined duct performance based on a 3d two port scattering matrix. In *Proceedings of meet. acoust.*, pages 1–14, 2008.

[5] Y. Auregan, M. Leroux, and V. Pagneux. Measurement of liner impedance with flow by an inverse method. In *Proceedings of the 10th AIAA/CEAS Aeroacoustics Conference*, pages 464–470, 2004.

[6] E. Piot, J. Primus, and F. Simon. Liner impedance eduction technique based on velocity fields. In *Proceedings of 18th AIAA/CEAS*, 2012.

[7] C.W. Zhou, J.P. Laine, M.N. Ichchou, and A.M. Zine. Multi-scale modelling for two-dimensional periodic structures using a combined mode/wave based approach. *Compos Struct*, 154:145–162, 2015.

[8] Y. Druon. *Étude de la propagation guidée et du rayonnement acoustiques par les conduits d'éjection de turboréacteur*. PhD thesis, Ecole Centrale de Lyon, Lyon, 2006.

[9] M. Abom. Measurement of the scattering matrix of acoustical two-ports. *Syst Signal Process*, 5:89–104, 1991.

[10] M. El bakkali, A. Lhémery, V. Baronian, and S. Grondel. A modal formulation for the propagation of guided waves in straight and curved pipes and the scattering at their junction. *J Phys Conf Ser*, 498:012012, 2014.

[11] M. Kharrat, M.N. Ichchou, O. Bareille, and W. Zhou. Wave diffusion sensitivity to angular positions of defects in pipes. *J Comput Acoust*, 23:1550013, 2015.

[12] W.P. Bi, V. Pagneux, D. Lafarge, and Y. Auregan. Modelling of sound propagation in a non-uniform lined duct using a multi-modal propagation method. *J Sound Vib*, 289:1091–1111, 2006.

[13] M. Taktak, J.M. Ville, M. Haddar, G. Gabard, and F. Foucart. An indirect method for the characterization of locally reacting liners. *J Acoust Soc Am*, 127:3548–3559, 2010.

[14] R. Marechal, E. Perrey-Debain, J.M. Ville, and B. Nenning. Fast computation of the scattering matrix of lined ducts containing passive components. *Acta Acust united Ac*, 97:966–973, 2011.

[15] A. Sitel and M.A. Galland. Scattering-matrix formulation for both measurement and prediction of acoustical performances of hybrid cells and their active and passive elements. *Acta Acust United Acust*, 97:579–589, 2011.

[16] S.W. Rienstra. *Fundamentals of Duct Acoustics*. Von Karman Institute Lecture Notes, 2015.

[17] W.P. Bi, V. Pagneux, D. Lafarge, and Y. Auregan. Sound propagation in nonuniform lined duct by the multimodal method. In *Proceedings of 10th ICSV*, pages 3229–3236, 2003.

[18] W.P. Bi, V. Pagneux, D. Lafarge, and Y. Auregan. An improved multimodal method for sound propagation in nonuniform lined ducts. *J Acoust Soc Am*, 122:280–290, 2007.

[19] B. Regan and J. Eaton. Modelling the influence of acoustic liner non-unifromities on duct modes. *J Sound Vib*, 219:859–879, 1999.

[20] M. Taktak, M. Haddar, J.M. Ville, A. Sitel, G. Gabard, and F. Foucart. Mesure de la matrice de diffusion multimodale d'un tronçon traité. In *Proceedings of 8th CFA*, 2006.

[21] A. Sitel, J.M. Ville, and F. Foucart. An experimental facility for measurement of acoustic transmission matrix and acoustic power dissipation of duct discontinuity in higher order modes propagation conditions. *Acta Acust United Acust*, 89:586–594, 2003.

[22] A. Sitel, J.M. Ville, and F. Foucart. Multiload procedure to measure the acoustic scattering matrix of a duct discontinuity for higher order mode propagation conditions. *J Acoust Soc Am*, 120:2478–2490, 2006.

[23] C. Droz, J.P. Laine, M.N. Ichchou, and G. Inquiete. A reduced formulation for the free-wave propagation analysis in composite structures. *Compos Struct*, 113:134–144, 2014.

[24] E. Manconi. *Modelling wave propagation in two-dimensional structures using a wave/finite element techniques*. PhD thesis, University of Parma, 2008.

[25] B.R. Mace and E. Manconi. Modelling wave propagation in two-dimensional structures using finite element analysis. *J Sound Vib*, 318:884–902, 2008.

[26] E. Manconi and B.R. Mace. Wave characterization of cylindrical and curved panels using a finite element method. *J Acoust Soc Am*, 125:154–163, 2008.

[27] J.M. Renno and B.R. Mace. Calculating the forced response of two-dimensional homogeneous media using the wave and finite element method. *J Sound Vib*, 330:5913–5927, 2011.

[28] Y. Fan, M. Collet, M. Ichchou, L. Li, O. Bareille, and Z. Dimitrijevic. Energy flow prediction in built-up structures through a hybrid finite element/wave and finite element approach. *Mech Syst Signal Pr*, 66-67:137–158, 2016.

[29] Y. Waki, B.R. Mace, and M.J. Brennan. Numerical issues concerning the wave and finite element method for free and forced vibrations of waveguides. *J Sound Vib*, 327:92–108, 2009.

[30] A. Kessentini, M. Taktak, M. Ben Souf, O. Bareille, M.N. Ichchou, and M. Haddar. Computation of the scattering matrix of guided acoustical propagation by the wave finite element approach. *Appl. Acoust.*, 108:92–100, 2016.

[31] K.S. Peat. The transfer matrix of a uniform duct with a linear temperature gradient. *J Sound Vib*, 123:43–53, 1988.

[32] T. Tanaka, T. Fujikawa, T. Abe, and H. Utsuno. A method for the analytical prediction of insertion loss of a two dimensional muffler model based on the transfer matrix derived from the boundary element method. *J Vib Acoust*, 107:86–91, 1985.

[33] A. D. Pierce. *Acoustics: An Introduction to its Physical Principles and Applications*. McGraw-Hill, 1981.

[34] M. Akoum and J.M. Ville. Measurement of reflection matrix of a discontinuity in a duct. *J Acoust Soc Am*, 103:2463–2468, 1998.

[35] C. Malmary. *Etude théorique et expérimentale de l'impédance acoustique de matériaux en présence d'un écoulement d'air tangentiel*. PhD thesis, Université de Maine, LeMans, 2000.

[36] J. Primus. *Détermination de l'impédance acoustique de matériaux absorbants en écoulement par méthode inverse et mesures LDV*. PhD thesis, INSA, Toulouse, 2012.

[37] J. Primus, F. Simon, and E. Piot. Validation of a direct propagation model for liner impedance eduction. In *Proceedings of 17th AIAA/CEAS*, 2011.

[38] J. Primus, E. Piot, and F. Simon. An adjoint-based method for liner impedance eduction: Validation and numerical investigation. *J Sound Vib*, 332:58–75, 2013.

[39] J. Primus, E. Piot, and F. Simon. Onera-nasa cooperative effort on liner impedance eduction. In *Proceedings of 19th AIAA/CEAS*, 2013.

[40] M. Taktak. *Mesure de la matrice de diffusion d'un tronçon traité cylindrique recouvert par un matériau: applications à la mesure de son efficacité et à la détermination de son impédance homogéneisée*. PhD thesis, ENIS, Sfax, 2008.

[41] M. Abramowitz and I.A. Stegun. *Handbook of Mathematical Functions*. Dover Publications, Inc., 1964.

[42] E. Redon, A.-S. Bonnet-Ben Dhia, J-.F. Mercier, and S. Poernomo Sari. Non-reflecting boundary conditions for acoustic propagation in ducts with acoustic treatment and mean flow. *Int. J. Numer. Meth. Engng*, 86:1360–1378, 2011.

[43] L.J. Eriksson. Higher order mode effects in circular ducts and expansion chambers. *J Acoust Soc Am*, 68:545–550, 1980.

[44] B. Ouedraogo. *Modélisation du rayonnement acoustique dans les guides traités par des matériaux absorbants à réaction localisée ou non localisée en présence d'écoulement par la méthode des éléments finis*. PhD thesis, Université de Bourgogne, Bourgogne, 2011.

[45] G.N. Watson. *A Treatise on the Theory of Bessel Functions*. Cambridge U.P., 1966.

[46] S.W. Rienstra and W. Eversman. A numerical comparison between the multiple-scales and finite-element solution for sound propagation in lined flow ducts. *J. Fluid Mech.*, 437:367–384, 2001.

[47] G.D. Furnell and D.A. Bies. Matrix analysis of acoustic wave propagation within curved ducting systems. *J Sound Vib*, 132:245–263, 1989.

[48] S. Marburg and B. Nolte. *Computational acoustics of noise propagation in fluids: finite and boundary element methods*. Springer, 2008.

[49] A. Brooks, C. Morgans, and H. Hansen. Learning acoustics through the boundary element method: an inexpensive graphical interface and associated tutorials. *Acoust Aust*, 33:89, 2005.

[50] A. Peplow and S. Finnveden. A super-spectral finite element method for sound transmission in waveguides. *J Acoust Soc Am*, 116:1389–1400, 2004.

[51] M. Taktak, J.M. Ville, M. Haddar, G. Gabard, and F. Foucart. A 3d multiport scattering matrix based-method for educing wall impedance of cylindrical lined duct section: Simulation and error evaluation. *Adv Acoust Vib*, 2009, 2009.

[52] J. M. Ville. Experimental methods in duct acoustics for higher order modes propagation conditions. In *Proceedings of forum acust*, 2014.

[53] H. Trabelsi, N. Zerbib, J.M. Ville, and F. Foucart. Méthode de mesure de la matrice de diffusion multimodale d'obstacles complexes en présence d'écoulement uniforme. In *Proceedings of 10th CFA*, 2010.

[54] C.W. Zhou, M. Ichchou, and J-.P. Laine. Free wave propagation in two-dimensional periodic beam grillage. In *Proceedings of 21th ICSV*, 2014.

[55] D.J. Mead. A general theory of harmonic wave propagation in linear periodic systems with multiple coupling. *J Sound Vib*, 27:235–260, 1973.

[56] J.M. Mencik and M.N. Ichchou. Multi-mode propagation and diffusion in structures through finite elements. *Eur J Mech A-Solid*, 24:877–898, 2005.

[57] B.R. Mace, D. Duhamel, M.J. Brennan, and L. Hinke. Finite element prediction of wave motion in structural waveguides. *J Acoust Soc Am*, 117:2835–2843, 2005.

[58] J.M. Mencik and M.N. Ichchou. Wave finite elements in guided elastodynamics with internal fluid. *Int J Solids Struct*, 44:2148–2167, 2007.

[59] E. Manconi, B. R. Mace, and R. Gaziera. Wave finite element analysis of fluid-filled pipes. In *Proceedings of NOVEM2009*, 2009.

[60] Y. Waki, B.R. Mace, and M.J. Brennan. Free and forced vibrations of a tyre using a wave finite element approach. *J Sound Vib*, 323:737–756, 2009.

[61] T. Gras, M.A. Hamdi, and M. Ben Tahar. Couplage wave finite element method (wfem) et finite element method (fem) pour le calcul de réponse forcée d'un rail infini à section complexe supporté périodiquement. In *Proceedings of 13th CFA/VISHNO*, 2016.

[62] Q. Serra. *Modèles réduits d'interfaces dissipatives en vibroacoustique par approche k-space*. PhD thesis, Ecole Centrale de Lyon, Lyon, 2014.

[63] Q. Serra, M.N. Ichchou, and J.-F. Deu. Wave properties in poroelastic media using a wave finite element method. *J Sound Vib*, 335:125–146, 2015.

[64] W.J. Zhou and M.N. Ichchou. Wave propagation in mechanical waveguide with curved members using wave finite element solution. *Comput Methods Appl Mech Eng*, 199:2099–2109, 2010.

[65] M. Kharrat, M.N. Ichchou, O. Bareille, and W. Zhou. Pipeline inspection using a torsional guided-waves inspection system. part 2: defect sizing by the wave finite element method. *Int J Appl Mech*, 6, 2014.

[66] C.W. Zhou. *Wave and modal approach for multi-scale analysis of periodic structures*. PhD thesis, Ecole Centrale de Lyon, 2014.

[67] J.-M. Mencik and M.N. Ichchou. A substructuring technique for finite element wave propagation in multi-layered systems. *Comput. Methods Appl. Mech. Engrg.*, 197:505–523, 2008.

[68] C. Droz, M.N. Ichchou, and J-.P. Laine. An improved wave/finite element formulation for studying high-order wave propagation in large-scaled waveguides. In *Proceedings of 11th WCCM*, 2014.

[69] C. Droz, C. Zhou, M.N. Ichchou, and J.-P. Laine. A hybrid wave-mode formulation for the vibro-acoustic analysis of 2d periodic structures. *J Sound Vib*, 363:285–302, 2016.

[70] WX. Zhong and FW. Williams. On the direct solution of wave propagation for repetitive structures. *J Sound Vib*, 181:485–501, 1995.

[71] A. Craggs. The application of the transfer matrix and matrix condensation methods with finite elements to duct acoustics. *J Sound Vib*, 132:393–402, 1989.

[72] C. Wilcox. Theory of bloch waves. *J Anal Math*, 33:146–167, 1978.

[73] A. Bocquillet, M. N. Ichchou, and L. Jezequel. Energetics of axisymmetric fluid-filled pipes up to high frequencies. *J Fluid Struct*, 17:491–510, 2003.

[74] Y. Waki. *On the application of finite element analysis to wave motion in one-dimensional waveguides*. PhD thesis, University of Southampton, 2007.

[75] C.W. Zhou, J.P Laine, M.N. Ichchou, and A.M. Zine. Wave finite element method based on reduced model for one-dimensional periodic structures. *Int J Appl Mech*, 7:1550018, 2015.

[76] E.D. Nobrega, F. Gautier, A. Pelat, and J.M.C. Dos Santos. Vibration band gaps for elastic metamaterial rods using wave finite element method. *Mech Syst Signal Process*, 79:192–202, 2016.

[77] G.R. Liu and S.S. Quek. *The finite element method: a practical course*. Butterworth-Heinemann, 2003.

[78] M.N. Ichchou, J.M. Mencik, and W. Zhou. Wave finite elements for low and midfrequency description of coupled structures with damage. *Comput Methods Appl Mech Eng*, 198:1311–1326, 2009.

[79] A. Klinger. Approximate pseudoinverse solutions to ill-conditioned linear systems. *J Optim Theory Appl*, 2:117–124, 1968.

[80] F. Bouchoucha, M. Akrout, T. Fakhfakh, M.N. Ichchou, and M. Haddar. Damage detection in cylindrical pipe through diffusion matrix in wave finite element method. *Adv Struct Eng*, 15:435–445, 2012.

[81] S.W. Rienstra. Contributions to the theory of sound propagation in ducts with bulk-reacting lining. *J Acoust Soc Am*, 77:1681–1685, 1985.

[82] S.W. Rienstra. Acoustic radiation from a semi-infinite annular duct in a uniform subsonic mean flow. *J Sound Vib*, 94:267–288, 1984.

[83] S. Redonnet and Y. Druon. Computational aeroacoustics of aft fan noises characterizing a realistic coaxial engine. *AIAA Journal*, 50:1029–1046, 2012.

[84] J.F. Bridge and S.W. Angrist. An extended table of roots of $j_n^{'}(x)y_n^{'}(\beta x) - j_n^{'}(\beta x)y_n^{'}(x) = 0$. *Maths Compt*, 16:198–204, 1962.

[85] C.L. Morfey. Rotating pressure patterns in ducts: Their generation and transmission. *J Sound Vib*, 1:60–87, 1964.

[86] B.S. Howard and S. Cazzolato. *Acoustic Analyses Using MATLAB and ANSYS*. Taylor Francis Group, 2014.

[87] G.H. Golub and C.F. Van Loan. *Matrix Computations , Third Edition*. The Johns Hopkins University Press, 1996.

[88] A. Neumaier. Solving ill-conditioned and singular linear systems: A tutorial on regularization. *SIAM Rev.*, 40:636–666, 1998.

[89] R. Kirby and F. Denia. Analytic mode matching for a circular dissipative silencer containing mean flow and a perforated pipe. *J Acoust Soc Am*, 122:3471–3482, 2007.

[90] X. Sun, L. Du, and V. Yang. A homotopy method for determining the eigenvalues of locally or non-locally reacting acoustic liners in flow ducts. *J Sound Vib*, 303:277–286, 2007.

[91] B. Nennig, E. Perrey-Debain, and M. Ben Tahar. A mode matching method for modeling dissipative silencers lined with poroelastic materials and containing mean flow. *J Acoust Soc Am*, 128:3308–3320, 2010.

[92] C. Chan, E. Perrey-Debain, J-M. Ville, and B. Poirier. Numerical determination of transmission losses of a turbofan inlet duct lined with porous materials. *Appl Acoust*, 117:86–93, 2017.

[93] T. Zandbergen. Are locally reacting acoustic liners always behaving as they should? In *Proceedings of 5th AIAA*, 1979.

[94] R. Kirby and A. Cummings. The impedance of perforated plates subjected to grazing gas flow and backed by porous material. *J Sound Vib*, 217:619–636, 1998.

[95] T. H. Melling. The acoustic impedance of perforates at medium and high sound pressure levels. *J Sound Vib*, 29:1–65, 1973.

[96] D. Maa. Potential of microperforated panel absorber. *J. Acoust. Soc. Am.*, 104:2861–2866, 1998.

[97] T. Elnady. *Modelling and Characterization of Perforates in Lined Ducts and Mufflers*. PhD thesis, The Royal Institute of Technology, Stockholm, 2004.

[98] C. Malmary, S. Carbonne, Y. Auregan, and V. Pagneux. Acoustic impedance measurement with grazing flow. In *Proceedings of 7th AIAA/CEAS*, 2001.

[99] A. W. Guess. Calculation of perforated plate liner parameters from specified acoustic resistance and reactance. *J Sound Vib*, 40:119–137, 1975.

[100] R. Tayong and P. Leclaire. Hole interaction effects under high and medium sound intensities for micro-perforated panels design. In *Proceedings of 10th CFA*, 2010.

[101] Y. Auregan and A. Starobinski. Determination of acousitcal energy dissipation/ production potentially from the acoustical transfer functions of a multiport. *Acta Acust united Ac.*, 85:788–792, 1999.

[102] S. Sack and M. Abom. Experimental characterization of acoustic multi-ports. In *Proceedings of forum acust*, 2014.

[103] M. Taktak, M.A. Majdoub, M. Bentahar, J.M. Ville, and M. Haddar. Caractérisation numérique d'un tronçon cylindrique traité avec écoulement. In *Proceedings of 10th CFA*, 2010.

[104] W.P. Bi, V. Pagneux, D. Lafarge, and Y. Auregan. Characteristics of penalty mode scattering by rigid splices in lined ducts. *J Acoust Soc Am*, 121:1303–1312, 2007.

[105] B. Ouedraogo, R. Maréchal, J.-M. Ville, and E. Perrey-Debain. Broadband noise reduction by circular multi-cavity mufflers operating in multimodal propagation conditions. *Appl. Acoust.*, 107:19–26, 2016.

[106] R.A. Scott. The propagation of sound between walls of porous material. In *Proceedings of the Phys. Soc.*, page 358, 1946.

[107] J.F. Allard and N. Atalla. *Propagation of Sound in Porous Media: Modelling Sound Absorbing Materials, Second Edition*. John Wiley and Sons, Ltd., 2009.

[108] D.J. Johnson, J. Koplik, and R. Dashen. Theory of dynamic permeability and tortuosity in fluid-saturated porous media. *J. Fluid. Mech.*, 176:379–402, 1987.

[109] Y. Champoux and J.F. Allard. Dynamic tortuosity and bulk modulus in air saturated porous media. *J. Appl. Phy.*, 70:1975–1979, 1991.

[110] N. Sellen. *Modélisation de l'impédance de surface d'un matériau par controle actif: application à la caractérisation et à l'optimisation d'un absorbant acoustique*. PhD thesis, Ecole Centrale de Lyon, Lyon, 2003.

[111] N. Sellen, M.A. Galland, and O. Hilbrunner. Identification of the characteristic parameters of porous media using active control. In *Proceedings of 8th AIAA/CEAS*, 2002.

[112] Y. Yasuda, S. Uenoy, and H. Sekine. A note on applicability of locally-reacting boundary conditions for delany-bazley type porous material layer backed by rigid wall. *Acoust. Sci. Tech.*, 36:459–462, 2015.

[113] E. Becache, A. S. Bonnet-Ben Dhia, D. Lafarge, and G. Legnedre. Perfectly matched layers for the convected helmholtz eqution. *SIAM J. Numer. Anal.*, 42:409–433, 2004.

[114] M. K. Myers. On the acoustic boundary condition in the presence of flow. *J Sound Vib*, 71:429–434, 1980.

[115] K.U. Ingard. Influence of fluid motion past a plane boundary on sound reflection, absorption, and transmission. *J Acoust Soc Am*, 31:1035–1036, 1959.

[116] E.J. Brambley. Viscous boundary layer effects on the myers impedance boundary condition. In *Proceedings of 15th AIAA/CEAS*, 2009.

[117] Y. Renou and Y. Auregan. On a modified myers boundary condition to match lined wall impedance deduced from several experimental methods in presence of a grazing flow. In *Proceedings of 16th AIAA/CEAS*, 2010.

[118] Y. Auregan, R. Starobinski, and V. Pagneux. Influence of grazing flow and dissipation effects on the acoustic boundary conditions at a lined wall. *J Acoust Soc Am*, 109:59–64, 2001.

[119] B. Betgen. *Comportement d'un absorbant actif en écoulement étude théorique et expérimentale*. PhD thesis, Ecole Centrale de Lyon, Lyon, 2010.

[120] M. Taktak, M.A. Majdoub, M. Bentahar, and M. Haddar. Numerical modelling of the acoustic pressure inside an axisymmetric lined flow duct. *Arch Acoust*, 37:151–160, 2012.

[121] M. Taktak, M.A. Majdoub, M. Haddar, and M. Bentahar. Numerical characterization of an axisymmetric lined duct with flow using the multimodal scattering matrix. *J Theor App Mech*, 51:313–325, 2013.

[122] X. Wang and X. Sun. Transfer element method with application to acoustic design of aeroengine nacelle. *Chin J Aeronaut*, 28:327–345, 2015.

[123] G. Dhatt and G. Touzot. *Presentation of the Finite Element Method*. Maloine S.A. Editeur, 2009.

[124] M. Taktak, H. Jrad, C. Karra, M. Bentahar, and M. Haddar. Numerical modeling of the acoustic propagation in a three-dimensional wave guide in the presence of flow. *Acta Acust United Acust*, 97:453–465, 2011.

[125] V. Pagneux and A. Maurel. Scattering matrix properties with evanescent modes for waveguides in fluids and solids. *J Acoust Soc Am*, 116:1913–1920, 2004.

[126] Y. Renou and Y. Aurégan. Failure of the ingard–myers boundary condition for a lined duct: An experimental investigation. *J Acoust Soc Am*, 130:52–60, 2011.

[127] Y. Renou. *Impédance des traitements acoustiques absorbants en conduit : effets de l'écoulement rasant et de la couche limite*. PhD thesis, Université du Maine, LeMans, 2010.

[128] S.W. Rienstra. A classification of duct modes based on surface waves. *Wave motion*, 37:119–135, 2003.

[129] J. Kooi and S. Sarin. An experimental study of the acoustic impedance of helmholtz resonator arrays under a turbulent boundary layer. In *Proceedings of AIAA 7th Aeroacoustics Conference*, 1981.

[130] W. Bell, B. Daniel, and B. Zinn. Acoustic liner performance in the presence of a mean flow and three-dimensional wave motion. In *Proceedings of AIAA 12th Aerospace Sciences Meeting*, 1974.

[131] J.C. Wendoloski. On the theory of acoustic flow measurement. *J Acoust Soc Am*, 110:724–737, 2001.

[132] Y. Wang, C. Zhang, L. Ren, M. Ichchou, M.A. Galland, and O. Bareille. Sound absorption of a new bionic multi-layer absorber. *Compos Struct*, 108:400–408, 2014.

[133] Z. Xiaodan and F. Xiangqian. Enhancing low frequency sound absorption of micro-perforated panel absorbers by using mechanical impedance plates. *Appl. Acoust.*, 88:123–128, 2015.

[134] M. Mirowska and K. Czyzewski. Estimation of sound absorption coefficients of porous materials. In *Proceedings of 14th ICSV*, 2007.

AUTORISATION DE SOUTENANCE

Vu les dispositions de l'arrêté du 25 mai 2016,

Vu la demande du Directeur de Thèse

Messieurs O. BAREILLE, M. ICHCHOU et M. TAKTAK

et les rapports de

M. N. GMATI
Professeur - LAMSIN - Ecole Nationale d'Ingénieurs de Tunis (ENIT) - BP 37 - 1002 Tunis
Tunisie

et de

M. N. BOUHADDI
Professeur - FEMTO-ST - Université de Bourgogne Franche-Comté
Département de Mécanique Appliquée - 24 chemin de l'épitaphe - 25000 Besançon

Monsieur KESSENTINI Ahmed

est autorisé à soutenir une thèse pour l'obtention du grade de **DOCTEUR**

Ecole doctorale MECANIQUE, ENERGETIQUE, GENIE CIVIL ET ACOUSTIQUE

Fait à Ecully, le 30 mai 2017

P/Le directeur de l'E.C.L.
La directrice des Etudes

ECOLE CENTRALE DE LYON Service Scolarité ECULLY

M-A. GALLAND